INFORMATION TO USERS

This manuscript has been reproduced from the microfilm master. UMI films the text directly from the original or copy submitted. Thus, some thesis and dissertation copies are in typewriter face, while others may be from any type of computer printer.

The quality of this reproduction is dependent upon the quality of the copy submitted. Broken or indistinct print, colored or poor quality illustrations and photographs, print bleedthrough, substandard margins, and improper alignment can adversely affect reproduction.

In the unlikely event that the author did not send UMI a complete manuscript and there are missing pages, these will be noted. Also, if unauthorized copyright material had to be removed, a note will indicate the deletion.

Oversize materials (e.g., maps, drawings, charts) are reproduced by sectioning the original, beginning at the upper left-hand corner and continuing from left to right in equal sections with small overlaps.

Photographs included in the original manuscript have been reproduced xerographically in this copy. Higher quality 6" x 9" black and white photographic prints are available for any photographs or illustrations appearing in this copy for an additional charge. Contact UMI directly to order.

ProQuest Information and Learning
300 North Zeeb Road, Ann Arbor, MI 48106-1346 USA
800-521-0600

NUMERICAL SIMULATION OF ONE- AND TWO-PHASE FLOWS IN UNPACKED AND PARTIALLY PACKED VESSELS

BY

SAIFUDDIN SHEIKH

A Thesis Presented to the

FACULTY OF THE COLLEGE OF GRADUATE STUDIES

KING FAHD UNIVERSITY OF PETROLEUM & MINERALS

DHAHRAN, SAUDI ARABIA

In Partial Fulfillment of the
Requirements for the Degree of

MASTER OF SCIENCE

In

CHEMICAL ENGINEERING

May 2001

KING FAHD UNIVERSITY OF PETROLEUM AND MINERALS
DHAHRAN 31261, SAUDI ARABIA

DEANSHIP OF GRADUATE STUDIES

This thesis, written by **SAIFUDDIN SHEIKH** *under the direction of his Thesis Advisor and approved by his Thesis Committee, has been presented to and accepted by the Dean, Deanship of Graduate Studies, in partial fulfillment of the requirements for the degree of*

MASTER OF SCIENCE *in* **CHEMICAL ENGINEERING.**

Thesis Committee

Dr. Habib D. Zughbi (Chairman)

Prof. Abdullah A. Shaikh (Member)

Dr. Kevin F. Loughlin (Member)

Prof. Abdullah. A. Shaikh
(Department Chairman)

Prof. Osama A. Jannadi
(Dean of Graduate Studies)

عمادة الدراسات العليا
DEANSHIP OF GRADUATE STUDIES

Date: 2006-2007

Dedicated to Dad, Mom, Noman

&

Marium

Acknowledgements

Praise and Glory to Allah (SWT) who gave me the intelligence, courage and patience to undertake this work and successfully complete it. Acknowledgement is due to King Fahd University of Petroleum & Minerals for providing financial support in the form of research assistantship. I am indebted to the Department of Chemical Engineering in KFUPM. The facilities and support of the Department made my work easier.

I am thankful to Dr. Habib D. Zughbi, my Thesis Advisor. His easy to approach attitude and a knack for tackling problems was very encouraging. It was a great experience working and learning with him. I am also thankful to Prof. Abdullah A. Shaikh, chairman of the Chemical Engineering Department and one of my committee members. Prof. Shaikh's constructive criticism helped in focussing my work better. Dr. Kevin. F. Loughlin's presence in my committee was very encouraging and I am thankful to him for the excellent editorial work for my Thesis. I would also like to thank Prof. Sharma, the 'authority in mixing' for his guidance and encouragement during this work. I am also thankful to Riasat Saab, our department secretary for his cooperation.

Special thanks to my parent's back home for their patience, prayers and support during this work. My brother's constant motivation also helped me in pursuing this research. I am also thankful to Baboo Uncle, Rukiya aunty, Hafeez and Marium for their trust in me.

The company of my friends in North Compound (NC) was a driving force in accomplishing this task. I am thankful to brother Sohel for his guidance. Mazhar's presence made my life easy in NC. Special thanks to Ifadat, my Boss, his guidance, timely help and good old chevy made my stay a memorable one. I am also thankful to

Rizwan for the encouragement and motivation. I am indebted to Zameer, Mozahar, Rakib, Hasib (Bangali guys), the Hyderabadi community of KFUPM especially Mujtaba baba and Imran, the Pakistani friends at NC namely Fareed, & Tariq. I would also like to thank Faiz, a great friend. Finally thanks to all the NC guys for their support and love. Last but not least, I am thankful to the Saudi graduate students, namely Tareg, Bashammakh, Abdullah, Nayef and Nabeel.

TABLE OF CONTENTS

List of Tables

List of Figures

Nomenclature

A	Cross-sectional area (m^2)
A_d	Droplet Area (m^2)
Bo*	Bond Number
$c_{\varepsilon 1}$	Turbulence model constant = 1.44
$c_{\varepsilon 2}$	Turbulence model constant = 1.92
C_D	Drag Coefficient
C_μ	Parameter of the Turbulence model
d	Droplet diameter (m)
d_p	Effective diameter of particle (m)
d_e, d_k	Rate of gain of k by diffusion and generation by mean strain
d_φ	Diffusive transport
$\sum \mathbf{f}_f$	Local volume averaged forces between the packing and fluid (Pa)
$\mathbf{f}_p$	Pressure force (Pa)
$\mathbf{f}$	Force generated by the fluid moving through the pellet interstices (Pa)
$f_{z,p}$	Pressure force (Pa)
F_D	Drag Force (N)
F_z	Pressure force in the z direction (Pa)
F_y	Pressure force in the y direction (Pa)
$F_{z,p}$	Pressure force (Pa)

g	Acceleration due to gravity (m^2/s)
G	Mass flowrate of the fluid (kg/s)
k	Turbulent kinetic energy.
p	Pressure (Pa)
G_k	Generation by body forces
P_k	Rate of gain of k by diffusion
Q	Volumetric flowrate (m^3/s)
R_i	Volume fraction of phase i
R_{ep}	Packed Bed Reynolds number
S_v	Specific surface (surface of solids per unit volume of solids)
S_{φ_i}	Source rate of φ_i per unit volume
S_e	Secondary source/sink term
$\overline{v_i v_j}$	Turbulent stresses
v	Superficial velocity (m/s)
v_r	Fluid velocity (m/s)
v_i	Velocity vector of phase *i*
v_s	Superficial velocity (m/s)
v_z	interstitial velocity in the z direction (m/s)
v_y	interstitial velocity in the y direction (m/s)
v_o	average empty tube flow velocity ($=\sqrt{v^2_{z,o} + v^2_{y,o}}$)

$v_{z,o}$ average empty tube flow velocity in z direction (m/s)

$v_{y,o}$ average empty tube flow velocity in y direction (m/s)

$\mathbf{v}$ Velocity of the fluid (m/s)

We Weber Number

Greek Letters

α Permeability

Γ_{φ_i} Exchange coefficient of ϕ in phase I

ε Dissipation rate

η Kinematic viscosity (m^2/s)

θ Void fraction

μ Dynamic viscosity (Pa.s.)

μ_{eff} Effective viscosity (Pa.s.)

μ_t Turbulent viscosity

μ_g Gas viscosity (Pa.s).

ϱ Density (kg/m^3)

ϱ_g Gas Density (kg/m^3)

σ Surface tension (kg/sec^2)

σ_φ Constant of the Turbulence model

τ Shear stress force

φ_i Any conserved property of phase i

THESIS ABSTRACT

Name:	SAIFUDDIN SHEIKH
Title:	Numerical Simulation of One- and Two-phase Flows in Unpacked and Partially Packed Vessels
Degree:	Master of Science
Major Field:	Chemical Engineering
Date of Degree:	May 2001

A Detailed description of flow distribution in packed and unpacked vessels is often necessary in order to obtain better understanding and explanation of a range of operations in the process industry. Computational Fluid Dynamics (CFD) is increasingly used to investigate flow distribution in chemical and petrochemical processes. In this study one- and two-phase flows in an unpacked and partially packed vessel of industrial dimensions are investigated.

The vessel considered is a horizontal cylinder, which is 18.2 m long and 4.9 m in diameter. It has three inlets and one outlet and fluid is entering the vessel at a velocity of 57 m/s.

The present work numerically simulates the flow in the vessel using a k- ε turbulence model. Flow in the packed bed is simulated using a modified Ergun equation. The effects of a) fluid flowrates, b) number of inlets and outlets, c) inserts such as annular discs, d) turbulence model, and the e) splits of phases (two-phase flow) on the patterns of flow have been investigated.

Results of single-phase flow for the unpacked vessel indicate that the flow is not evenly distributed in the current design. Results of two-phase flow also showed similar uneven flow distribution. Results also showed that the distribution of flow in the partially packed vessel depends on the value of the friction forces between the packing and the fluid with a certain degree of maldistribution (significantly less than the unpacked case) observed.

Flow distribution in the unpacked vessel is significantly improved by using two or more outlets. The emplacement of annular discs or conical like inserts above the inlets further improved the flow distribution. The two-phase flow results exhibited similar patterns except for an increased deposition of the heavier phase at some parts of the surface of the vessel and/or on the surface of the inserts.

Master of Science Degree
King Fahd University of Petroleum & Minerals
Dhahran, Saudi Arabia
May 2001

مـــــلخص الرســـالة

الأسم : سيف الدين شيـــــخ.

العنوان : المحاكاة العددية للتدفق ذي الطور والطورين في الأوعية الغير محشوة والمحشوة جزئياً.

الدرجة : مـــــاجســـــتير.

التخصص: هندسة كيميائية.

التاريخ : مايو ٢٠٠١م.

يُعْتَبَرُ الوصف التفصيلي لتوزيع التدفق في الوعاء المحشو وغير المحشو ضرورياً للحصول على شرح كافٍ ومفهوم أفضل في مجال العمليات الصناعية . يستخدم ديناميكا السوائل العددية (CFD) لبيان وإعطاء صورة لتوزيع التدفق في العمليات الكيميائية والبتروكيميائية. في هذه الدراسة تم دراسة التدفق ذي الطور والطورين في الوعاء المحشو والمحشو جزئياً لأبعاد صناعية.

الوعاء موضوع الدراسة هو ذو شكل إسطواني أفقي بطور ١٨,٢م وقطر ٤,٩ م وهو ذو ثلاثة مداخل ومخرج واحد وسرعة السائل الداخل للوعاء ٥٧ م/ث.

يحاكي العمل الحالي عددياً التدفق داخل الوعاء باستخدام نموذج (k - ε turbulence model). وتمت محاكاة التدفق في الوعاء المحشو باستخدام معادلة (Ergun) المعدّلة وتمت دراسة تأثير العوامل التالية: (١) معدل التدفق، (٢) عدد المداخل والمخارج، (٣) الإضافات داخل الوعاء مثل القرص الحلقي، (٤) نموذج الاضطراب المستخدم، (٥) انشطار الطورين بمجال تدفق السائل.

أعطت نتائج التدفق ذي الطور الواحد والطورين نفس النتائج وإشارات إلى أن التدفق في التصميم الحالي للوعاء الغير محشو غير موزع بشكل متناظر وأشارت النتائج أيضاً إلى أن توزيع التدفق في الوعاء المحشو جزئياً يعتمد على قوى الاحتكاك ما بين السائل على المواد المستخدمة للحشو.

تم تحسين توزيع التدفق في الوعاء الغير محشو بشكل ملحوظ باستخدام مخرجين أو أكثر بدلاً من مخرج واحد. بالإضافة إلى ذلك ، أعطت محاكاة التدفق ذي الطورين نفس النتائج إلا أن هناك ترسيباً للطور الثقيل عند بعض أجزاء السطح الداخلي للوعاء أو سطح الإضافات داخله.

درجة الماجستير في العلوم

جامعة الملك فهد للبترول والمعادن

مايو ٢٠٠١م

Chapter 1

1.1 Introduction

Fluid flow plays a significant role in a wide range of operations in the oil, chemical and petrochemical industry. Successful reactor engineering crucially depends on the ability to predict and control the fluid dynamics and mixing occurring in industrial reactors. Therefore a good understanding of flow behavior and flow distribution is often crucial for proper design and operation of equipments such as packed and unpacked reactors and mixers. However, the detailed knowledge about the flow in industrial vessels is rather limited mainly because most vessels are operated at high temperature and pressure, which makes measurements of velocities a difficult task.

Fluid flows are usually unsteady, three-dimensional and involve fluids that are to some degree compressible[1]. In order to model the main flow features, many simplifying assumptions are usually made, such as assuming that the flow is steady, or restricted to less than three dimensions or that it is practically incompressible. The form of the resulting continuum equations as derived from the conservation law of physics, therefore depends on these assumptions about the flow and fluids involved.

Computational Fluid Dynamics (CFD) offers the possibility of predicting the detailed flow and turbulence of the reactor under different geometrical and operating conditions. Over the past two decades, CFD has undergone a rapid transformation and is nowadays an integral part of research related to fluid flow, heat and mass transfer problems. CFD is

now well established for single-phase flow problems, and is gaining widespread recognition for solving multiphase flow problems and problems involving chemical reactions.

CFD contributes to the analysis of fluid flow and related phenomena such as heat and/or mass transfer, mixing and chemical reaction. Usually, the domain of interest is divided into a large number of control-volumes or computational cells, which have relatively small size in comparison with macroscopic volume of the domain of interest. For each control-volume a discrete representation is made after which an iterative solution procedure is invoked to obtain the solution of the non-linear equations. CFD is based on the conservation laws for mass, momentum and (thermal) energy.

Flow related problems in the industry are numerous. Oleimans[2] and Coleman[3] have described many of these problems in details. The present work is concerned with the detailed understanding of one-and two-phase flows in packed and unpacked vessels. An example of single-phase flow in packed beds can be found in catalytic converters. Two-phase flow in an unpacked vessel is commonly found in the inlets of polymerization reactors. Such an industrial case constitutes very complex problems, which may include in addition to highly turbulent flows, complex geometry of very large scale, (5-20m), chemical reactions, heat and mass transfer.

Obtaining a rigorous model of one or more of these industrial applications with all aspects included is beyond the scope of this work for many reasons including the computational power required to execute such a three-dimensional complex model. This work concentrates on resolving the flow fields for one-and two-phase flows in unpacked and partially packed vessels mainly in two-dimensions. The effects of flowrates, number

and arrangement of inlets and outlets, geometric inserts and physical properties are investigated. Such flow models may be very helpful in offering a better understanding of the problem. The degree of understanding depends on the problem. For example, such a two-dimensional model properly simulates axisymmetric, unreactive and isothermal flow.

In the following sections single- and two-phase flows and flow through packed beds are introduced.

1.2 Single-Phase Flow

Single-phase flow is by far the most common phenomena in day to day life, from the simple flow of water through a tap to many complex industrial operations. For single-phase isothermal systems involving laminar flows the conservation equations (Continuity and Navier-Stokes) are firmly established[4]. These equations are discussed in detail in section 3.4. For the closure of the continuity and the Navier-Stokes equations, an equation for the density is required. For non-isothermal systems, the transport equations have to be supplemented with a thermal energy equation whereas for systems involving chemical conversion, species conservation equations (reaction rates) have to be added.

The conservation equations discussed above are also valid for turbulent flows, but within the context of CFD, a very high resolution in space and time would be required to capture all the details of the turbulent flow field. Such a resolution is still out of reach for most modern day computers. There are various turbulence models in the literature and they are discussed in detail in section 3.9.

Once the governing equations are framed, turbulence model selected, the next step is to formulate the relevant boundary conditions and then select the appropriate numerical

technique to solve these equations. A suitable computer code is required to implement these numerical techniques. The numerical results then need to be validated. These steps are discussed in section 3.3.

Single-phase flow modeling by CFD has received considerable attention over the last two decades. Single-phase CFD modeling has found application in civil engineering for solving the problems involving flow dynamics of rivers, lakes and estuaries and external flow around buildings. Furthermore, CFD has been applied to calculate air currents throughout the buildings in order to arrive at improved designs of ventilation systems.

In chemical engineering CFD modeling of single-phase flows has been applied to gas and liquid flows through reaction vessels[5] (packed/unpacked). Wang and Andrews[6] have presented CFD simulation results for laminar flow of a Newtonian liquid in a helical duct. Mier *et al.*[7] have carried out simulations of single phase laminar and turbulent flows at the entrance of a tube, and flow through an orifice plate. Abid *et al.*[8] have studied the blending/mixing of highly viscous (miscible) liquids encountered in a variety of industrial operations.

1.3 Two-Phase Flow

A two-phase flow is one in which dynamic interactions and sometimes chemical reactions between two-phases or components in a flowing system take place, e.g., liquid-liquid, gas-liquid, liquid-solid particles and gas-solid particles. Sometimes the two phases consist of the same chemical substance, as in distillation equipment or they can be different chemical substances, like dust particles in air.

Due to the great complexity of two-phase flow systems compared to single-phase flow, assumptions are made that direct the research into three broad areas of approach. In one approach[9] the two-phase flow is represented by a fictitious single-phase flow, wherein the fluid properties such as density and viscosity are defined in such a way as to maximize the effectiveness of representation. This is at best a crude approximation of the actual flow. Another approach deals with separated flow models, wherein the fluid dynamic equations are developed separately for each phase. These equations can then be combined to describe the total flow, or boundary conditions can be assumed between the two phases to couple the two sets of equations. The third and most phenomenological approach breaks the analysis of two-phase flow into several flow regimes. Some regimes are almost continuous whereas for other regimes there is a discrete, pronounced structural change. The flow regime is broken down in terms of the actual structure existing between the two-phases. The flow regime is defined in terms of the actual resultant flows, even though there are too many operative factors to predict with accuracy which of these regimes will occur in a given flow system. This description of regimes is therefore necessarily of a qualitative, subjective nature.

Theoretical and experimental studies of two-phase flow are becoming increasingly important because of their widespread applications in industry. This relevance is being given a great stimulus by the expanding needs of modern industrial societies. The application of two-phase flow research to problems in the petrochemical industries is clear from systems such as reactors, boilers, evaporators, distillation towers, and turbines. Transportation and extraction of the products of oil are other obvious applications. As movement toward such alternative energy sources as coal gasification, nuclear energy,

and solar energy, new applications of two-phase technology become even more important[9]. Quite apart from the oil, petrochemical and industries concerned with the development of energy supplies, two-phase flow occurs in such varied industries as food processing, paper manufacturing, and steel manufacturing.

Many applications outside industry also exist. Rain, snow, dust storms, and fog and cloud formation all involve interactions of two phases. Bioengineering, from the study of blood flow to the inhalation of air-suspended particulate matter, finds a need for understanding of two-phase flow phenomena.

Coleman[3] has discussed the use of the CFD approach in understanding unit operations in the chemical industry. He has presented a detailed study of some cases at BP Amoco Chemicals, wherein CFD was used not only to aid in understanding and solving existing process problems but also to assist in the design of new process operations. A detailed case history of distribution of an evaporating spray in a reactor inlet is presented, which is of significant relevance to the present investigation.

The widespread availability of fast computing facilities and the rapid advance of powerful numerical techniques and software offers the best possibility of numerical simulation of two-phase flow problems.

1.4 Flow Through Packed Beds

Fluid flow through packed beds is commonly encountered in industrial applications involving mass and heat transfer both with and without chemical reactions. Complete understanding of the fluid flow distribution in packed beds is of considerable practical importance due to its significant effect on transport and reaction rates. Packed beds could

be either fixed bed or moving bed type. The fixed bed catalytic reactor is widely used in the chemical industry[10]. In chemical engineering processes, packed beds are frequently used as catalytic reactors, filters, or separation processes like absorption, adsorption and distillation. In design of these devices, fluid dynamics plays an important role, since the transport of chemical species, mixing or contacting catalytic surfaces, is entirely described by the fluid dynamical conservation laws.

Some common design elements that need to be considered first when dealing with packed beds include pressure drop, flow maldistribution, interfacial and intra-particle gradients and the effect of catalyst characteristics on the process or hydrodynamic design. The present work investigates the flow distribution in partially packed beds.

The analysis of fluid flow, heat transfer processes and coupled chemical conversion in packed bed reactors has traditionally received considerable attention from chemical engineers. Coleman[3] has discussed the use of CFD in solving some industrial scale cases involving the used of packed beds and the ability of CFD in identifying the problem areas and their successful solution.

1.5 Objectives of the Study

Although many single- and two-phase flow problems in unpacked and packed vessels have been investigated experimentally and numerically, there does not seem to be many published references that deal with flow distribution in large industrial vessels. Most of the research in this area has been concentrated on some theoretical model developments, and generally on a very small scale.

The present study uses some of the techniques mentioned in this chapter to simulate the flow in unpacked and partially packed vessels. The vessel simulated in the present study has actual industrial dimensions and operating conditions. The geometry and operating conditions of the vessel though appears to be very simple but actually from the flow distribution point of view, causes a lot of flow maldistribution, thereby reducing the overall efficiency of the vessel. The study aims to improve this flow situation using some alternatives. The study aims at simulating single-and two-phase flows in the vessel while unpacked and partially packed. The effects of vessel geometry, inlet and outlet boundary conditions, fluid flowrates and physical properties, split of phases (volume and mass percentages), turbulence model, and interphase friction (two-phase flows) on the patterns of fluid flow are investigated.

The work is motivated by operating problems faced in the local industry in the above mentioned and other vessels.

In the above-mentioned vessel, a part of the catalyst constituting the packed bed is found to be underutilized during shutdowns. This may be partly due to flow maldistribution. Other vessels where two-phase flows are used face other problems such as accumulation of liquid in certain undesirable locations. Such accumulation may result in surging of compressors and/or in off specification polymerization products.

This study is not meant to offer final solutions to such problems, partly because it is a 2D study and partly because it does not include chemical reactions. Nevertheless, it is expected to provide a valuable contribution towards a better understanding of the flows under investigation and factors affecting such flows.

Chapter 2

Literature Review

2.1 Introduction

In recent years Computational Fluid Dynamics (CFD) has emerged as a powerful tool for engineers and scientists alike, providing valuable information on the temporal and spatial distribution of key variables in a flow field. CFD can be applied with confidence to solve a variety of single-and multiphase flow problems. CFD is a discipline that encompasses the numerical solution of the equations of mass, momentum and energy conservation in a flow-geometry of interest, together with subsidiary sets of equations reflecting the problem at hand. Examples of such subsidiary equations include (1) equations for turbulence quantities in the context of the Reynolds-averaged formulation of the equations of fluid motion, (2) equations describing chemical species present in the flow and (3) equations describing the dynamics of solid particles, liquid droplets and gas bubbles dispersed in the flow. Further complicating factors could be due to the fact that the flow occurs in a complex geometry, the fluid has non-Newtonian properties, and/or the chemical kinetics contains many steps. All these factors have to be accounted for in an appropriate way in a CFD calculation[12].

The continuing development of the CFD technology has meant that the CFD calculations are now increasingly being seen as an integral part of optimization or development plans for a much wider range of chemical processes. Although, in many

cases optimizing the flow may only result in an increase in selectivity of one or two percent, the low margins in the industry mean that this can represent a staggering increase in profitability. The realization of this has already motivated the application of detailed flow models to specific processes involving chemical reactions. These calculations help to identify the possible problems occurring in existing systems and provide useful insights in the design of experiments. Furthermore, once they are accepted as a reasonably accurate description of the processes in a reactor they can be used for scale up[12].

There has been an extensive research in the area of single-phase flow applications in stirred tanks, packed bed reactors, polymeric flows and chemically reactive flows[13]. The next section highlights a review of the investigations in single-phase flow modeling using CFD.

2.2 Single-phase flow

Single-phase flow modeling has received considerable attention since the advent of Computational Fluid Dynamics. Within single-phase systems a further distinction can be made between systems involving i) laminar flows in complex geometries, ii) turbulent flows, iii) flows with complex rheology, and iv) fast chemical reactions[11]. CFD has been successfully used for single-phase flow simulation in open channels and stirred tanks. CFD simulations of flow in baffled stirred tank reactors (BSTRs) are desirable because they provide a useful supplement to the poorly established scale-up criteria that are traditionally used to design reactors in conjunction with the results of laboratory or pilot-scale tests. The first two-dimensional CFD simulation of BSTRs was carried out by Harvey and Greaves[14]. The overall flow patterns obtained in these simulations were in

encouragingly good agreement with experiments and paved the way for further development of BSTR modeling using CFD.

Harris *et al.*[12] have reported results of single-phase CFD simulations of industrial scale BSTRs. They have carried out three-dimensional simulations of stirred tanks using a variety of meshing techniques and have found good agreement with experimental work. They have concluded that although an enormous amount of progress has been made in the past decade, simulation predictions for mean velocities and turbulence quantities are still not entirely satisfactory, even for single-phase non-reacting flows. Improved turbulence modeling and high performance computing have a particularly important role to play in the future application of CFD to this type of reactor

Harris *et al.*[12] have also carried out single-phase CFD simulation for non-Newtonian, non-isothermal flow (polymeric flow) in an extruder. The main feature of their work was that the viscosity of the fluid, which was a novel type of polymer, exhibited a combined shear-rate and temperature dependence through a complex geometry. CFD modeling was successful in optimizing the extrusion process by improving the residence time distribution of the fluid so as to avoid hot spots, which caused polymer degradation. A challenge with this modeling is the experimental validation of these complex rheological models.

Mier *et al.*[7] have presented numerical results for single and multiphase flows using staggered and collocated grids in the finite volume methods for four standard flows: developing laminar single-phase flow at the entrance of a tube; developing turbulent single-phase flow at the entrance of a tube; incompressible flow through an orifice plate and developing turbulent gas-solid flow in a vertical pipe. They analyzed the

convergence rate, the stability of the pressure-velocity coupling, the dependence of the solution on the grid size and the capability of reproduction of experimental data and/or analytical solutions. The numerical results when compared with experimental data were in a good agreement. The results showed that the staggered arrangement of the grid has an advantage when dealing with high-pressure gradient and multiphase flows. The number of iterations were largest using the staggered grids for single-phase flows. This probably occurs due to the fact that coarse collocated grids guarantees the conservation law in a larger control volume for the same grid concentration.

Another critical issue in single-phase flow modeling is the behavior of the jets. Lane[15] has presented a detailed account of the jet behavior in tanks. A jet may be either laminar or turbulent depending on the jet Reynolds number. Lane has given the ranges of the jet Reynolds number for characterizing whether a jet is laminar or turbulent. In this investigation, since the inlet velocity is very high (57 m/s), the jets are turbulent. The jet expansion plays a very crucial role in the flow distribution pattern. Turbulent jets have a lower expansion than laminar jets. The cone angle of the jet gives an indication of the jet. The cone angle[15] for turbulent jets that have been reported in literature vary between 8-20°. In this investigation, the cone angle of the jet is about 10°, which is due to very high jet velocity which hampers the jet from spreading sideways. If the angle of spread or expansion is more, it would be beneficial as it can reduce the size of low velocity zones between the adjacent jets. In the vessel under consideration, these jets are far apart and the adjacent jets do not connect and this can lead to considerable low velocity zones, in between the jets themselves.

2.3 Two-Phase Flow

By a combination of rigorous model development, advanced computational techniques, and a number of small-and large-scale supporting experiments, considerable progress has been made in understanding and predicting two-phase phenomena. Current approaches towards developing multiphase models depend on some form of averaging. Analytical methods for the development of the basic equations for two-phase flow include:

1. Homogeneous model/drift flux model
2. Separate-flow model (two-fluid model)

The first model is more suited to dealing with mixed flow such as bubble flow and slug flow, while the second is more suited to cases where flow is separated, as in stratified and annular flow. Numerical methods for two-phase modeling include:

1. One Fluid Approach
2. Two-Fluid Model (Euler-Euler)
3. Mixed Approach (Euler-Lagrange)

Numerical methods are dealt with in detail in Section 3.3.

2.3.1 Homogeneous Model/ Drift Flux Model

The homogeneous model[16] treats the mixture as a whole, and consequently the physical properties are represented by the average value of the mixture. This treatment assumes that the gas and liquid phases possess the same velocity (or the slip velocity is neglected). This model was used extensively in the past, because of its simplicity. The six unknowns to be determined, as in single-phase flow, are the velocity vectors (in three

directions), pressure, temperature, and density. The number of equations (Continuity, 3 momentum equations, energy equation and equation of state for density) is thus equivalent to the number of unknowns.

The homogeneous model seems to be well suited for the description of complex systems, such as nuclear reactors, which cannot take into account a detailed separate-phase flow model because of their complexity. The model does not seem to be very popular due to its inaccuracy for two-phase flow in comparison with the separate flow model.

2.3.2 Separate Flow Model (Two-Fluid Model)

As both phases occupy the full flow field concurrently, two sets of conservation equations corresponding to these two phases can be written and must be complemented by a set of interfacial jump conditions (discontinuities). The separate flow model[17] takes account of the fact that the two phases can have differing properties and different velocities. Separate equations of continuity, momentum and energy, if required, are written for each phase and these equations are solved simultaneously. The equations are coupled by the fact that the summation of liquid and gas volume fraction in each cell is always equal to one. In its simplest form, only one parameter, such as velocity, is allowed to differ for the two phases while conservation equations are only written for the combined flow.

The separate flow model considers the phases to be artificially segregated into two streams; one of liquid and one of gas. Each stream is assumed to travel at a mean velocity. For the case where the mean velocities of the two phases are equal the equations reduce to those of the homogeneous model. The basic premises upon which the separated flow

model is based are the assumptions of (a) constant but not necessarily equal velocities for the two phases, and (b) the attainment of thermodynamic equilibrium between the phases.

The model may be developed with various degrees of complexities. In this investigation a similar type of approach will be used, but turbulence equations will also be solved for the two-phase situation, which is dealt with in details in section 3.6.

2.3.3 Flow Patterns in Two-Phase Flow

From an engineering viewpoint, the final objective of studying two-phase flow is to determine the heat transfer and pressure drop characteristics of a given flow. The hydrodynamic behavior of two-phase flow, such as pressure drop, volume fractions, or velocity distribution, varies in a systematic way with the observed flow pattern or regime, just as in the case of a single-phase flow, whose behavior depends on whether the flow is in the laminar or turbulent regime. However, in contrast to single-phase flow, there exists a lack of generalizing principles for gas-liquid flow that could serve as a framework for solving practical problems. For instance, for a two-phase flow, we do not have such comfortable phenomenological principles as Prandtl's mixing-length theory, the methods of analogies such as Colburn's '*j*' factors, or the simplifications allowed by boundary-layer theory. The identification of a flow regime automatically provides a picture of the phase boundaries. The location of the phase boundaries in turn allows one to make various order-of-magnitude calculations using integrated forms of the momentum and continuity equations. Such calculations suggest which variables might be worthwhile investigating and what kind of hydrodynamic behavior is to be expected. Two-phase flows are frequently characterized by two important quantities:

(i) The gas volume fraction, R_1, which is defined as the ratio of the volume of gas to the total volume of gas and liquid in a flow.

$$R_1 = \frac{\text{volume of gas}}{\text{total volume}}$$

The fractional volume of the liquid (R_2) then becomes (1 - R_1).

(ii) The superficial gas velocity, v_s, which is the ratio of the gas volumetric flow rate Q, at a given flow cross section, to the cross-sectional area A.

$$v_s = Q / A$$

2.3.4 Flow Regimes in Two-Phase Flow

The main interest in this work is concentrated on flow in a large vessel (a horizontal cylinder, 18.2 m long, and 4.9 m in diameter). However, it is beneficial when talking about two-phase flows to be aware of the possible flow regimes. Such regimes are better defined for two-phase flows in pipes. Typical flow patterns in vertical and horizontal pipes[18] are shown in Figures 2.1a and 2.1b respectively. Flow patterns identified in these figures can be described as follows:

(i) *Bubbly flow*. In bubbly flow, the gas phase is moving as isolated bubbles in a liquid continuum. This flow pattern occurs at low gas volume fractions.

(ii) *Slug flow*. In vertical slug flow, bubbles that have nearly the same diameter as the tube and have a characteristic rounded front and move along separated by liquid slugs, which may contain a dispersion of smaller bubbles. In horizontal slug flow, large liquid slugs move behind bubbles large enough to cover the entire diameter. Such flow occurs with moderate gas volume fractions and relatively low flow velocity, and can be considered a

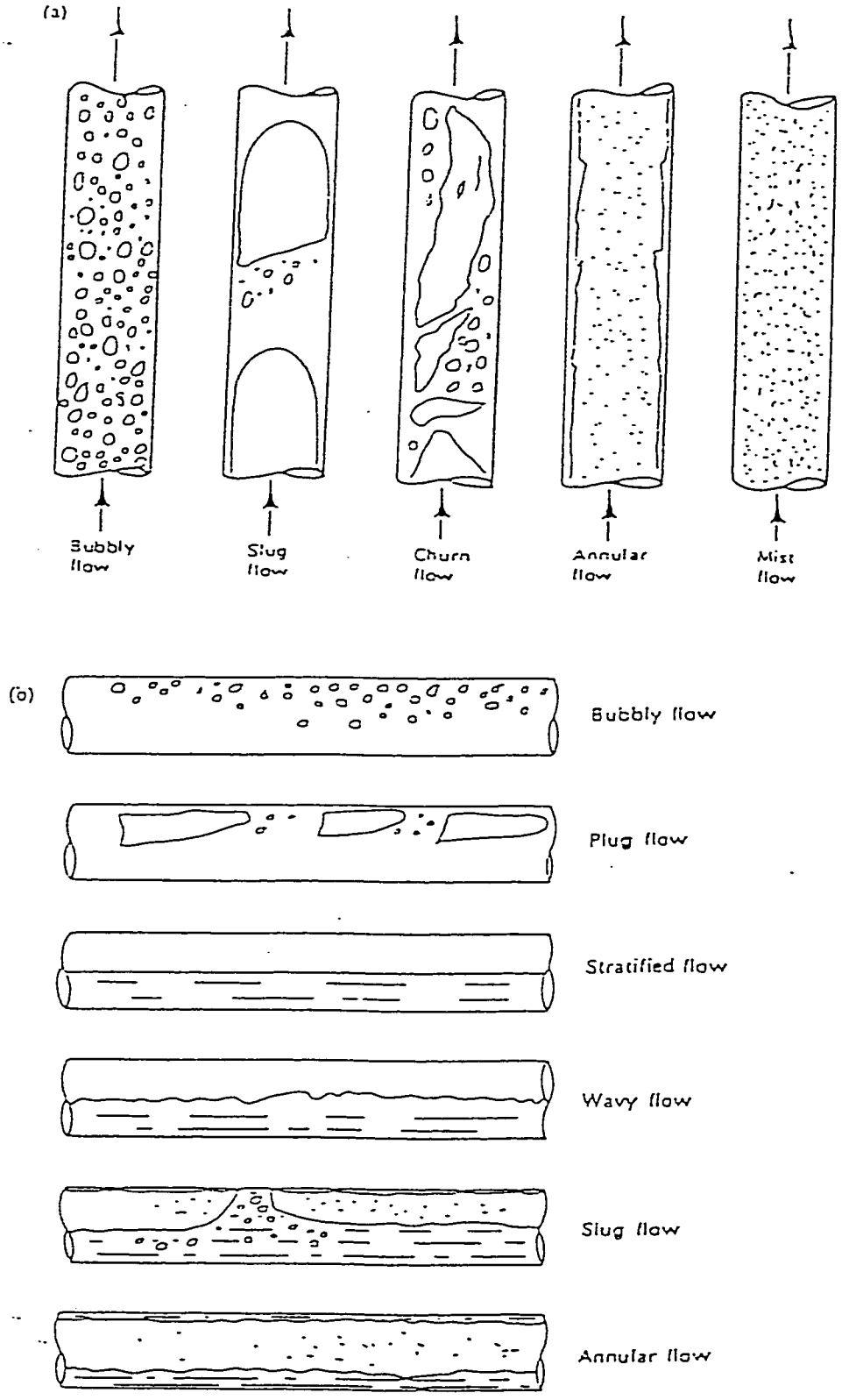

Figure 2.1 Typical two-phase flow patterns: (a) flow patterns in vertical flow (b) flow patterns in horizontal flow (after Tong & Tang[18])

transition between bubbly and annular flow. Such transitions may take place in more than one step, as shown for the next two flow regimes.

(iii) *Plug flow.* This is applicable only to horizontal flow, as shown in Figure 2.1 b. It consists of elongated gas bubbles. Although the name is sometimes used interchangeably with slug flow, it is differentiable in horizontal flow by the shape of the gas cavity.

(iv) *Churn flow.* As the gas velocity is increased, the slug flow regime begins to break down and the gas bubbles become unstable, leading to an oscillating, "churning" flow (especially in air-water systems). Thus an alternative name for this region is unstable slug flow.

(v) Wispy annular flow. In wispy annular flow, the central region of the flow is gaseous except for wisps of droplets bunched into discrete groupings. Such a flow usually occurs at high mass-flow rates.

(vi) *Annular flow.* In annular flow there is a continuous liquid in an annulus along the wall and a continuous gas/vapor phase in the core. The gas core may contain entrained droplets, dispersed mist, while the discontinuous gas phase appears as bubbles in the annulus. This flow pattern occurs at high void fractions and high flow velocities. A special case of annular flow is that where there is a gas/vapor film along the wall and a liquid core in the center. This type is called inverse annular flow and appears only in sub cooled stable film boiling.

(vii) *Mist flow.* This type of flow is common in cases of high velocity gas-continua in which the liquid phase is dispersed and occurs at very high gas volume fractions.

(viii) *Stratified* and *Wavy Flows* are characteristics of horizontal flow as gravitational forces inhibit such a regime in case of vertical flows.

All the above regimes are for very high L/D (Pipe length: Pipe diameter) ratios. In the current investigation, this ratio is not high since the diameter is very large. Therefore the flow regime in the vessel under consideration may not be directly related to the previously considered regimes. However this is not crucial because the flow is solved in a rigorous manner and the interphase friction estimated based on a bubble or droplet diameter. The phases are considered interdispersed in the large vessel.

2.4 Literature Review of Two-Phase Flow Problem

Although CFD can be applied with confidence to solve a variety of single-phase flow problems, a considerable effort still has to be made before CFD can be applied to the study of gas-liquid two-phase flows with the same level of confidence. Several problems have yet to be solved, for instance there seems to be no general agreement on the definitive form of the governing equations. There is also an ongoing debate about which modeling approach (Euler-Euler or Euler-Lagrange) is most suited for the study of gas-liquid two-phase flow. Furthermore, CFD modeling of gas-liquid two-phase flows is complicated by considerable ambiguity about the correct description of bubble dynamics and about the interplay between the bubbles and the turbulent eddies.

Nevertheless, CFD modeling of dispersed gas-liquid/two-phase flow has shown remarkable progress over the past two decades. The flow could be either that of a liquid continuum-gas phase dispersed or a gas continuum-liquid phase dispersed. Two most common approaches to modeling gas-liquid two-phase flows are the Euler-Euler or two fluid approach and the Euler-Lagrange or discrete bubble approach. In the Euler-Euler approach, both phases are modeled as two interpenetrating continua. In the Euler-

Lagrange approach, the volume averaged Navier-Stokes equations are used to describe the motion of the continuous phase and each bubble is tracked on basis of a balance of forces acting upon the bubble and an equation of motion.

There has been an extensive research in the area of gas-liquid two-phase flow in bubble columns. Delnoij *et al.*[19] have reported a three dimensional numerical model for gas-liquid bubble columns (liquid continuum-gas phase dispersed) using an Euler-Lagrange approach. The model resolves the time-dependent three-dimensional motion of small, spherical gas bubbles in a liquid. It incorporates all relevant forces acting on a bubble rising in a liquid, and accounts for two-way momentum coupling between the phases. Their results underlines the importance of dynamic modeling and it further strengthens the case for the development of (pseudo) two-phase instantaneous, whole field measurement techniques, rather than, measurement techniques that produce time-averaged data.

Spicka *et al.*[5] carried out numerical studies of the hydrodynamics of gas-liquid flow in a 2D acrylic reactor with internal dimensions of 200 by 600 by 2 mm, packed/unpacked rectangular reactor (liquid continuum-gas phase dispersed). They reported experimental data that was obtained using different techniques of imaging such as laser velocimetry, and pressure drop dynamics. They investigated the hydrodynamic parameters such as gas-holdup, interfacial area, bubble velocity, liquid turbulence intensity, and pressure drop. Their experimental results were in excellent agreement with the CFD predictions.

Al-Dahhan *et al.*[23] investigated two-phase flow in trickle-bed reactors. One of the major challenges in the design of trickle-beds is the prevention of liquid flow maldistribution, which causes portions of the bed to be incompletely wetted by the

flowing liquid. Their numerical results were in good agreement with their experimental results

Kuipers and Van Swaaij[11] suggested the use of a mixed Eulerian-Lagrangian approach for solving dispersed multiphase flow. They also studied bubble formation at a single orifice in gas-fluidized beds (liquid continuum-gas phase dispersed) and reported good agreements of numerical simulations with experimentally observed bubble size using the two-fluid model.

Ranade and Van den Akker[21] carried out extensive studies of two-phase flow using a computational snapshot approach and found good agreement of predicted results with experimental data. Ranade[22] has also studied gas-liquid flows for bubble column reactors using the two fluid model approach (liquid continuum-gas phase dispersed) and concluded that sparger characteristics and resistance play a crucial role in determining the fluid dynamics of bubble columns.

There is an extensive amount of literature on gas-liquid flows, but most of the cases discussed above are those of liquid continuum in which the gas phase is dispersed in rather smaller scale geometry. In this study we aim to investigate numerically two-phase flow in a large size vessel.

2.5 Flow Through Packed Beds

A detailed knowledge of the fluid flow profile is essential for a proper design of packed beds. CFD can be used to model a wide variety of flows through porous media, including flow through packed beds, perforated plates, flow distributors and tube banks. In one type of modeling, a zone is defined in which the porous media model is applied

and the pressure loss in the flow is determined via user-defined inputs. Heat transfer through the medium can also be represented, subject to the assumption of thermal equilibrium between the medium and the fluid flow. Typically a porous media model incorporates an empirically determined flow resistance in a region of the model defined as porous. A porous media model is nothing more than an added momentum sink in the governing momentum equations.

A number of early studies showed that reaction and radial heat transfer can only be modeled correctly if the non-uniformities of the bed structure are properly accounted for[24, 25]. Therefore over the years, a number of studies investigated the radial variation of the axial gas velocity in packed beds. These studies included axial velocity measurements at various radial positions, measurement of radial porosity profiles[26-28] and modeling of the radial variations of axial velocity[29, 30]. It was noted, however, that in industrial packed beds, some nonuniformities either due to the presence of internal structures[31, 32] or due to irregular gas inlet design[33] could cause the flow not to be one-dimensional and the gas velocity to vary in both radial and axial direction. Such a two-dimensional flow is called "non-parallel" flow in the literature[34]. Hence, for industrial applications of packed beds, it is certainly important to be able to effectively model the non-parallel gas flow. In general, three types of mathematical models have been developed for the treatment of non-parallel gas flow in packed beds[20]. They are:

1) Vectorized Ergun equation model

2) Equations of motion model

3) Discrete cell model (DCM)

The Vectorized Ergun equation model is based on the assumption that a packed bed can be treated as a continuum. The model utilizes the empirical Ergun equation, which holds well for overall pressure drop in the macroscopic beds with unidirectional flow, for an infinitesimal length of the bed and applied in the direction of flow. A number of investigators [31, 33, 35] utilized this method to model two- and three-dimensional flow in packed beds.

The Equations of motion model, in principal, solves the mass and momentum conservation equations for the flowing phase provided the solid boundaries are precisely specified. Such a direct numerical simulation (DNS) however is beyond the reach at present for large industrial-scale packed beds[36]. By employing the effective viscosity as an adjusting factor, Ziolkowska and Ziolkowski[29] and Bey and Eigenberger[28] have developed a mathematical model for the interstitial velocity distribution.

Another possibility of modeling packed bed reactors involves the use of a so-called Discrete Cell Model (DCM)[20] approach which is based on the concept that the packed bed may be represented by a number of interconnected discrete cells with the bed porosity allowed to vary in two directions from cell to cell. The fluid flow is assumed to be governed by the minimum rate of total energy dissipation in the packed bed (i.e. flow follows the path of least resistance). It is assumed that the Ergun equation is applicable at the cell scale. Therefore, the solution for velocity at each cell interface can be achieved by solving the non-linear multivariable minimization problem. Jiang *et. al.*[20] compared the numerical simulation results with CFD predictions and found reasonable agreement.

Fluid flow between particles in packed beds is characterized by a random packing geometry, high turbulence and strong velocity fluctuations. Any realistic flow model must

therefore be based on some averaging assumptions. One generally accepted procedure[28] is to assume angular symmetry (in case of cylindrical coordinate system) of the flow profile and to consider a continuous distribution of the void fraction in the packing. Then any fluid flow will create continuously distributed interstitial velocity. The flow field can be described by the Navier-Stokes equations if additional terms for fluid-particle interactions are incorporated. Vortemeyer and Schuster[37] proposed the application of the extended Brinkman equation where the fluid-particle interactions is described by a two-dimensional Ergun pressure correlation and the fluid wall friction is separately taken into account. This allows the application of a no-slip boundary condition at the wall where the void fraction approaches unity. The conceptual difficulty that fluid-wall friction is treated differently from fluid-particle friction is considered acceptable since fluid-wall friction affects the flow profile only in the immediate vicinity of the wall, whereas inside the packing Ergun pressure drop, describing fluid-particle interaction is by far dominating.

Vortemeyer and Schuster[37] have used this variational approach to evaluate the steady two-dimensional velocity profiles for isothermal incompressible flow in rectangular and cylindrical packed beds. They used the continuity equation, Brinkman's equation and a semi empirical expression for the radial porosity profile in the packed bed to compute these profiles. Their results showed that significant preferential wall flow occurs in cases where the ratio of channel diameter and particle diameter becomes sufficiently small. Although their study was done for an idealized situation, it has laid the foundation for more detailed studies[28] . The momentum equations for interstitial velocity have been used assuming laminar viscosity. Bey and Eigenberger[28] used the increased "turbulent viscosity" which accounts for the highly turbulent interstitial flow. They took

measurements outside the fixed bed behind a monolith. Hence, before and behind the monolith the fluid shifts from the region near the wall to the centre. When the comparison was carried out between measured velocity profiles outside the bed with simulations, they concluded that these changes have to be taken into account. These researchers[28, 37] have used a two-dimensional model containing the continuity equation and the momentum balance equations in the radial and axial direction. The momentum balances are composed of the Ergun equation and of shear stress and inertia effects.

In this investigation the approach of Bey and Eigenberger[28] has been used, but the model equations are for a Cartesian coordinate system instead of the cylindrical system used by them. The details are discussed in section 3.5. The pressure drop in the packing has been evaluated by the well-established correlation of Ergun[38] wherein factors determining the (energy loss) pressure drop in packed beds should be considered. These factors are the: (1) rate of fluid flow, (2) viscosity and density of the fluid, (3) closeness and orientation of the packing, and (4) size, shape, and surface of the particles. The first two variables concern the fluid while the last two the solids. In this investigation, the first two factors have been considered for modeling the pressure drop through the packed bed while the values of the other two factors are assumed to remain constant.

The literature survey for the present investigation is summarized in the following Tables.

Table 2.1: Summary of Published work in Single Phase Flow

Investigators	**Reference**	**Year**	**Technique Used**
Abid *et al.*	8	1992	Experimental and CFD
Wang & Andrews	6	1995	CFD

Harris *et al.*	12	1996	CFD
Mier *et al.*	7	1999	Experimental and CFD

Table 2.2: Summary of Published work in Two-Phase Flow

Investigators	**Reference**	**Year**	**Technique Used**
Ranade & Akker	21	1994	Experimental and CFD
Ranade	22	1995	Experimental and CFD
Kuipers & Van Swaaij.	11	1997	Experimental and CFD
Al-Dahhan *et al.*	23	1999	CFD and DCM
Delnoij *et al.*	19	1999	CFD
Spicka *et al.*	5	1999	Experimental and CFD
Coleman	3	1999	CFD

Table 2.3: Summary of Published work in Flow through Packed Beds

Investigators	**Reference**	**Year**	**Technique Used**
Ergun	38	1952	Experimental
Stanek & Szekely	35	1974	Theoretical and Simulation
Szekely & Poveromo	33	1975	Experimental and Simulation
Lerou & Froment	26	1977	Experimental
Vortemeyer & Schuster	37	1983	Simulation
McGreavy *et al*	27	1983	Experimental

Delmas & Froment	24	1988	Experimental and Simulation
Bey & Eigenberger	28	1997	Experimental and Simulation
Jiang *et al*	20	2000	CFD and DCM

From the above extensive literature review, it can be concluded that the importance of uniform flow distribution had been recognized for a long time, but all the investigations were attempted for lab scale models and there is a scarcity of data for large industrial scale vessel as is considered in this investigation. From the literature review for two-phase flow. the two-fluid model seems to be the most promising model and the same has been used in this investigation. Also the $k-\varepsilon$ turbulence model is the most widely used for turbulence modeling and the same is incorporated in this investigation. Lastly the modified Ergun equation is the most popular equation for analyzing flow through packed beds and the same has been used in simulating the flow through packed beds.

2.6 Experimental Validation of Results

Experimental validation of CFD results is considered a prerequisite to pave the way for widespread acceptance of CFD in the chemical engineering community, especially in connection with multiphase flow applications[11]. The available experimental techniques can be classified according to the following aspects:

1.Type of quantity measured

2. Local or whole field measuring

3. Instantaneous or time-averaged quantities

4. Intrusive or non-intrusive method.

For the measurement of pressure, temperature, phase concentrations, composition and velocities in single and multiphase systems, a variety of experimental methods are available, ranging from the simple probe techniques to sophisticated whole-field measuring methods. Thermal anemometry, electrical sensing techniques, light scattering and optical methods, electromagnetic wave techniques and ultrasonic techniques have all been used to study complex fluid flows. Some commonly used techniques for CFD validation are:

- Laser Doppler Anemometry (LDA)
- Particle Image Velocimetry (PIV)
- Nuclear Magnetic Resonance Imaging (NMR)
- Laser Induced Fluorescence (LIF)
- Particle Tracking Method (CARPT)
- Tomographic Techniques

Significant progress has been made in recent years with respect to development of experimental techniques for both single and multiphase flow applications. Clearly, CFD has partly generated the driving force, which has led to the development of some of the above stated advanced techniques and will continue to do so in future.

2.7 Computer Codes for CFD simulations

It is necessary to translate the already described solution procedure into computer codes to generate useful simulations of engineering equipment. A CFD code needs to be designed to give appropriate importance to general applicability, ease of use and economy of computations.

Instead of expanding the capacities of the in-house research purpose code to carry out real life, complex engineering flow simulations, it might be more efficient to use a commercially available CFD code. A number of CFD codes are available commercially, each with its own particular set of features. Most of these codes however provide user-friendly facilities for modeling complex geometries and grid generation. The powerful post-processing facilities developed by professional programmers also aid the user in the interpretation of simulated results. It should be noted here that, although a variety of ready-to-use commercial codes are available, the experience and insight gained through the use of in-house codes may turn out to be very valuable.

Dombrowski *et al.*[39] have reviewed the various available CFD codes. PHOENICS, FLUENT, CFX and FIDAP are the major codes available presently. The first three codes use a finite volume approach and the fourth one uses finite elements. Almost all-modern CFD codes have a $k-\varepsilon$ model for describing the turbulence. Most of these codes also provide for more advanced models like algebraic stress models or Reynolds stress models. Provision for non-Newtonian flow modeling is one of the important features, which is most relevant to the chemical and process industries. Most of the codes can handle power law and Bingham models of non-Newtonian fluids. FIDAP provides more complex models like the Carreau model together with the power law. Multiphase flow modeling is another important area for the chemical and process industries, and only a few codes provide this facility. PHOENICS provides three types of multiphase flow modeling, including two interpenetrating continua, particle tracking and free surface flows.

An important feature of a CFD code from the point of view of a complex application is the ability to incorporate or extend the code via user-written modules because, no

matter how general the code is, it will be necessary to develop specific sub models to simulate specific reactors. Some codes provide the ability to incorporate user defined physical property models and also enable new numerical features to be included. PHOENICS was chosen to carry out the present study as it has been tried before to simulate one-and two-phase flow problems in complex geometries[40, 41].

Chapter 3

Mathematical Formulation

3.1 Introduction

Numerical Simulation of flow in a vessel, involves specifying the governing conservation equations using an appropriate turbulence model, specifying the proper boundary and initial conditions and then solving these equations.

Thus resolving the flow in a desired equipment includes formulation of governing transport equations, formulation of necessary constitutive and closure equations, formulation of appropriate boundary conditions, selection of numerical techniques to solve these governing equations, development or selection of a suitable computer code to implement these numerical techniques, validation of techniques and codes, and flow simulation strategies for the desired equipment. All of these aspects will be discussed in the following sections.

3.2 Mathematical Formulation of Single-Phase Flow

The choice of a co-ordinate system and the meshing technique chosen depends on the shape of the geometry. Most shapes can be represented by either Cartesian, or cylindrical polar co-ordinates. For more complex geometries what is called as Body-fitted co-ordinates can be used.

Single-phase flow is based on the conservation laws for mass, momentum and energy which can be expressed in Cartesian coordinates as[4] :

(1) Mass conservation (Continuity Equation):

$$\frac{\partial \varrho}{\partial t} + \nabla . \varrho \, v = 0 \tag{3-1}$$

(2) Momentum equation (Navier- Stokes equation)

$$\varrho \frac{Dv}{Dt} = -\nabla p + \mu \nabla^2 v + \varrho \, g \tag{3-2}$$

(3) Energy equation

$$\varrho \frac{D}{Dt}\left(\frac{1}{2}v^2\right) = -\left(v.\nabla p\right) - \left(v.\left[\nabla.\tau\right]\right) + \varrho\left(v.g\right) \tag{3-3}$$

The mass, momentum and energy conservation differential equations can also be written in the more general form, which is used by PHOENICS[42]:

$$\frac{\partial\left(R_i \varrho_i \varphi_i\right)}{\partial t} + \mathrm{div}\left(R_i \varrho_i v_i \varphi_i - R_i \Gamma_{\varphi_i} grad \varphi_i\right) = R_i S_{\varphi_i} \tag{3-4}$$

Transient Convection Diffusion Source

where

R_i volume fraction of phase *i*

φ_i any conserved property of phase *i*

v_i velocity vector of phase *i*

Γ_{φ_i} exchange coefficient of ϕ in phase *i*

S_{φ_i} source rate of φ_i per unit volume

Thus, the continuity equation for phase *i* becomes:

$$\frac{\partial(R_i \varrho_i)}{\partial t} + \mathrm{div}(R_i \varrho_i v_i) = R_i S_{\varphi_i} \tag{3-5}$$

where

ϱ_i is the density of phase *i*

and the conservation of momentum for variable φ_i becomes:

$$\mathrm{div}(R_i \varrho_i v_i \varphi_i - R_i \mu_{eff} grad \varphi_i) = R_i S_{\varphi_i} \tag{3-6}$$

where

μ_{eff} is the effective viscosity

For the single-phase model the term $i = 1$ and the equations are reduced to one phase only. Gravitational body forces are represented in PHOENICS by way of sources of momentum in the equations for each of the six velocity components (3 for each phase). Such sources are specified in a way that ensures the multiplication of the acceleration due to gravity by the mass of the phase in the velocity cell, which results in the source being set to the force acting on the velocity cell.

3.3 Modeling of Two-Phase Flow

Two-Phase flow in reactors is mostly turbulent. In some cases the liquid is assumed to be a continuum while the second phase, usually a gas, exists in the form of dispersed bubbles. In other cases the gas may be a continuum while the liquid exists in the form of dispersed droplets. Therefore it is necessary to select an approach for simulating turbulence and the effects of the dispersed phase on flow characteristics.

Two-phase flow can be resolved using one of the many available techniques. These include (i) one fluid approach, where one set of continuity and momentum equations is solved. In such a case one needs to assume a distribution of void fraction for a liquid continuum-dispersed bubbles case, (ii) two fluids approach where two sets of momentum and mass conservation equations are solved, one for each phase. This method gives generally more accurate results. However it requires additional information such as the interphase friction coefficient (Euler-Euler) and (iii) one set of equations is solved for one phase while the second phase is treated by a Langrangian technique (Euler-Lagrange). Another key issue in two-phase flow simulation is turbulence. A number of models are available to simulate turbulence effects. The $k-\varepsilon$ model is used in the present study with one selected case re-run using the Reynolds stress model. The modeling of turbulence is discussed in section 3.9.

The effects of heat transfer on two-phase flow can be accounted for by solving the energy equation. The effects of phase change (evaporation or condensation) can also be taken into account.

In this study the second option that is solving two sets of equation is used. The two sets of equations are coupled by the fact that the summation of liquid and gas volume fraction in each cell is always equal to one. The interphase friction also needs to be calculated. This depends on the size of the dispersed droplets or bubbles. The method of estimating the droplet/bubble diameter is explained in section 3.4.1.

The effects of heat transfer or chemical reactions in the present study are not included. The continuity and momentum equation formulation is the same as for one-phase except that the term i = 2 contrary to that for single-phase flow.

A general-purpose multiphase three-dimensional CFD package, PHOENICS is used for solving the equations. In modeling two-phase flow, a set of the full conservation equations for mass and momentum in primitive variables for steady flow (the Navier-Stokes and the continuity equations) are solved for each phase to determine the pressure and flow fields. The two sets are coupled by the fact that for each computational cell, the summation of the liquid and gas volume fractions is equal to one. A solution algorithm based on the SIMPLE algorithm given by Patankar[43] is used for discretization. For multiphase flows, additional coupling between two phases through interphase forces needs to be handled. IPSA[44] (Inter Phase Slip Algorithm) is one way of handling two-phase flow problem in the CFD package. IPSA can be used along with the SIMPLE algorithm to treat pressure-velocity coupling. In most of the two-phase flow cases, therefore, the transparency and ease of implementation often dictate the choice of algorithm for pressure velocity coupling.

The interphase friction between the liquid and gas phases is calculated based on the assumption that the flow consists of a gas continuum with the liquid phase represented by droplets. The droplet size has a significant effect on the value of interphase friction. This is calculated using empirical correlations as in Section 3.4.2.

The real difficulty in the calculation of the velocity field lies in the unknown pressure field. The pressure gradient forms a part of the source term for a momentum equation. Yet, there is no obvious equation for obtaining the pressure. The pressure field is indirectly specified via the continuity equation. When the correct pressure field is substituted in the momentum equations, the resulting velocity field satisfies the continuity equation. This indirect specification, however, is not very useful, unless a direct solution

of the whole set of discretization equations resulting from momentum and continuity equations is attempted. Since iterative methods of solving the discretization equations even for a single dependent variable are preferred, the direct solution for the entire set of velocity components seems out of question. The alternative of vorticity based methods is also ruled out as it cannot be extended to three-dimensional situations, for which a stream function does not exist. Also the pressure, which is eliminated, happens to be an important desired result.

Patankar[43] has suggested the use of a staggered grid where a different grid is employed for each dependent variable. He has suggested pressure and velocity corrections to be :

$$p = p^* + p'$$

where p is the corrected pressure, p^* is the guessed pressure, p' is the pressure correction. Also the velocity components v_x, v_y, v_z can be represented by:

$$v_x = v_x^* + v_x' \qquad v_y = v_y^* + v_y' \qquad v_z = v_z^* + v_z'$$

where $v_x^*, v_y^* v_z^*$ are the imperfect velocity fields based on the guessed pressure p^*. The above expressions form the basis of the SIMPLE algorithm, which is most widely used for numerical simulation purposes. SIMPLE, stands for *S*emi-*I*mplicit *M*ethod for *P*ressure *L*inked *E*quations. Its sequence of operation can be stated in the following points:

1. Guess the pressure field p^*.
2. Solve the momentum equations to obtain $v_x^*, v_y^* v_z^*$.
3. Solve the p' equation.

4. Calculate p by adding p' to p^*.
5. Calculate v_x, v_y, v_z from their starred values using the velocity correction formulas.
6. Solve the discretization equations for other $\phi's$ (such as temperature, concentration, and turbulence quantities) if they influence the flow field through fluid properties, source terms, etc.
7. Treat the corrected pressure p as a new guessed pressure p^*, return to step 2, and repeat the whole procedure until a converged solution is obtained.

PHOENICS uses an in built SIMPLE-based algorithm for solving the discretized equations. Results include plots of the full velocity fields and the liquid and gas volume fraction for each model that shows clearly the effects of parameters under investigation including geometry, boundary conditions, physical properties and flow rates.

The following section present a detailed procedure of the calculation of the interphase friction and the mean droplet diameter, which are essential for modeling two-phase flow.

3.4 Calculation of Interphase Friction

Interphase friction plays an important role in determining the transport of momentum between the phases. For the conditions under consideration, the flow is represented by droplets of a specific (or a range of) diameter(s) entrained in a gas continuum. The interphase-transport coefficient is estimated based on these conditions. To do that first the size of the drops entrained in the gas stream is estimated. There are many expressions in the literature for the maximum diameter, mean diameter, most probable diameter etc. An area averaged value of the droplet diameter and not the maximum value is required.

Following the estimation of average droplet diameter a value of the interphase transport coefficient (CFIPS) is then fed into the CFD package.

3.4.1 Calculations of Droplet Mean Diameter

The use of high gas velocities and perforated plates having relatively large free areas leads to the spray regime operation The behavior of droplets in the spray regime differs from the more commonly used froth regime in industrial operations. The spray regime on a perforated plate (distributing plate) corresponds to the jetting regime appearing at a single orifice. Hence, the mechanism of droplet formation in the spray and jetting regimes must be similar, whereas few investigations on droplet size in the jetting regime have been reported. The mean droplet diameter can be calculated using either a correlation for falling droplets or another correlation for annular dispersed flow, both given by Kataoka and Ishii[45]. Miyahara and Takahashi[46] have studied two-phase flows (air- water system) over a specific range of densities, surface tensions and viscosities.

In this investigation the correlations of Miyahara and Takahashi[46] are used. The mean diameter of droplets is first calculated for the present system using empirical correlations given by Miyahara and Takahashi[46].

For steady jetting:

$$Bo^* = 0.58 We^{-0.067} \qquad 1.5 \times 10^4 < We < 1.5 \times 10^5 \qquad (3\text{-}7)$$

$$Bo^* = 0.42 \qquad 3.0 \times 10^3 < We < 3.5 \times 10^5 \qquad (3\text{-}8)$$

where

$$\mathrm{Bo}^* = \left(\varrho_l g d^2/\sigma\right)^{\frac{1}{2}} \qquad \textit{Bond number} \qquad (3\text{-}9)$$

$$\mathrm{We} = \left(\varrho_l v^2 d/\sigma\right) \qquad \textit{Weber number} \qquad (3\text{-}10)$$

where v is the fluid velocity, g is the acceleration due to gravity, d is the diameter of the droplet and σ is the surface tension.

The above correlations give an approximate mean droplet diameter. In this investigation, the liquid density chosen is 600 kg/m^3 which is a typical value for hydrocarbons, As most organic liquids have surface tension (σ) values between 0.02 and 0.03 kg/sec^2, some mid-range values can be selected to arrive at a suitable droplet diameter.

Calculations can be also performed using correlations by Ganic and Rohsenow[47], Wallis[17] and the equation of Nukiyama-Tanasawa given by Wallis[17].

3.4.2 Calculation of the Interphase Friction Coefficient

The interphase transport coefficient (CFIPS) can be calculated by the following correlations:

The drag force exerted on a droplet is given by Miyahara and Takahashi[46]:

$$F_D = -0.5 C_D \varrho_g v_r |v_r| A_d \tag{3-11}$$

where

$$C_D = 10.67 / Re^{0.5} \tag{3-12}$$

and

$$Re = \varrho_g v_r d / \mu_g \tag{3-13}$$

and the interphase transport coefficient (CFIPS) can be estimated by:

$$CFIPS = 3 \varrho_g C_D v_s / 4d \tag{3-14}$$

3.5 Initial and Boundary Conditions

In setting up a flow-simulating computation it is crucial to correctly specify the proper initial and boundary conditions. In particular, it involves the specification of convective and diffusive fluxes at surfaces bounding the domain. In this study the inlet condition corresponds to the flow conditions. In PHOENICS defining an inlet condition means specifying the cells through which the fluid is introduced, the velocities (x-,y- and z-direction), and the pressure of the phases (mass flux- specification).

An outlet condition refers to the physical conditions at flow exit. Specification involves the location of cells, which are desirable to be kept open, and the exit pressure. In this study, we specify these conditions at the distributing plate of the vessel by specifying those cells that are to remain open or closed.

Wall conditions are also required to be specified for a complete description of the boundary conditions. For this study a general no-slip condition is imposed on all solid walls. A similar condition is required for any solid boundary within the computational domain including any baffles or inserts that may be present.

3.6 Mathematical Formulation for Packed bed flow

The modeling of the fluid flow in packed beds is based on the continuity equation and the momentum balances in the two direction (i.e. y and z) in the Cartesian coordinate system. The steady state continuity equation is

$$0 = \nabla.(\theta \varrho \mathbf{v}) \tag{3-15}$$

where the void fraction θ and the velocity $\mathbf{v}$ are assumed to be continuously varying functions.

In Cartesian coordinates, with v_y and v_z as dependent variables, the continuity equations can be written as

$$0=\frac{\partial(\theta \varrho\, v_y)}{\partial y}+\frac{\partial(\theta \varrho\, v_z)}{\partial z} \tag{3-16}$$

The stationary momentum balances are formulated according to Bey and Eigenberger[28].

$$-[\nabla.\theta \varrho_f \mathbf{vv}]-\nabla\theta\, p-[\nabla\theta\tau]-\sum \mathbf{f}_f-\theta\varrho\, g=0 \tag{3-17}$$

The terms $\sum \mathbf{f}_f$ are local volume averaged forces between the packing and the fluid. These forces are formed by the pressure force ($\mathbf{f}_p$) and the force generated by the fluid moving through the pellet interstices ($\mathbf{f}$).

$$\sum \mathbf{f}_f = \mathbf{f}_p + \mathbf{f} \tag{3-18}$$

A pressure force results, if a voidage change occurs. For the one-dimensional case

$$F_{z,p}=-A\,p(\theta_{z+\Delta z}-\theta_z) \tag{3-19}$$

Division of equation (3.19) by the volume and for $\Delta z \rightarrow 0$

$$f_{z,p}=-p\frac{\partial\theta}{\delta z} \tag{3-20}$$

The multi-dimensional analog is

$$\mathbf{f}_p=-p\nabla\theta \tag{3-21}$$

Equation (3.21) inserted in to equations (3.16) and (3.17) gives

$$-[\nabla.\theta \varrho_f \mathbf{vv}]-\theta\nabla p-[\nabla.\theta\tau]-\mathbf{f}-\theta\varrho\, g=0 \tag{3-22}$$

In Cartesian coordinate system the definition of the del operator is:

$$\nabla = \hat{i}\frac{\partial}{\partial x} + \hat{j}\frac{\partial}{\partial y} + \hat{k}\frac{\partial}{\partial z} \tag{3-23}$$

$$\mathbf{vv} = \left(v_x\hat{i} + v_y\hat{j} + v_z\hat{k}\right)\left(v_x\hat{i} + v_y\hat{j} + v_z\hat{k}\right) \tag{3-24}$$

$$\begin{aligned}\mathbf{vv} = &\left(v_x{}^2\hat{i}.\hat{i} + v_x v_y\,\hat{i}.\hat{j} + v_x v_z\hat{i}.\hat{k}\right)\\ &+\left(v_y v_x\,\hat{j}.\hat{i} + v_y{}^2\hat{j}.\hat{j} + v_y v_z\hat{j}.\hat{k}\right)\\ &+\left(v_z v_x\,\hat{k}.\hat{i} + v_z v_y\,\hat{k}.\hat{j} + v_z{}^2\,\hat{k}.\hat{k}\right)\end{aligned} \tag{3-25}$$

Thus $\nabla.(\theta \varrho_f \mathbf{v}\,\mathbf{v})$ can be written as:

$$\begin{aligned}\nabla.(\theta \varrho_f \mathbf{v}\,\mathbf{v}) = &\frac{\partial\left(\theta \varrho_f v_x{}^2\hat{i} + \theta \varrho_f v_x v_y\hat{j} + \theta \varrho_f v_x v_z\hat{k}\right)}{\partial x}\\ &+\frac{\partial\left(\theta\, v_y v_x\,\hat{i} + \theta \varrho_f v_y{}^2\hat{j} + \theta \varrho_f v_y v_z\hat{k}\right)}{\partial y}\\ &+\frac{\partial\left(\theta\, v_z v_x\,\hat{i} + \theta \varrho_f v_z v_y\hat{j} + \theta \varrho_f v_z{}^2\hat{k}\right)}{\partial y}\end{aligned} \tag{3-26}$$

Cancellation of all the terms with v_x leads to:

$$\nabla.(\theta \varrho_f \mathbf{v}.\mathbf{v}) = \frac{\partial\left(\theta \varrho_f v_y{}^2\hat{j} + \theta \varrho_f v_y v_z\hat{k}\right)}{\partial y} + \frac{\partial\left(\theta \varrho_f v_z v_y\,\hat{j} + \theta \varrho_f v_z{}^2\hat{k}\right)}{\partial z} \tag{3-27}$$

Also:

$$\nabla p = \frac{\partial p}{\partial x}\hat{i} + \frac{\partial p}{\partial y}\hat{j} + \frac{\partial p}{\partial z}\hat{k} \tag{3-28}$$

$$\nabla.\theta\tau = \theta\begin{pmatrix}\tau_{xx}\hat{i}.\hat{i} + \tau_{xy}\hat{i}.\hat{j} + \tau_{xz}\hat{i}.\hat{k}\\ +\tau_{yx}\hat{j}.\hat{i} + \tau_{yy}\hat{j}.\hat{j} + \tau_{yz}\,j.\hat{k}\\ +\tau_{zx}\hat{k}.\hat{i} + \tau_{zy}\hat{k}.\hat{j} + \tau_{zz}\hat{k}.\hat{k}\end{pmatrix} \tag{3-29}$$

Cancellation of terms with x component yields:

$$\nabla.\theta\tau = \frac{\partial}{\partial y}\left(\theta\tau_{yy}\hat{j} + \theta\tau_{yz}\hat{k}\right) + \frac{\partial}{\partial z}\left(\theta\tau_{zy}\hat{j} + \theta\tau_{zz}\hat{k}\right) \tag{3-30}$$

The various shear stresses in terms of velocity gradients and fluid properties for Newtonian fluids is given by Bird *et al.*[4] as follows:

$$\tau_{yy} = -\mu\left[2\frac{\partial v_y}{\partial y}\right] \tag{3-31}$$

$$\tau_{yz} = -\mu\left[\frac{\partial v_y}{\partial z} + \frac{\partial v_z}{\partial y}\right] \tag{3-32}$$

$$\tau_{zy} = -\mu\left[\frac{\partial v_y}{\partial z} + \frac{\partial v_z}{\partial y}\right] \tag{3-33}$$

$$\tau_{zz} = -\mu\left[2\frac{\partial v_z}{\partial z}\right] \tag{3-34}$$

Collecting all the terms for the ***z* component**:

$$0 = -\frac{\partial}{\partial z}\left\{\left(\theta\,\varrho_f\,v_y\,v_z\right) - \theta\,\mu\left(\frac{\partial v_z}{\partial y} + \frac{\partial v_y}{\partial z}\right)\right\} - \theta\,\frac{\partial p}{\partial z} - \frac{\partial}{\partial z}\left[\theta\,\varrho_f\,v_z^{\,2} - 2\theta\,\mu\,\frac{\partial v_z}{\partial z}\right] - F_z \tag{3-35}$$

Collecting all the terms for the ***y* component**:

$$0 = -\frac{\partial}{\partial y}\left\{\left(\theta\,\varrho_f\,v_y^{\,2}\right) - \frac{\partial}{\partial z}\left(\theta\varrho_{\ f}\,v_y\,v_z\right)\right\} - \theta\,\frac{\partial p}{\partial y} + \frac{\partial}{\partial y}\left[2\theta\mu\ \frac{\partial v_y}{\partial y}\right] + \frac{\partial}{\partial z}\left(\theta\,\mu\left(\frac{\partial v_y}{\partial z} + \frac{\partial v_z}{\partial y}\right)\right) - F_y \tag{3-36}$$

3.7 Pressure Drop correlations for Packed Bed

Ergun[38] in his classic paper has given an expression for pressure losses in packed beds which is caused by simultaneous kinetic and viscous energy losses, and derived the following comprehensive equation applicable to all types of flow.

$$\frac{\Delta P}{L} g_c = 150 \frac{(1-\theta)^2}{\theta^3} \frac{\mu v_m}{d_p^2} + 1.75 \frac{1-\theta}{\theta^3} \frac{G v_m}{d_p} \qquad (3\text{-}37)$$

$$d_p = \frac{6}{S_v} \qquad (3\text{-}38)$$

where:

$\frac{\Delta P}{L}$ is the pressure drop per unit length of the packed bed.

g_c is the gravitational constant

θ is the fractional void volume in the packed bed

μ is the absolute viscosity of the fluid

v_m is the superficial velocity measured at average pressure

d_p is effective diameter of particle

G is the mass flowrate of the fluid = $\varrho\ v_m$

S_v is the specific surface (surface of solids per unit volume of solids).

Brinkman[48] was the first to formulate the differential equation which describes the artificial flow profile within a porous medium bounded by a rigid wall restricting himself to the Darcy flow regime and extending Darcy's law by a viscosity term. Vortemeyer and Schuster[37] have used the extended Brinkman's equation for their formulation for higher

flow rates by incorporating the Ergun pressure loss relation given above. They obtained the pressure loss term as:

$$\frac{\partial p}{\partial z} = -f_1 v - f_2 v^2 + \mu \frac{\partial^2 v}{\partial x^2} \tag{3-39}$$

for flow within a rectangular duct: The factors f_1 and f_2 have the form,

$$f_1 = 175 \varrho \frac{(1-\theta)}{\theta^3 d_p} \tag{3-40}$$

$$f_2 = 1.75 \varrho \frac{(1-\theta)}{\theta^3 d_p} \tag{3-41}$$

where v is the flow velocity and the other terms have the same meaning as stated earlier. Bey and Eigenberger[28] have represented the pressure drop in the packing by modifying the Ergun equation for a cylindrical coordinated system. In the Cartesian coordinate system the pressure forces can be calculated by the following equations:

$$F_z = 150 \mu_f \frac{(1-\theta)^2}{\theta^3 d_p^2} v_{z,o} + 1.75 \varrho_f \frac{(1-\theta)}{\theta^3 d_p} v_{z,o} |v_o| \tag{3-42}$$

where

$$v_z = \frac{v_{z,o}}{\theta} \tag{3-43}$$

$$F_y = 150 \mu_f \frac{(1-\theta)^2}{\theta^3 d_p^2} v_{y,o} + 1.75 \varrho_f \frac{(1-\theta)}{\theta^3 d_p} v_{y,o} |v_o| \tag{3-44}$$

where

$$v_y = \frac{v_{y,o}}{\theta} \tag{3-45}$$

where

F_z is the pressure force in the y direction

F_y is the pressure force in the z direction

μ_f dynamic viscosity (kg/ms)

θ void fraction

ϱ_f fluid density (kg/m^3)

v_z interstitial velocity in the z direction (m/s)

v_y interstitial velocity in the y direction (m/s)

v_o average empty tube flow velocity ($=\sqrt{v^2_{z,o} + v^2_{y,o}}$)

$v_{z,o}$ average empty tube flow velocity in z direction (m/s)

$v_{y,o}$ average empty tube flow velocity in y direction (m/s)

The F_z and F_y obtained from equations (3.42 - 3.44) can be substituted in the momentum balance equations (3.35 - 3.36) respectively and solved. In the present equations the modified form of Ergun equation given by Bey and Eigenberger[28] as given from equations (3.42 - 3.45), have been used for calculating the pressure drop in the z- and y- directions

3.8 Modeling of Turbulence

Turbulence is a three-dimensional, time-dependent, nonlinear phenomenon. The instantaneous velocity field in a turbulent flow is described by Navier-Stokes equations. However, because of the existence of an extremely wide range of space and time scales in

turbulent flows, the exact numerical simulation of turbulent flows is possible only at relatively low Reynolds number if the geometry is simple. For most engineering applications, it is still necessary to use turbulence models along with time-averaged Navier-Stokes equations. It must be realized that most of the available turbulence models obscure the actual physical processes like eddies, high vorticity regions, large structures which stretch and engulf, and so on. However, the cautious application and interpretation of turbulence models have proved to be valuable tools in engineering research and design, despite their physical deficiencies.

A turbulence model is a set of equations that express relations between unknown terms appearing in averaged Navier-Stokes equations with known quantities. The starting point of most of these models is the formulation of an expression for the Reynolds stress terms. A large class of models of the Reynolds stresses normally uses an eddy viscosity hypothesis.

The turbulence models most often applied can be summarized as follows[11]:

- Constant eddy viscosity model
- Prandtl's mixing length model
- Prandtl-Kolmogorov model
- $k-\varepsilon$ model
- Renormalization group (RNG)
- Algebraic stress model (ASM)
- Reynolds stress model (RSM)
- Large eddy simulation (LES)

All models mentioned above require some form of empirical input, which imply that they are not generally applicable to any type of turbulent flow problem. However, the most complex models such as ASM and RSM offer the greatest predictive power. Many of the older turbulence models are based on Boussinesq's eddy viscosity, which assumes that in analogy with the viscous stresses in laminar flows, the Reynolds stresses are proportional to the gradients of the time-averaged velocity. Within the framework of the models, which use the eddy viscosity concept, the task of the turbulence model is the description by means of algebraic or differential equations of the turbulent viscosity. The constant eddy viscosity model and Prandtl's mixing length model belong to the class of zero-equation models since no transport equations are involved for the turbulence quantities. These two models are not suitable when convective or diffusive transport processes of turbulence are important. The Prandtl-Kolmogorov model belongs to the class of single equation models because one conservation equation for the turbulent kinetic energy k is solved. The weak point of this model is the specification of the characteristic length L: especially for complex flows, it is difficult to specify the length scale (distribution) and therefore two-equation models have become more popular. Here an additional transport equation is invoked to obtain the length scale (distribution) L. In the $k-\varepsilon$ model two transport equations are solved for, k, the kinetic energy of turbulence and its dissipation rate, ε.

Renormalisation group (RNG) theory based models of turbulence have been developed by Orszag *et al.*[49]. In RNG based $k-\varepsilon$ models, the value of model parameters are evaluated by the theory. Moreover, modifications of a standard $k-\varepsilon$ model such as low Reynolds number modification, extra term of rate of strain, etc., are given by the

RNG theory. These models have not yet been sufficiently tested for the engineering flow simulations; however, initial results of these models are promising.

Computational experience has revealed that the two-equation models, employing transport equations for the velocity and length scales of the fluctuating motion, often offer the best compromise between width of application and computational economy.

There are however certain type of flows where the $k-\varepsilon$ model fails, such as complex swirling flows and in such simulations more advanced turbulence models (ASM or RSM) are required which do not involve the eddy viscosity concept. According to the Algebraic stress model (ASM) and the Reynolds stress model (RSM), the six components of the Reynolds stress tensor are respectively obtained from a complete set of algebraic equations and a complete set of transport equations. These models are conceptually superior with respect to the older turbulence models such as the $k-\varepsilon$ models but computationally they are much more involved and consequently much more expensive.

Due to the advances in computer technology and numerical solution procedures two powerful simulation types of turbulent flows have recently received particular attention, namely Direct Numerical Simulation (DNS) and Large Eddy Simulation (LES)[11] . As stated earlier, turbulent flows are also governed by the Navier-Stokes equations and in principle the solution of these equations with a sufficiently high temporal and spatial resolution should provide all the details of the turbulent flow without the necessity of turbulence modeling. Due to the fact that turbulent motion contains element with a linear dimension which is typically a factor 10^{-3} smaller than the linear dimensions of the macroscopic flow domain, a DNS simulation in three dimension requires 10^{9} grid points which is still difficult from the storage capacity point of view of present day computers. It

should be however noted that the ratio of the dimension of the macroscopic system and the dimension of the smallest eddies present in the turbulent flow depend on the Reynolds number: the smaller the Reynolds number the smaller is this ratio.

In Large Eddy Simulation (LES) the spatial resolution of the computational mesh is deliberately chosen in such a manner that only the large-scale turbulent motion (eddies) is resolved. The consequence of this approach is the necessity to use sub-grid models, which in fact model the turbulent stresses on a scale smaller than the computational grid. Due to the fact that the small-scale turbulence is isotropic, the specification of sub-grid models is far less difficult than the aforementioned closure models for the Reynolds stresses. The advantage of LES in comparison with DNS is the possibility it offers to study (with a given number of grid points or control volumes) turbulent flows at significantly higher Reynolds numbers.

In conclusion, the two equation turbulence models are the simplest ones that promise success for flows in which length scales cannot be prescribed empirically. The $k-\varepsilon$ model is the most widely tested model for a variety of complex flows. Many modifications such as multiple scale $k-\varepsilon$ models or extra terms to compensate for shortcomings of the standard $k-\varepsilon$ model have been developed. At present these two equation models form the basis for most of the engineering simulations of complex flows. More advanced models, such as (ASM and RSM) which do not use the assumption of isotropic turbulent viscosity or the concept of turbulent viscosity itself are available but will increase the computational requirements significantly.

Based on the above discussion, the governing equations in this investigation are formulated using a standard $k-\varepsilon$ model. The $k-\varepsilon$ model is described below in detail.

One case was also run with RSM for comparison purposes.

3.8.1 The $k-\varepsilon$ Turbulence Model

The most common approach to determining the kinetic energy of turbulence k and its dissipation rate ε, is to solve transport equations for these quantities in parallel with the solution of the mean momentum equations. In symbolic forms the equations may be written as[2]:

$$\frac{Dk}{Dt}=d_k+P_k+G_k-\varepsilon \tag{3-46}$$

$$\frac{D\varepsilon}{Dt}=d_e+c_{\varepsilon 1}+\frac{\varepsilon}{k}(P_k+G_k)-c_{\varepsilon 2}\frac{\varepsilon^2}{k}+S_e \tag{3-47}$$

where d_e, d_k, P_k and G_k denote the rate of gain of k at a point by diffusion and generation by mean strain and body forces, and $c_{\varepsilon 1}$, $c_{\varepsilon 2}$ are the coefficients having standard values (primary source/sink terms). In most cases the secondary source/sink term S_e has been taken as zero. Habitually, diffusive transport is represented by the simple gradient form:

$$d_\varphi=\frac{\partial}{\partial x_j}\left(\frac{v_t}{\sigma_\varphi}\frac{\partial \varphi}{\partial x_j}\right) \tag{3-48}$$

where φ stands for k or ε and the σ_φ are the constants of order unity. While the k equation may be regarded as exact, the ε transport equation rests on nothing more than dimensional analogy (with the k equation). Standard values for the coefficients of the primary source and sink terms are $c_{\varepsilon 1}$ = 1.44 and $c_{\varepsilon 2}$= 1.92.

The effects of turbulence on mean flow behavior is solved. The k-ε model relates the turbulent stresses $\overline{v_i v_j}$ and the average velocity gradient *du/dx* by a simple relationship:

$$\overline{v_i v_j} = \varepsilon \frac{\partial v_i}{\partial x_i} + \frac{\partial v_i}{\partial x_i} - \frac{2}{3} k \delta_{ij} \tag{3-49}$$

where δ_{ij} is the Kronecker delta and k is the turbulent kinetic energy.

By assuming isotropic turbulence, two dependent variables can be defined. The first is turbulent kinetic energy, k :

$$k = \frac{1}{2} \overline{v_i v_j} \tag{3-50}$$

and the second is the viscous rate of turbulent energy, ε :

$$\varepsilon = v \overline{v_{ij} v_{ij}} \tag{3-51}$$

The transport equations of these two variables follow the same form as other dependant variables as explained above. The turbulent viscosity μ_t is written as:

$$\mu_t = \rho C_\mu \frac{k^2}{\varepsilon} \tag{3-52}$$

where

C_μ is the parameter of the $k-\varepsilon$ model and

3.8.2 The Reynolds Stress Turbulence Model (RSM)

The $k-\varepsilon$ turbulence model is based on the isotropic eddy-viscosity concept for closure of the Reynolds stresses. In some situations, such as when body forces or complex strain fields are present, this assumption is too simple. The RSMs[50] allow not only for both the transport and different development of the individual Reynolds stresses, they also have the advantage that terms accounting for anisotropic effects are introduced automatically in the stress transport equations. These non-isotropic characteristics of the

turbulence play a very important role in flows with significant buoyancy, streamline curvature, swirl, or strong recirculation.

A full RSM consists, in general of 6 transport equations for the Reynolds stresses, 3 transport equations for the turbulent fluxes of each scalar property and one transport equation for the dissipation rate of turbulence energy. The solution of all these equations together with those of the mean flow is computationally expensive. In addition there is a considerable numerical disadvantage arising from the use of the RSM in that the stabilizing effects of an eddy-viscosity field are absent in the mean flow equations.

Thus, although RSM can provide a more realistic and rigorous approach for complex engineering flows, they may be too expensive in terms of storage and execution time for three-dimensional flows. In this investigation, RSM will be applied for analyzing the effect on flow distribution and to check whether the results differ significantly from those obtained using the $k-\varepsilon$ model.

Chapter 4

Results of Single-Phase Flow in Unpacked Vessel

4.1 Single-Phase Flow

The domain or the geometry of interest in this work is a three-dimensional industrial sulfur converter wherein the flow distribution is analyzed for a single-phase flow in an unpacked vessel. In this investigation only a two-dimensional model is built and simulated. A full three-dimensional model requires very high computational power, which is not possible for the present investigation, thus only a two-dimensional model is simulated.

4.1.1 Vessel Geometry and Operating Conditions

The sulfur converter is a horizontal cylinder 4.9 m in diameter and 18.2 m long. A gas stream is injected into the bottom of the vessel through three inlets each of 0.6-m diameter. The vessel has a single 1.0 m diameter outlet as shown schematically in Figure 4.1.

A two-dimensional model is constructed of this vessel. A mesh of 182 cells in the y-direction and 49 cells in the z-direction is chosen. This implies a uniform grid of 10 cm a side (Figure 4.2). In the y-direction, the inlets are located between cells 21-26, 89-94 and cells 157-162. The outlet is located at z = 4.9 m and in the y-direction has cells 50-59 open as shown in Figure 4.1.

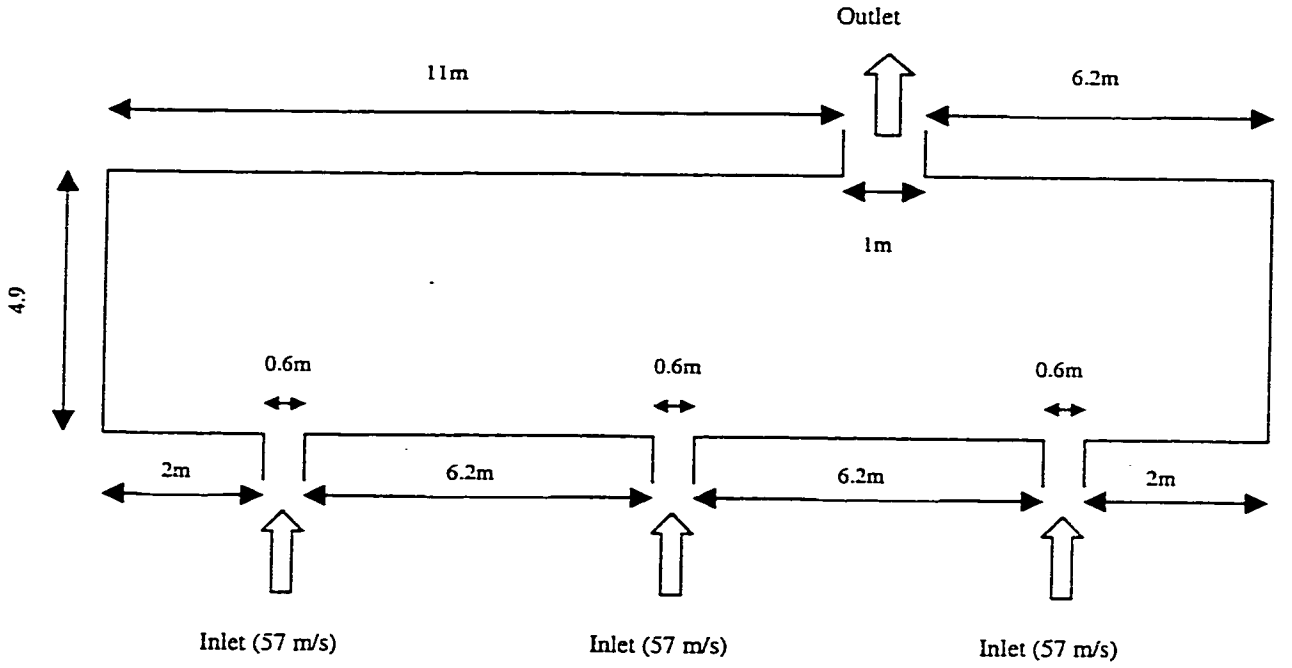

Figure 4. 1. Schematic of the Vessel

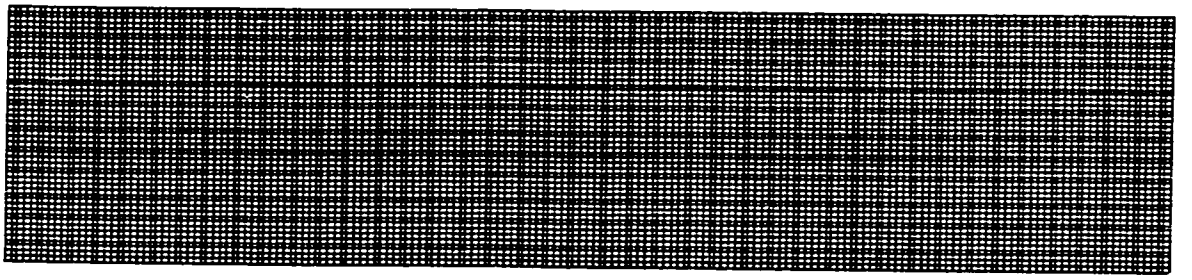

Figure 4.2. Vessel Grid (182 x 49 cells)

The feed gas is a mixture consisting mainly of CO_2, H_2S, SO_2 and H_2O with trace concentrations of other components such as methane and hydrogen. The density of the inlet gas is 1.36 kg/m^3 and its kinematic viscosity is 2.18×10^{-5} m^2/s or a dynamic viscosity of 2.96×10^{-5} Pa.s.

The gas is injected into the converter at a velocity of 57 m/s. The effects of chemical reactions and heat transfer are not included and only the flow and the pressure fields are resolved.

4.1.2 Simulation Results of Single Phase Flow

In this study one-phase flow is investigated using CFD simulations. The effects of various factors on the flow fields are investigated. These factors include the vessel geometry, inlet and outlet boundary conditions, fluid flowrates and turbulence model.

The simulation was done for a two-dimensional situation using the standard $k-\varepsilon$ model. The inlet velocity was 57 m/s at each of the three inlets. The model was run until a final converged solution was obtained by comparing the mass balances from the result file generated during the simulation. The model gives the two-dimensional plots for the velocity vectors, velocity contours, turbulence characteristics and pressure drop in the vessel.

Figure 4.3 (a) illustrates the velocity field for flow in the unpacked vessel. The results indicate that the jets hit the opposite wall of the converter with a high velocity and subsequently move towards the outlet. Despite a high injection velocity of 57 m/s, there are many zones inside the converter where the velocities are very small. These zones are referred to as zones with low velocities and sometimes as 'dead' zones. These zones are

more pronounced in the regions between two adjacent jets and are more prominent in the lower half of the vessel and near the vessel center. In the upper half, there is a good flow distribution, which is due to the jets striking the upper walls and heading towards the outlet. As discussed earlier the jet angle plays a major indication of the degree of flow distribution. The jet angle of expansion in this case is about 10° which fits well within the experimental values[15]. The flow shows a low velocity zone between two adjacent jets. The ultimate objective is to reduce the size of such zones and to increase the velocity in these zones. In the packed bed, such dead zones which are a result of flow distribution problems could lead to over-utilization of catalyst in one zone of flow domain and consequently under-utilization of the catalyst in certain zones leading to inefficiencies in the process.

Figures 4.3 (b) and Figure 4.3 (c) illustrates the contours of the velocity in the y- and z-directions respectively. These velocities are referred to as V1 and W1 in all the following numerical results. When the flow is mainly unidirectional, these contour plots of V1 and W1 could be very useful.

Figure 4.4 (a) illustrates a plot of the V1 velocity in the vessel at a distance of 2.5 m from the vessel bottom, or at a slab where z corresponds to the 25^{th} row of cells, and Figure 4.4 (b) is a similar plot of the z-directed velocity. These values have been monitored at a z = 25 in the flow direction which corresponds to the central slab which is seen to be the area of largest low velocity or the dead zones. Figures 4.4 (a. b) are reflections of the colored plots, i.e, the first jet on the colored plots refers to the first jet on the right, whereas on Figures 4.4 (a, b), this first jet is depicted as the first jet from the left of the Figure. The three peaks in Figure 4.4 (b) represent the three incoming jets. The zones of low velocity can be seen in the plots as a major part of the area between two

consecutive jets. One way to quantify the extent of dead zoning or low velocity zones from these plots is by drawing two horizontal lines on these plots at +5 m/s and -5 m/s. The extent of low velocity zones can then be found by accurately examining the number of cells that lie in this region. This is reflected in Figure 4.4b, which when closely examined shows that the number of cells contained within the + 5 m/s and - 5 m/s lines between the second and third jet is significantly higher than that between the first two jets.. The variation in case of Figure 4.4 (a) (V1 velocities) shows that the velocities in most of the cells lie in the +5 to - 5 m/s range.

A comparison of the vectors as well as contour plots with those of the Figures 4.3a and 4.3 (b) indicates that there is significant recirculation in between the jets and near the vertical wall, whereas near the bottom corners there is substantial dead zoning. Also evident from Figures 4.3 (a) and 4.3 (b) is the fact that in between the first two jets, the low velocity zones are small compared to those between the second and the third jet. It can be seen from Figure 4.4 (b), that in between the first two jets there are 7 cells, whereas in between the second and third jet, there are 11 cells. The more the number of cells, the wider the low velocity zones.

4.1.3 Effects of the fluid flowrate

Increasing the flow rate may be useful in increasing the circulation and in reducing the sizes of the dead zones. It is expected that increasing the velocity should lead to variations in the flow profiles inside the vessel. This increase may not be always practically possible due to limits on compressors or other equipment. However, it may useful to investigate the effects of varying the injection velocity. Figures 4.5 (a, b, c) illustrates a comparison of the flow fields for cases with injection velocities of 45, 57 and 70 m/s receptively. The

(a)

(b)

(c)

Figure 4.3 (a) Velocity Field for 57 m/s, (b) Contours of the velocity in the z- direction (W1) and (c) Contours of the velocity in the y-direction (V1)

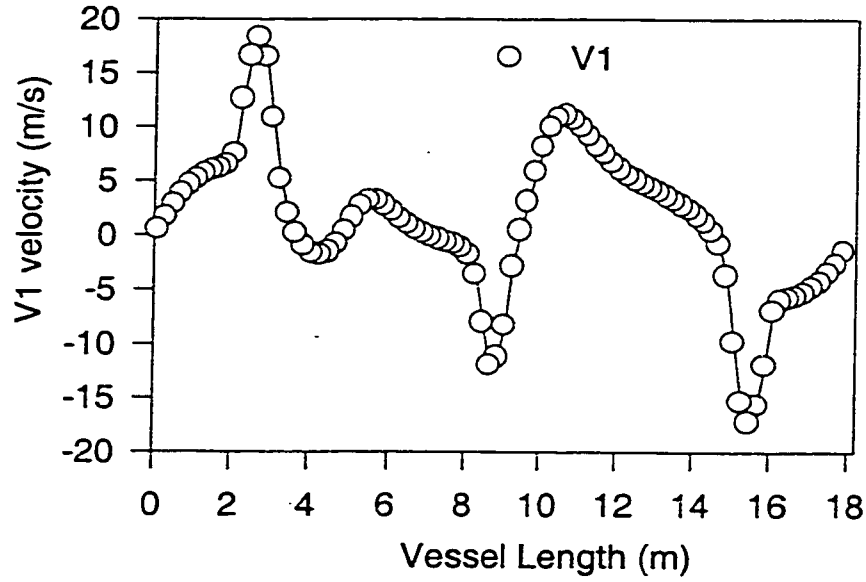

(a)

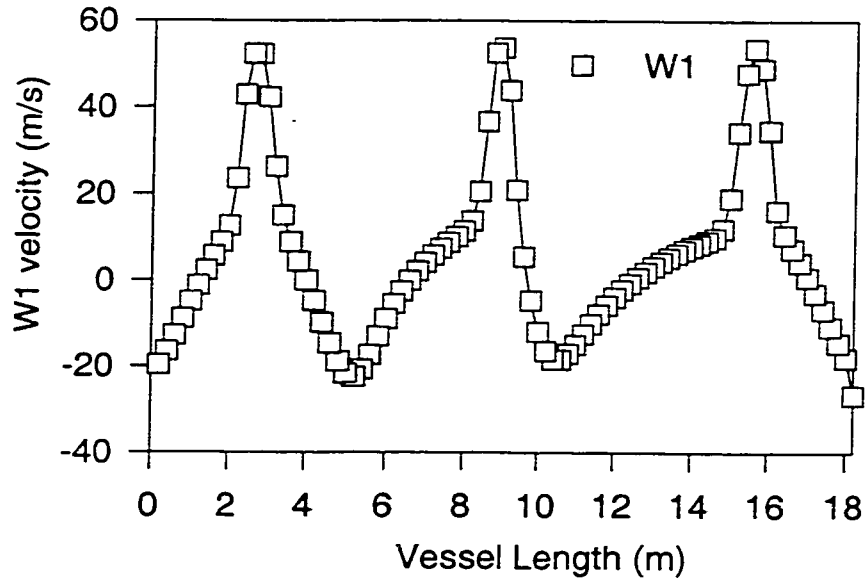

(b)

Figure 4.4. A plot of the (a) V1 velocity across the vessel at slab 25, and (b) W1 velocity across the vessel length at slab 25

injection velocity was increased keeping the length of the inlets constant. Results show no appreciable improvement in the flow distribution as the injection velocity is increased by 55.6%, i.e., from 45 m/s to 57 and 70 m/s. Figure 4.6 (a, b) illustrates this comparison of V1 and W1 respectively for slab 25 (corresponding to the 25^{th} row of cells) for the three cases. A horizontal line drawn between + 5 m/s and –5 m/s range shows that although the low velocity zones is smaller in case of the higher velocity (70 m/s), it cannot be taken as an appreciable improvement in the flow distribution when compared to the economics of operation., viz. costs on pumping or compressors. The velocity profile in the chosen slab shows mostly a translation due to the higher velocity but no significant increase in the values of the velocity in the zones with low velocity. The biggest increase in the values of the velocity was observed with the jets themselves.

Such an increase in the injection velocity would have made a much bigger impact if the flow conditions were different. For example, a significantly better improvement would have been noticed if there was a stronger re-circulation component of the flow. Such recirculating flow is likely to occur if, for example the outlet was through a distributing plate rather than through a single large outlet.

4.1.4 Effects of Different Arrangements of Inlets & Outlets

An intuitive approach to improve the flow distribution in a vessel is a better design and arrangement of the inlets and outlets. Figure 4.7 (a) illustrates a comparison of the flow field for three selected arrangements keeping the same inlets and varying the number of outlets. When the number of outlets is changed, the total area is kept constant, that is if two outlets are used instead of one, this means that the area of each outlet in this case is one half the area of outlet in the single outlet case. The arrangements compared are one

(a)

(b)

(c)

Figure 4.5. (a) Velocity Field for 45 m/s, (b) 57 m/s, and (c) 70 m/s.

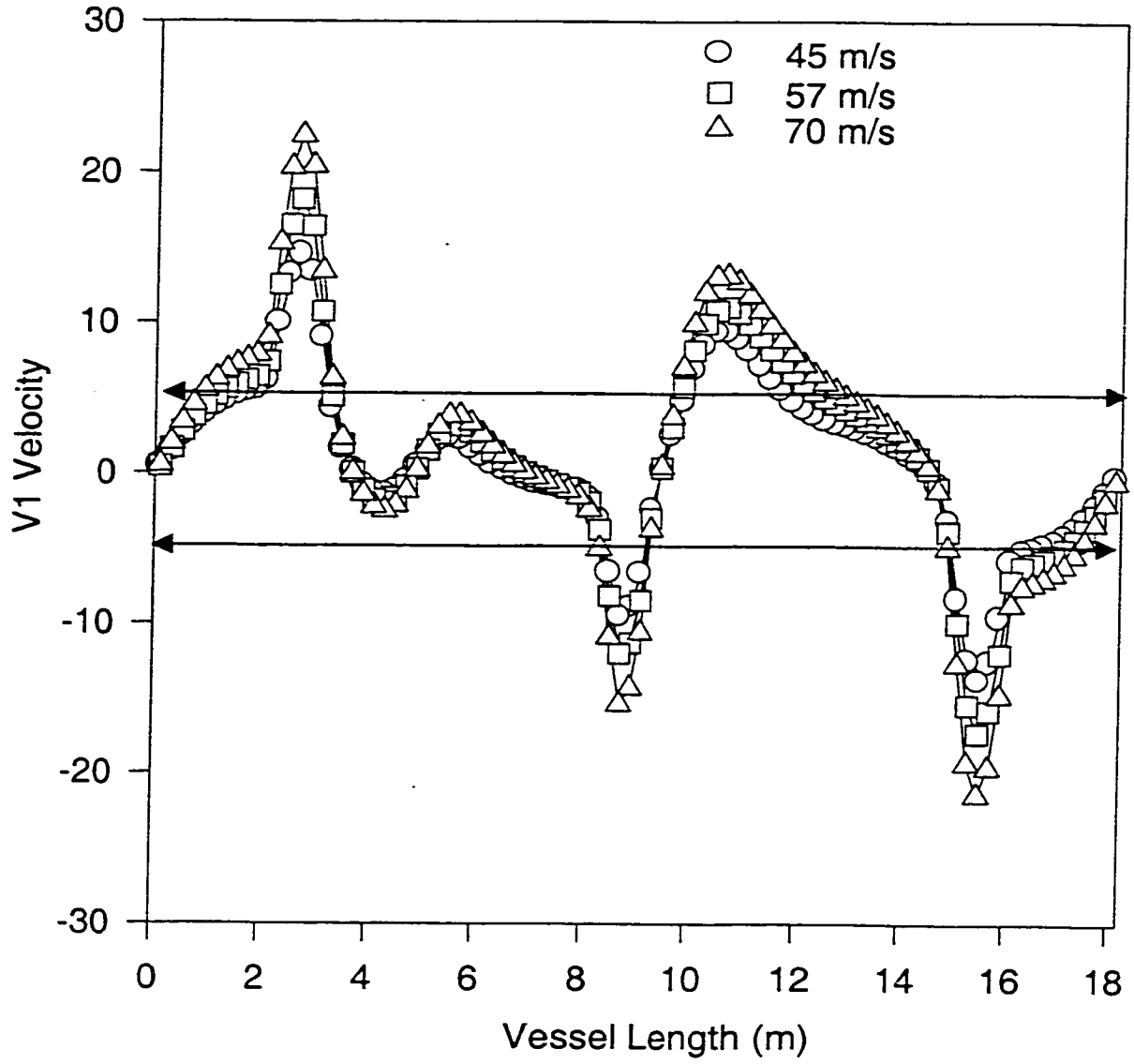

Figure 4.6 (a). A plot of V1 versus the vessel length for slab 25 at three different injection velocities

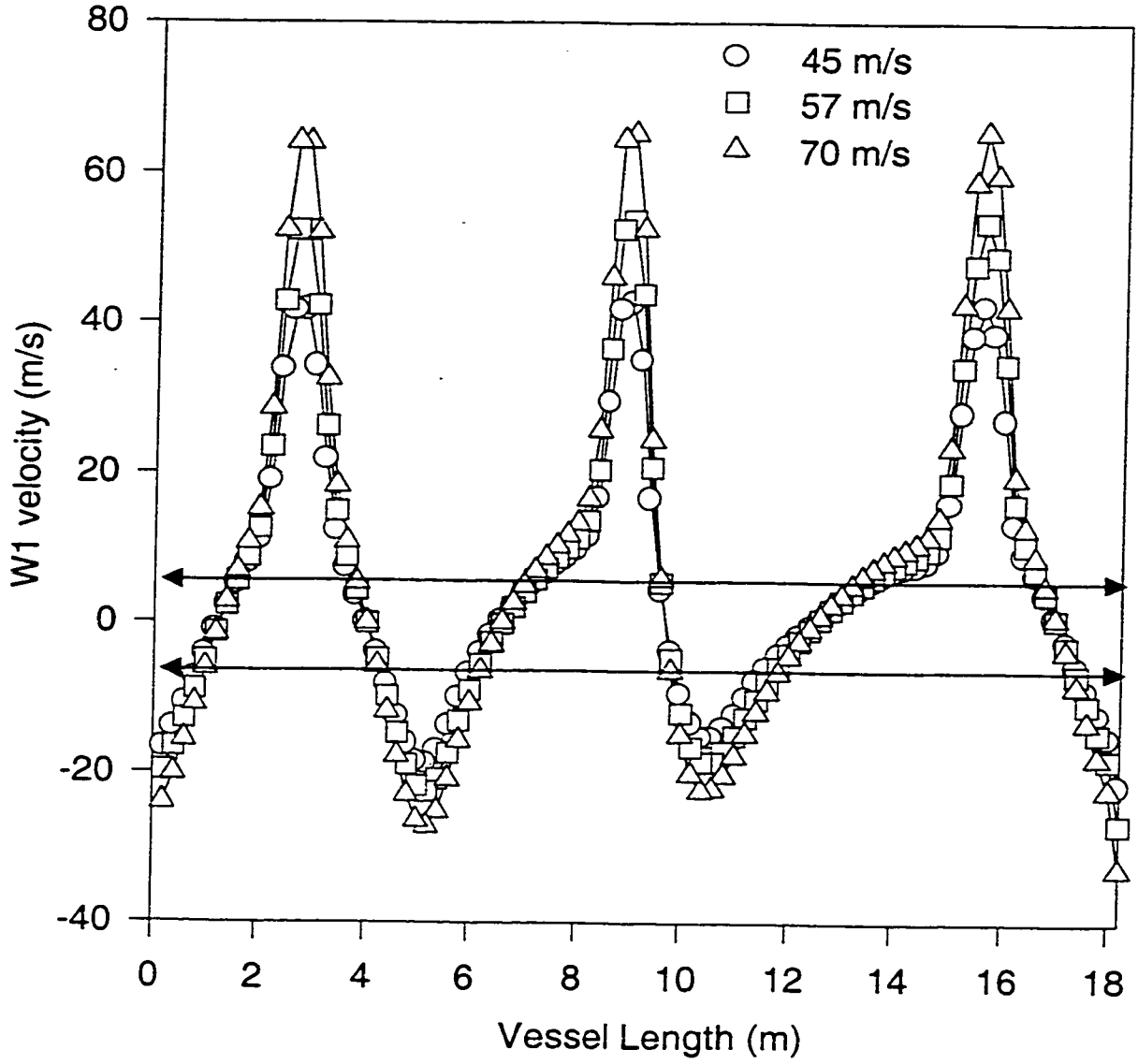

Figure 4.6. (b) A plot of W1 versus the vessel length for slab 25 at three different injection velocities

with a single outlet (Figure 4.7 a), one with two outlets (Figure 4.7 b) and one with multiple outlets (Figure 4.7 c). For all 3 cases the inlet cells are 21-29, 89-94 and 157-162. For Figure 4.7 (b), the 10 cells which makeup the 1 meter diameter outlet are 50-54 and 123-127. This arrangement is chosen- such that there is no short-circuiting of any of the three inlet jets although this may not strictly be the best one. The outlets are almost centered between the three inlets. The aim is to generate a good flow circulation and consequently to minimize the size of the low velocity zones. In Figure 4.7 (c), which is the multiple outlets case, the open cells are 13, 34, 51 etc. Figure 4.7 illustrates that the size of the zones with low velocity is smaller in the case of two-outlets compared to that of one outlet. It can also be seen that these low velocity zones are the smallest for the case with a multiple outlet.

Figure 4.8 illustrates the contour plots for comparing the three cases, i.e. single outlet (4.8 a), two outlets (4.8 b) and multiple outlets (4.8 c). The same trend can also be seen in these plots. The areas of low velocity (-3 to 6) m/s , (-7 to 1) m/s and (-4 to 3) m/s seem to decrease progressively in Figure 4.8 (a), (b) and (c).

Figure 4.9 (a), (b) illustrates a comparison plot for the V1 and W1 velocities for the three cases in the slab at z = 25. Figure 4.9 (a) illustrates that the variation in the V1 velocity for the case with multiple outlets is reduced substantially. The peaks of V1 have been reduced form - 20 and + 20 m/s to less than 10 m/s. The case with 2 outlets shows a major difference from the original case of 1 outlet in that no peak was observed around the middle of the vessel (around 9m).

(a)

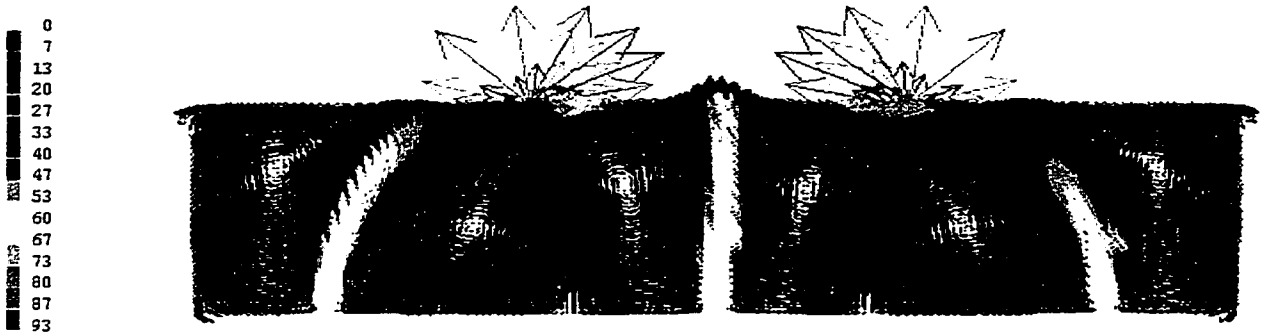

(b)

(c)

Figure 4.7. Velocity Field for an injection velocity of 57 m/s, three inlets and (a) one outlet , (b) two outlets and (c) multiple outlets

(a)

(b)

(c)

Figure 4.8. Contours of velocity in the z- direction (W1) at 57 m/s for (a) one outlet, (b) two-outlets and (c) multiple outlets.

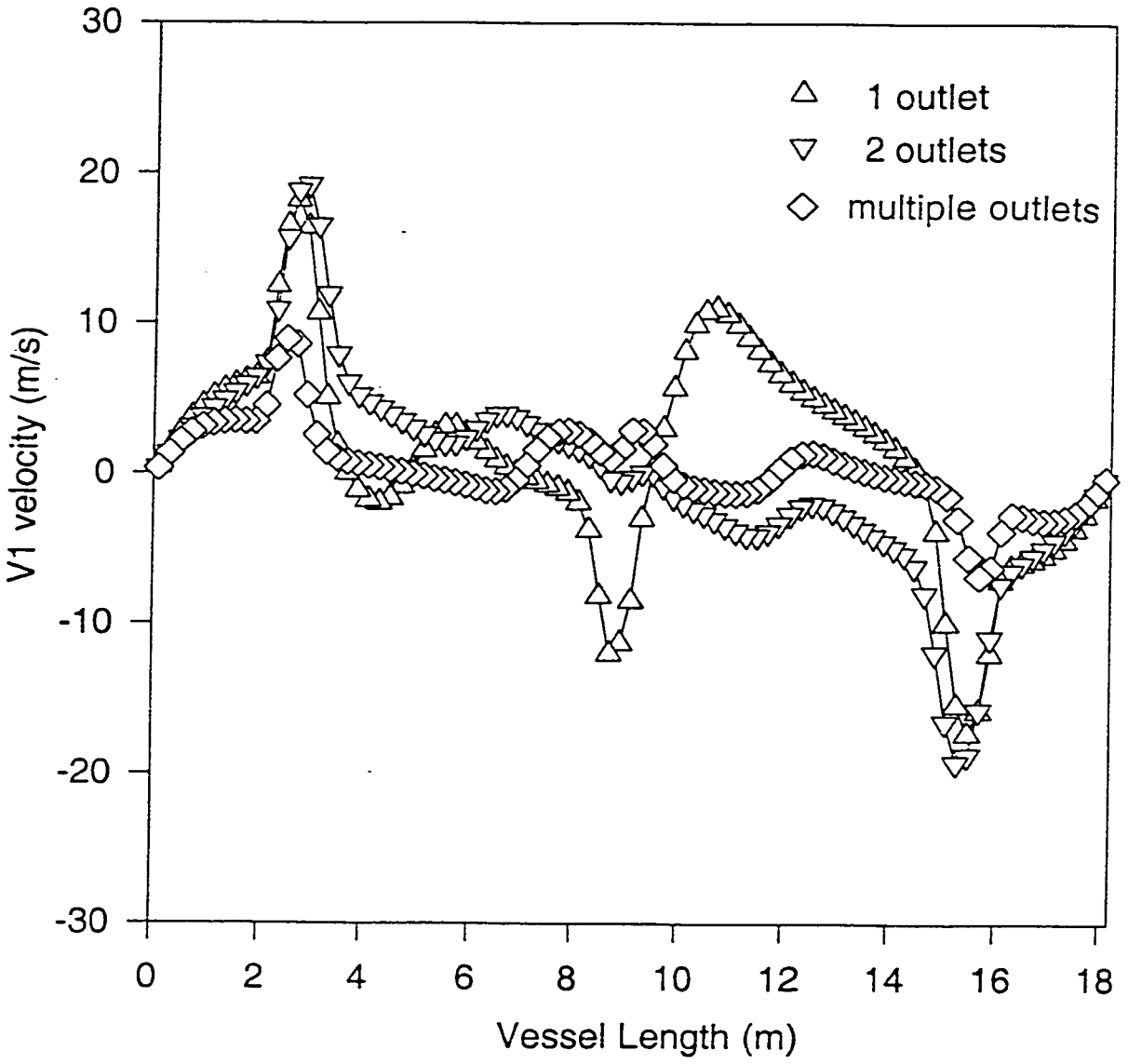

Figure 4.9 (a) A plot of V1 versus the vessel length for slab 25 for three different outlet arrangements.

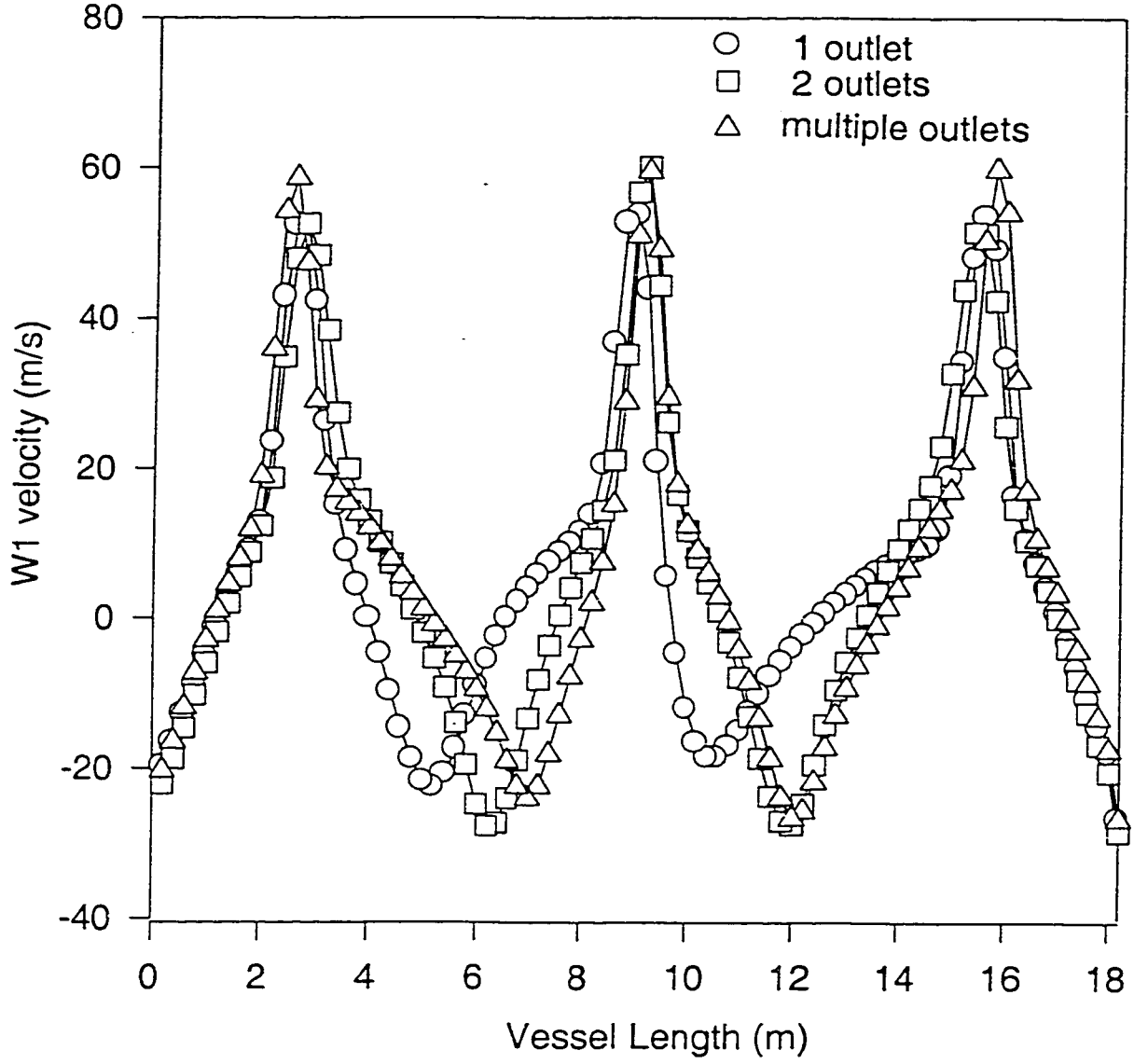

Figure 4.9 (b). A plot of W1 versus the vessel length for slab 25 at three different outlet arrangements.

Figure 4.9 b illustrates clearly that the length of the zones enclosed by the + 5 m/s and - 5 m/s has been significantly reduced in the case of two and multiple outlets compared with the single outlet case. This forms a quantification of the observation made based on Figures 4.8 and 4.9.

Figure 4.10 (a), (b), (c) compares the flow field for cases involving multiple inlets, single outlet and multiple inlet- multiple outlet. In Figure 4.10 (a) the incoming gas is distributed over six inlets keeping the total length of injection constant (1.8 m). The injection cells are 10-12, 20-22, 85-87, 95-97, 160-162 and 170-172, which sums up to 18 cells.

In Figure 4.10 (b) 8 inlets are used, which are 10-11, 20-21, 45-46, 85-87, 95-97, 137-138, 161-162 and cells 171-172, which again sums up to 18 cells. Figure- 4.10 (c) uses distributed inflow and outflow.

Figure 4.11 (a, b) are the comparison plots of the V1 and W1 velocities in the slab (z = 25), which means at 2.5 m from the bottom of the vessel, for the three cases.

From Figures 4.10 and 4.11, it can be stated that all the three arrangements of inlets and outlets did not give a much superior flow distribution and did not succeed in eliminating the zones of low velocities. The total size of these low velocity zones may change from case to case, however the flow distribution in 6-inlets/ 1 outlet and 8-inlets/ 1 outlets does not form a major step change from the standard case. These arrangements were chosen to investigate the effects of recirculation flow but no great difference was observed. The 6- and 8 inlet configuration chosen was not evenly distributed and it is expected that a more even and optimized distribution of these inlets could lead to a better distribution of flow in the vessel. The present arrangement is not an optimum one.

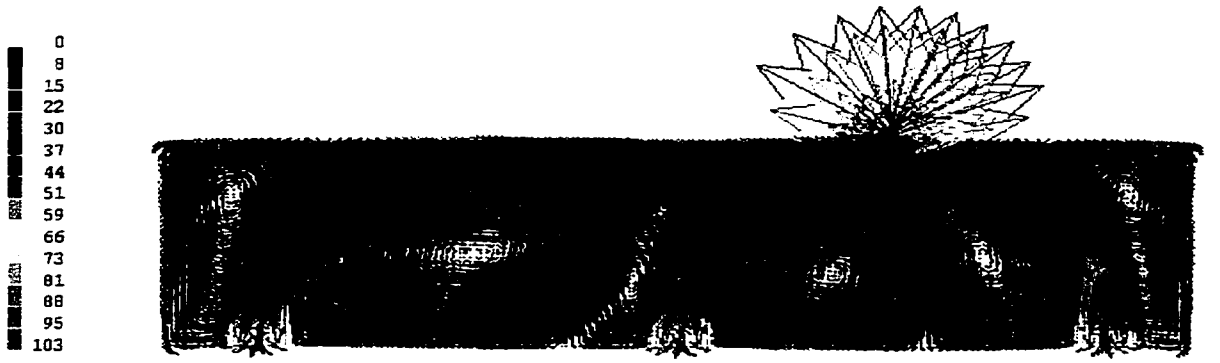

(a)

(b)

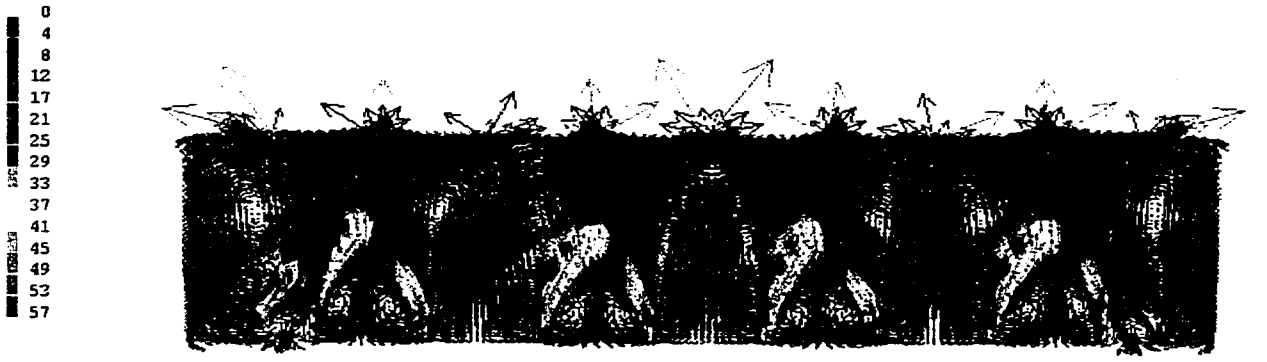

(c)

Figure 4.10. (a) Velocity Field for 6 cell inlet, (b) Velocity Field for 8 cell inlet, and (c) Velocity Field for a multiple inlet/ multiple outlet

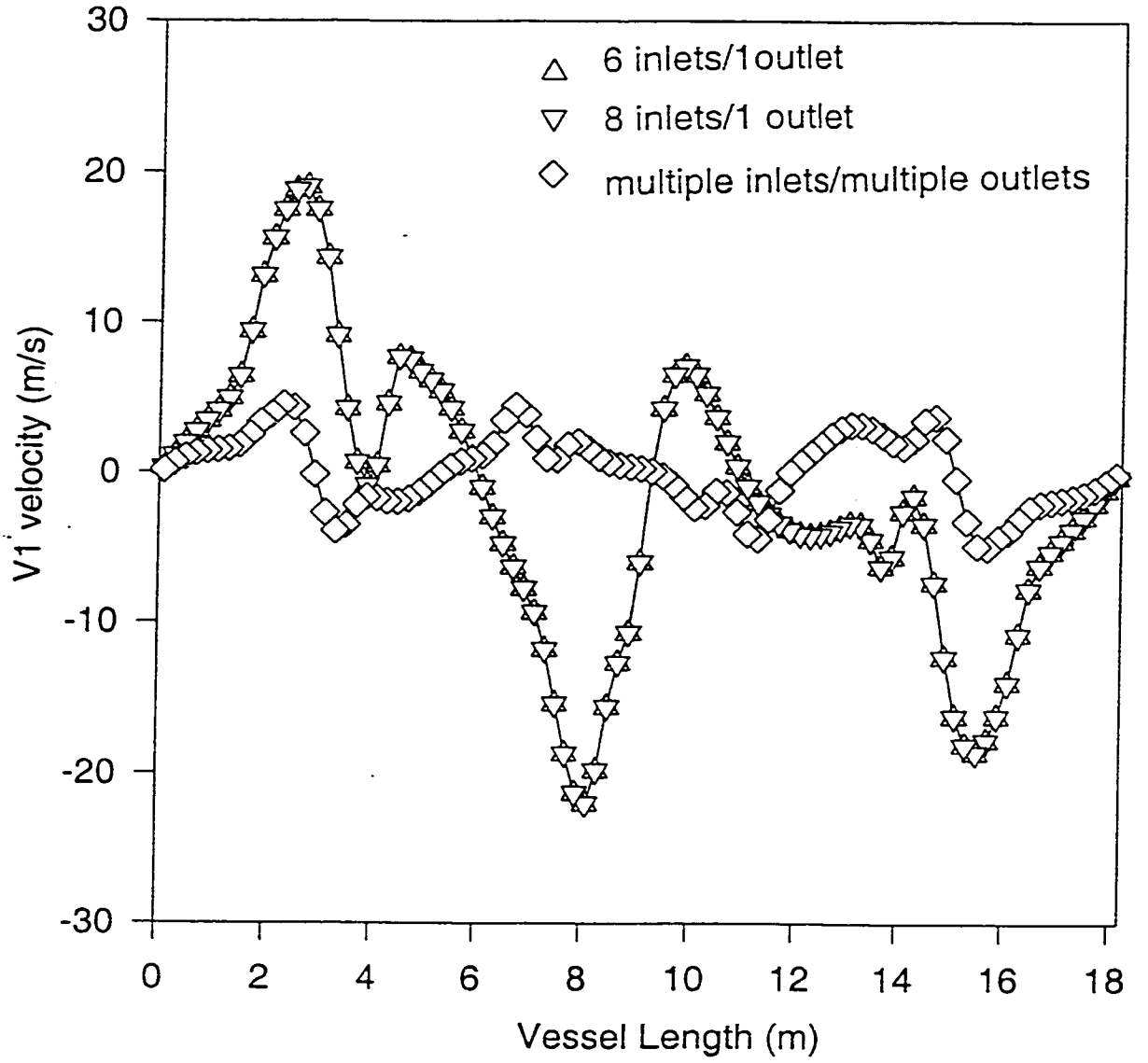

Figure 4.11 (a) A plot of V1 versus the vessel length for slab 25 for three different inlet/outlet arrangements.

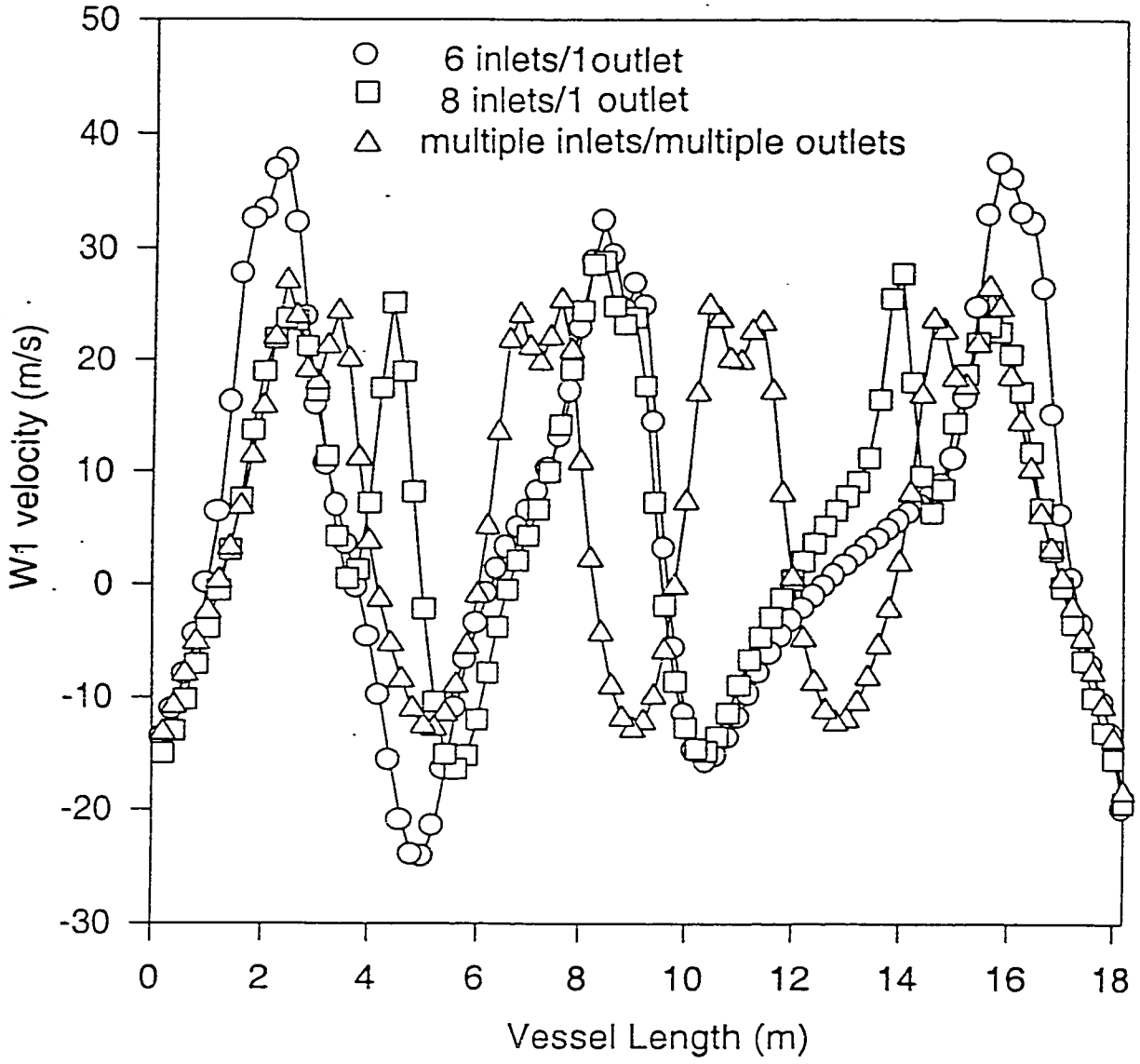

Figure 4.11 (b) A plot of W1 versus the vessel length for slab 25 for three different inlet/outlet arrangements.

The multiple inlet/outlets case showed as expected some improvement in limiting the size of the low velocity zones, however the expansion angle of the jets is rather limited (about 10 °) in the numerical results. This mean that there is still some low velocity zones between the adjacent jets.

4.1.5 Effects of Internal Geometric Improvements

Effects of geometric improvements can be effectively investigated using CFD modeling. In Computational Fluid Dynamics various shapes, inserts and other enhancements can be tested with the aim of choosing a design with a better flow distribution in the vessel. As a possible way of improving the flow distribution inside the unpacked vessel, annular discs are inserted above each incoming jet in the original vessel geometry. Figure 4.12 (a) illustrates the velocity field with three discs inserted. Each disc has an inner (open) diameter of 0.4 m and an outer diameter of 1.6 m. These discs are placed 0.6 m above the incoming jets. Figure 4.12 (b, c) illustrates the corresponding V1 and W1 contours respectively. These results show clearly that due to the fact that the open orifice is less than the inlet diameter, side jets are now active in addition to the main jets in the z- direction. This resulted in significantly higher velocities at the bottom section of the vessel. However no significant change was observed in the sizes of the zones with low velocities around the middle of the vessel.

A possible improvement in the insert design is to lessen the open area so that there is an increased throttle of the flow. Figure 4.13 (a), (b), (c) illustrates the velocity field and contours of W1 and V1, respectively for similar discs but now with an open diameter of 0.2 m and an outer diameter of 1.0 m. Results show remarkable improvements in the flow

patterns as compared to the previous case. The bigger dead zones which were visible in Figure 4.12 for the larger disc have been greatly minimized. There is appreciable recirculation near both vertical walls, which causes a good activity in the zone near the walls. Small low velocity areas are visible right on the insert plate itself. This could cause severe problems in case of multiphase flows, e.g., polymeric flows, wherein there can be a polymer film development on the insert. But in this case, since there is a single-phase gas flow, this problem may not be of serious concern.

Another feasible option, which may be investigated, is to vary the shape and size of the inserts. Figure 4.14 (a), (b), (c) illustrates the velocity field, W1 and V1 contours respectively for the case with conical inserts, which can throttle the flow gradually and uniformly. The insert has 0.2 m diameter at the base which is gradually increased to 1.4 m at the top. This insert is placed at a distance of 0.4 m from the vessel bottom. Although the low velocity zones do not seem to have reduced, there is a good potential for a similar insert to split and guide the flow in order to minimize the size of the low velocity zones. It should be noted that all the three jets unite near the outlet with a high velocity. This arrangement may lead to a substantial elimination of low velocity zones in the vessel, because the discs provide a bi-directional jet, which maintains high activity to its left as well as to its right. There is a need to modify this insert, possibly to revert to a wider open base, say 0.4 m instead to 0.2 m and to narrow the cone angle. For this geometry, it is clear from Figure 4.14 (a), that across the middle plane at slab, the low velocity zones has been significantly reduced. However larger low velocity zones are now observed in upper or lower parts of the vessel.

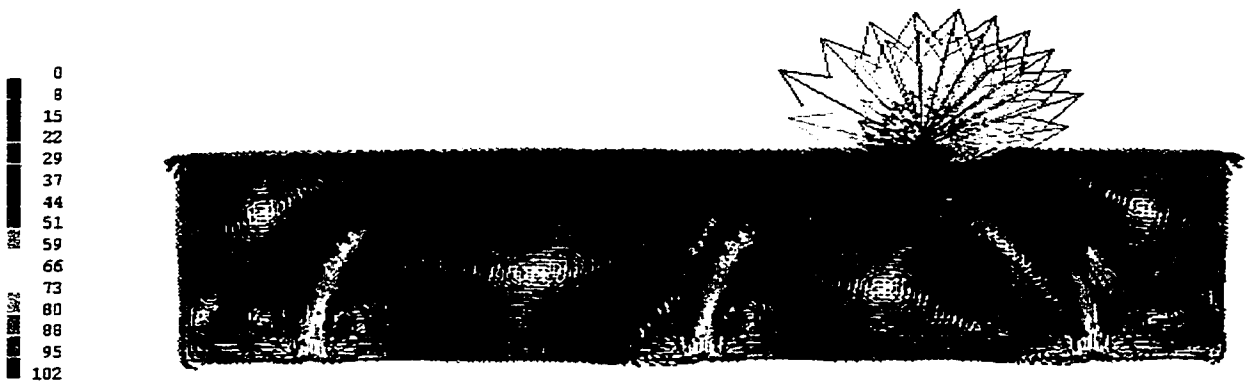

(a)

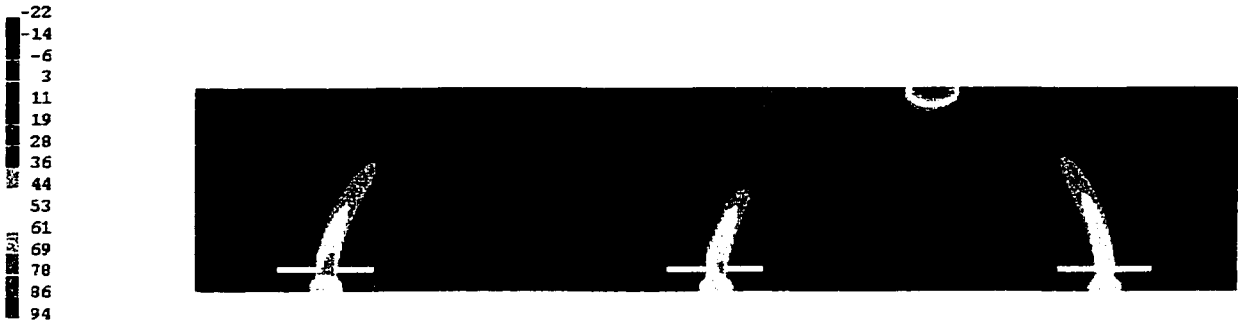

(b)

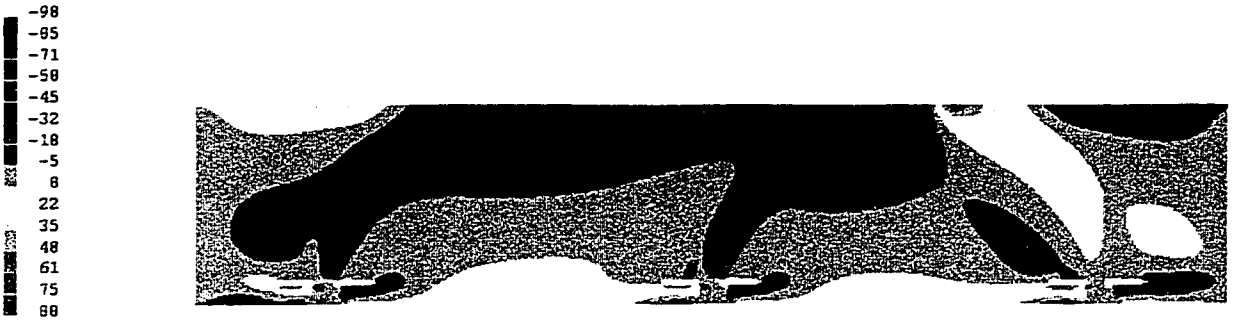

(c)

Figure 4.12. Annular Disc 0.4 m ID and 1.6 m OD (a) Velocity Field at 57 m/s, (b) Contour of the velocity in the z- direction (W1) and (c) Contour of the velocity in the y- direction (V1).

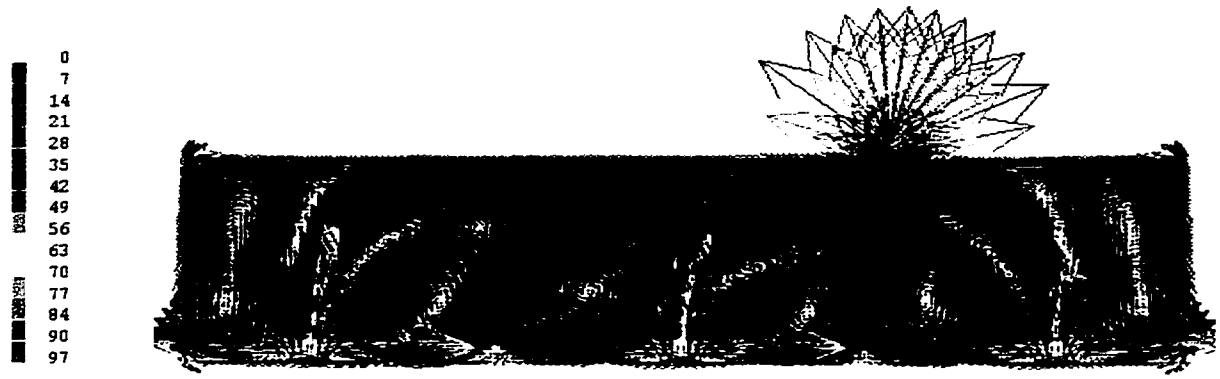

(a)

(b)

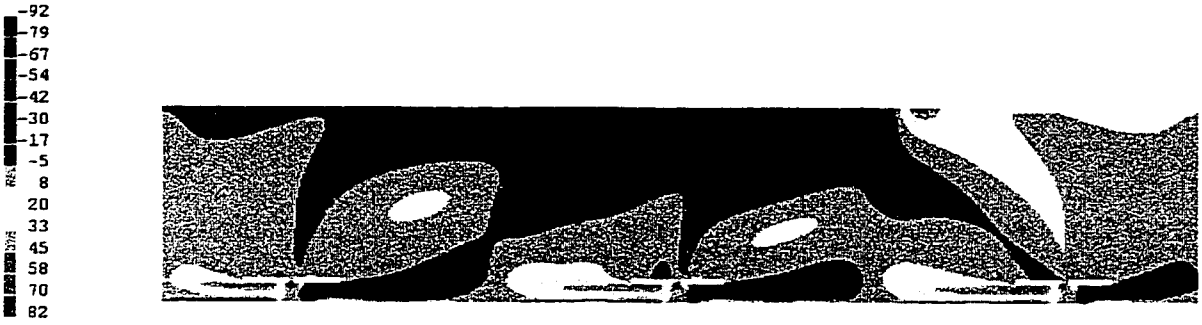

(c)

Figure 4.13. Annular Disc 0.2 m ID 1. m OD. (a) Velocity field at 57 m/s, (b) Contour of the velocity in the z- direction (W1) and (c) Contour of the velocity in the y- direction (V1).

(a)

(b)

(c)

Figure 4.14. (a) Velocity Field for a conical insert. (b) Contour of the velocity in the z- direction (W1) and (c) Contour of the velocity in the y- direction (V1)

4.1.6 Effects of Turbulence Model

Figure 4.15 (a, b, c) illustrates the results of the base case (3 inlets, 1 outlet, no inserts) with turbulence modeled using the Reynolds Stress Turbulence Model (RSM) for the standard case. The RSM is likely to provide a more realistic and rigorous approach for complex engineering flows. In this investigation, there seems to be some differences in the flow fields when RSM is used instead of the standard $k-\varepsilon$ model. The low velocity zones which were visible with the $k-\varepsilon$ model near the walls have been reduced to some extent. This result is expected, as the RSM is a more rigorous turbulence model, which takes into account the individual Reynolds stresses. Results with RSM show higher recirculation than the $k-\varepsilon$ model leading to a better flow distribution near the walls. Although the RSM model has improved the flow situation to some extent, the computation time was almost 50% more than that with the $k-\varepsilon$ model. Thus the choice of the $k-\varepsilon$ model for this investigation is justified, considering the saving in computation time and accuracy in predicting the flow distribution in the vessel.

4.1.7 Effects of the Grid Size

The grid size may play an important role in resolving the flow. The grid size has to be of a certain value before the flow is properly resolved. This means that a numerical solution could be grid dependent. To ensure that the present results are grid independent, a case with a finer grid size was considered. The case discussed in the previous sections had a grid of 182 x 49 cells. A case with a grid of half the previous size is used, i.e. the number of grid cells is now quadrupled to 364 x 98 cells. The inlets and outlet locations have been kept as before. Figure 4.16 (a, b) illustrates the velocity flow fields for the cases

of standard (182 x 49) and fine (364 x 98) grid sizes. The flow fields for both the cases are almost identical. Both cases showed the same flow distribution especially the size and shape of the low velocity zones. It can be safely concluded that the solution with the grid chosen (182 x 49) is grid independent.

(a)

(b)

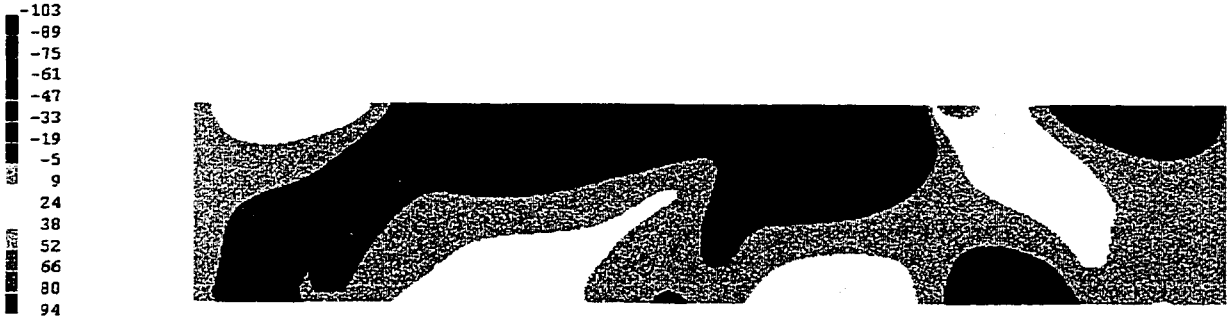

(c)

Figure 4.15. (a) Velocity Field at 57 m/s for the Reynolds Stress Turbulence Model (b) Contour of the velocity in the z-direction (W1) and (c) Contour of the velocity in the y-direction (V1)

(a)

(b)

Figure 4.16. (a) Velocity Field for a finer grid (364x98) and

(b)) Velocity Field for the standard grid (182x49).

Chapter 5

Results of Two-Phase Flow in Unpacked Vessel

5.1 Introduction

Few things are more central to chemical engineering than multiphase flow chemical reactors: they are used in industry to produce a variety of chemicals, where economy of scale remains the driving factor.

Good contacting between the phases in multiphase reactors is essential to promote interphase transport of species and energy. However, in many instances this is hard to achieve, as the state of uniform spatial distribution of the various phases is unstable and gives way to nonuniform structures spanning a wide variety of length and time scales.

The most practical approach to simulating the hydrodynamics of commercial-scale multiphase reactors is through continuum models that treat the coexisting phases as interpenetrating continua. The general structure of the continuity and momentum balance equations is the same for all dispersed two-phase flow problems, although the closure equations are system dependent.

Two-phase flow simulations were carried out in the same sulfur converter, which was earlier simulated for the single-phase flow situation. The converter is a horizontal cylinder having a diameter of 4.9 m and a length of 18.2 m. A gas-liquid (two-phase) stream is injected into the vessel through three inlets each with a 0.6-m diameter each. The tank has a single 1.0 m diameter outlet as earlier shown schematically in Figure 4.1. The two-

dimensional mesh used is the same as in a one-phase flow with 182 cells in the y-direction and 49 cells in the z-direction. This means a uniform grid of 10 cm a side has been chosen as was shown in Figure 4.2. The inlets are located at the bottom of the vessel between cells 21-26, 89-94 and cells 157-162. The outlet is located at at the top of the vessel (z = 4.9 m) and has cells 50-59 (y-direction) open as shown Figure 5.1.

Similar to the single-phase case the feed mixture consists mainly of CO_2, H_2S, SO_2 and H_2O with trace concentrations of other components such as methane and hydrogen and some liquid hydrocarbons. The density of the inlet gas is 1.36 kg/m^3 and its kinematic viscosity is 2.18×10^{-5} m^2/s or a dynamic viscosity of 2.96×10^{-5} Pa.s, whereas the density of the liquid is 600 kg/m^3 and its kinematic viscosity is 1.34 x 10^{-4}. Numerical simulations of two-phase flow were carried out. The effects of various factors on the flow fields are investigated. These factors include the vessel geometry, arrangement and number of inlet and outlets, fluid flowrates and turbulence models.

The gas-liquid mixture is injected into the converter at a velocity of 57 m/s. The analysis is done for a two-dimensional unpacked vessel. The effects of chemical reactions and heat transfer are not included and only the flow and the pressure fields are resolved. The inlet composition on the basis of volume fraction is 99% by volume gas (18.3% by-weight) and 1% liquid (81.7% by weight).

5.2 Simulation of the standard case

Figure 5.1 illustrates the velocity field for flow in the unpacked vessel. The results are similar to those in one-phase flow with no change in the size and location in the low velocity zones. Although the velocity with which the jets rise is slightly lower than in the

single-phase case. Figure 5.2 (a) illustrates the contours of velocity in the z- direction (W1) for the gas phase and Figure 5.2 (b) illustrates the z-velocity contours for the liquid phase (W2). On comparing these flow contours with Figure 4.3 for single-phase flow, it is evident that the dead zoning problem is more or less unchanged in case of a two-phase situation. Figure 5.3 (a) shows the contours of the velocity in the y- direction (V1) for the gas phase and Figure 5.3 (b) shows the contours of the velocity in the y- direction for the liquid phase (V2). These plots also confirm that there is no improvement in the flow situation. Figures 5.4 (a, b) illustrates the gas volume fraction (R1) and liquid volume fraction (R2) in the vessel. Figure 5.4 (b) illustrates that the liquid tends to concentrate near the edges, the dark orange colors on the contour map show the severity of this problem. In case of polymeric material this may precipitate at the corners thereby reducing the vessel efficiency. This is an unfavorable phenomena and needs careful study for its subsequent elimination or minimization.

5.2.1 Effects of variation in fluid flowrate

As in the case of single-phase flow, the flowrates were also changed for the two-phase situation. As discussed earlier, this change may not always be economically/practically feasible due to limits on the pumps and/or compressors. Figures 5.5 (a, b, c) illustrates a comparison of the flow fields for cases with an injection velocity of 45, 57 and 70 m/s respectively. The injection velocity was increased keeping the area of the inlets constant. Results show no major improvement in the flow distribution as the injection velocity is increased by 55.6% i.e. (from- 45-70 m/s.). The change in the size of the low velocity zones and in the magnitude of the velocity with injection velocity is similar to that in the single-phase case and will not be discussed in detail here.

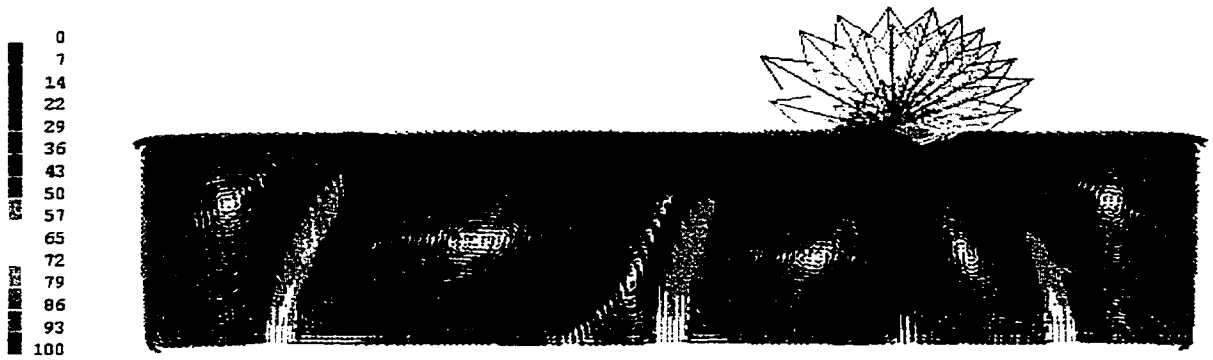

Figure 5.1. Velocity Field for two-phase flow at 57 m/s.

Figure 5.2 (a). Contour of velocity in the z- direction (W1) for phase 1.

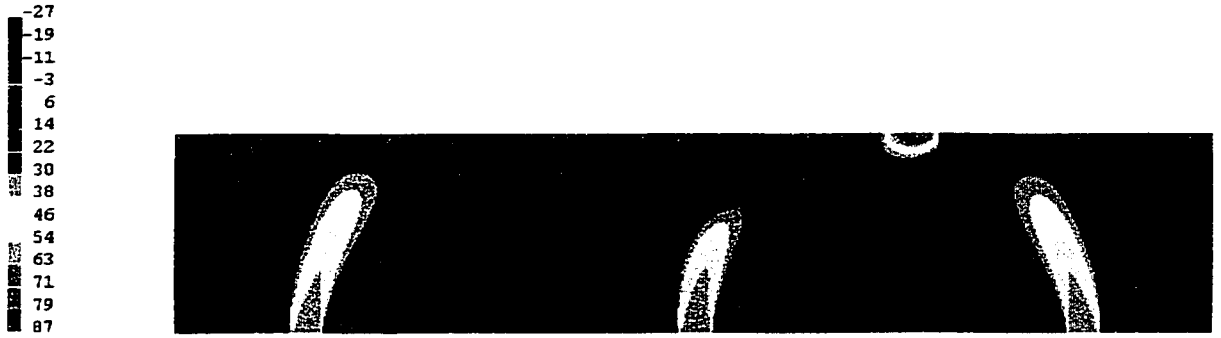

Figure 5.2 (b) Contour of velocity in the z- direction (W2) for phase 2.

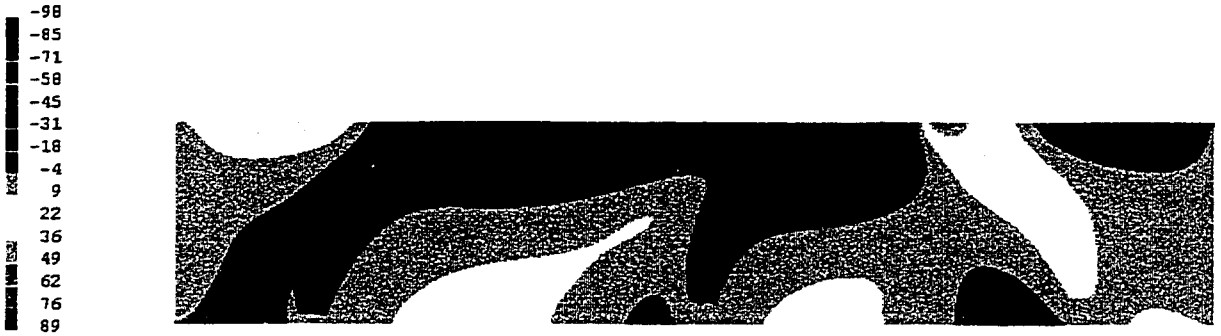

Figure 5.3 (a). Contour of the velocity in the y- direction for phase 1 (V1)

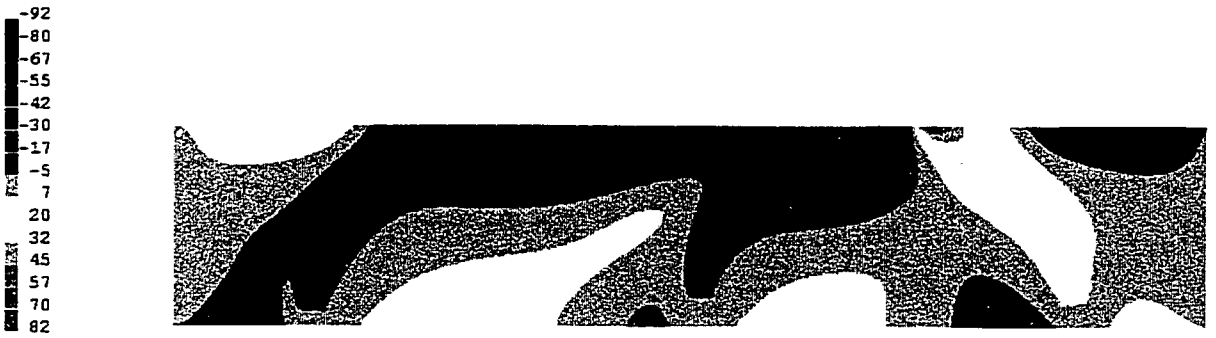

Figure 5.3 (b). Contour of the velocity in the y- direction for phase 2 (V2)

(a)

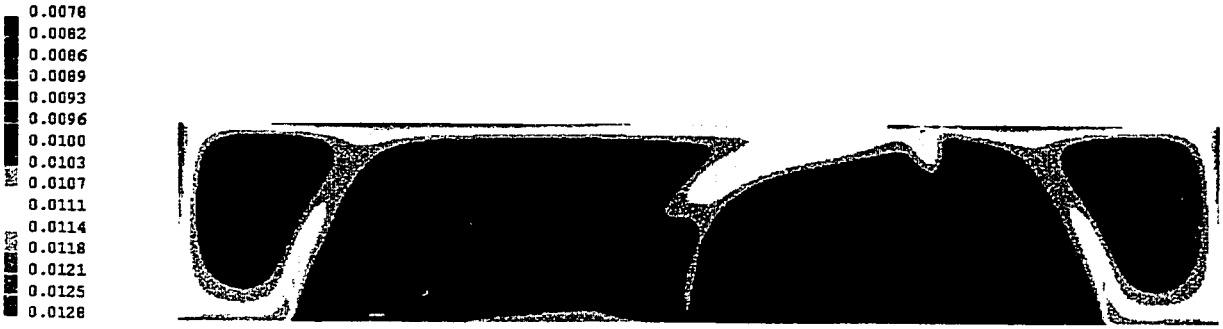

(b)

Figure 5.4. (a) Gas volume fraction (R1) and (b) Liquid volume fraction (R2) for an injection velocity of 57 m/s.

Figure 5.6 (a, b, c) illustrates the contours of the liquid volume fraction (R2) for the three injection velocities i.e., 45 m/s, 57 m/s and 70 m/s respectively. The locations of high liquid concentration seem to be unchanged when these plots are compared for each velocity. A minor improvement for the case of 70 m/s is observed and is represented by slightly lower liquid concentration at the bottom of the vessel.

5.2.2 Effects of different arrangements of Inlets & Outlets

Akin to improving the flow distribution in a vessel through a better design and arrangement of the inlets and outlets in case of one-phase flow, the same alterations are applied for two-phase situation. The arrangements compared are one with a single outlet (Figure 5.7 a), one with two outlets (Figure 5.7 b) and one with multiple outlets (Figure 5.7 c). The arrangement of open cells is the same as in for single phase. The outlets are almost centered between the three inlets in an attempt to obtain better flow circulation and consequently to minimize the low velocity zones. While the number of outlets is changed, the total open cells are kept constant, that is if two outlets are used instead of one, this means that the length of each outlet in this case is one half the length of outlet in the single outlet case. In comparison with the same arrangement for the single-phase flow this had shown similar improvements, i.e., the multiple outlets produced the best results. Figure 5.8 illustrates a comparison of the liquid volume fractions for the standard case, a case with two outlets and three-inlet arrangement and the multiple outlet case. The three inlets/ multiple outlet case illustrated that the high liquid concentration zones are smaller in size; however at some restricted points high concentration is observed.

Figure 5.9 (a) gives the velocity field for a case involving six inlets and a single outlet. In Figure 5.9 the incoming gas is distributed over six inlets keeping the total length

of injection, constant (1.8 m). The injection cells are 10-12, 20-22, 85-87, 95-97, 160-162 and 170-172, which sums up to 18 cells. From Figure 5.9 (a), it is clear that the size of the dead zones is comparable to the standard three-inlet case. This result was also true for the single-phase situation. Also from the liquid volume fraction (R2) Figure (5.9 b), it is clear that the liquid tends to get accumulated heavily in the lower half of the vessel.

As a possible way of overcoming this problem, 2 more inlets were introduced so as to minimize the liquid accumulation in the lower half. The second case (Figure 5.10 a) uses 8 inlet cells which are 10-11, 20-21, 45-46, 85-87, 95-97, 137-138, 161-162 and cells 171-172, which again sums up to 18 cells, thereby keeping the inlet length constant. From the velocity field plot, it is clear that the low velocity zones, which were visible in the 6 inlet-cell case, have been decreased. Also from the liquid volume fraction (R2) contour (Figure 5.10 b) it is clear that the liquid accumulation has been decreased.

The third case (Figure 5.11) uses distributed inflow and outflow. The inlet cells are 10, 20-21, 40-41, 60-61, 80-81, 100-101, 120-121, 140-141, 160-161 and 172^{nd} cell. The outlet cells are 13, 35, 57, 79-80, 103-104, 126, 147, and 170^{th} cell. From Figure 5.11, it can be seen that although the jets reach the vessel outlets at about 25-30 m/s, their distribution is more even, but there seems to be some small low velocity zones especially at the corners. From the liquid volume fraction (Figure 5.11b) plot, it seems that there is lesser liquid accumulation in this case when compared with the 6- and 8-inlet cell case. The liquid accumulation is lesser near the walls. Thus from all the cases which were simulated with different arrangements of inlets and outlets, the multiple inlet/multiple outlet case seems to give the most promising results from the liquid accumulation point of view.

(a)

(b)

(c)

Figure 5.5.Velocity Field for (a) 45 m/s, (b) 57 m/s and (c) 70 m/s

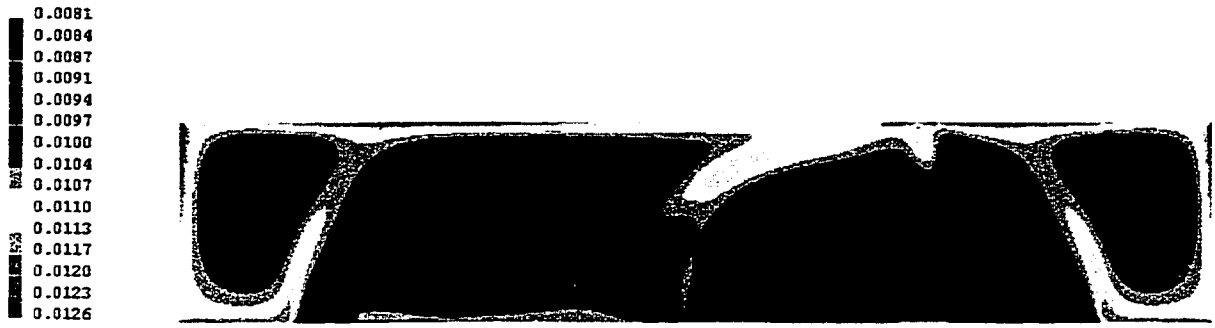

(a)

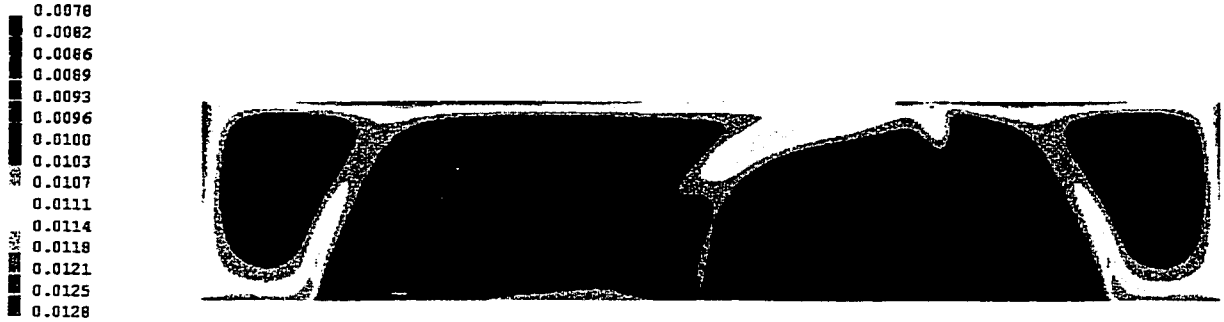

(b)

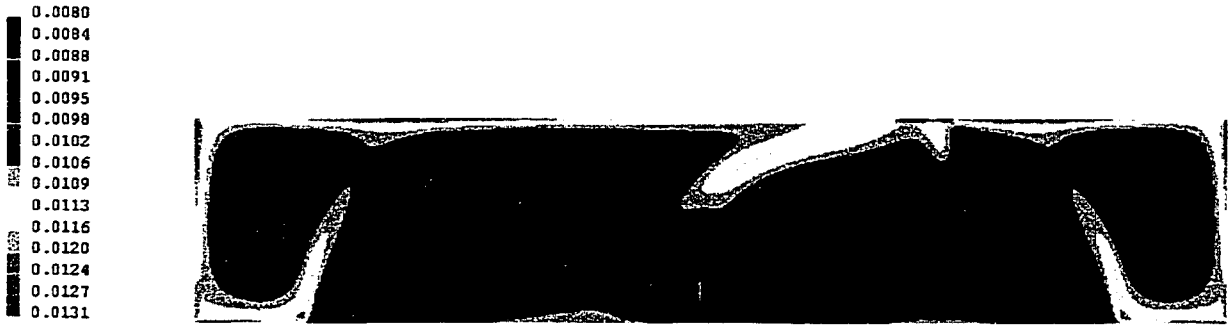

(c)

Figure 5.6. (a) Contours of the Liquid volume fraction (R2) at an injection velocity of (a) 45 m/s, (b) 57 m/s and (c) 70 m/s.

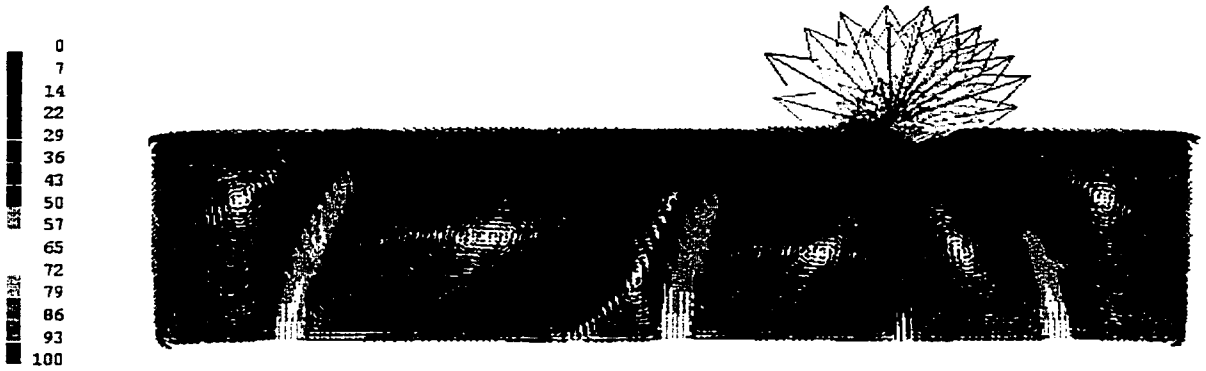

(a)

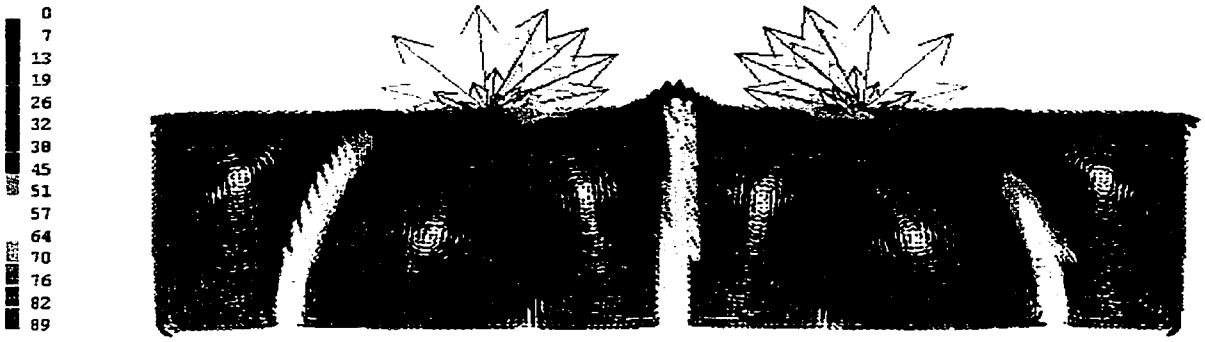

(b)

(c)

Figure 5.7. Velocity Field for (a) single outlet, (b) two outlets and (c) multiple outlets

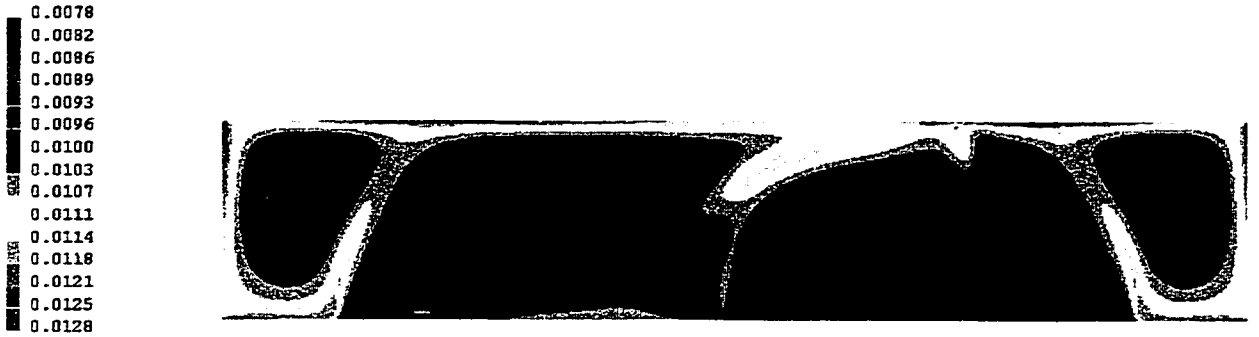

(a)

(b)

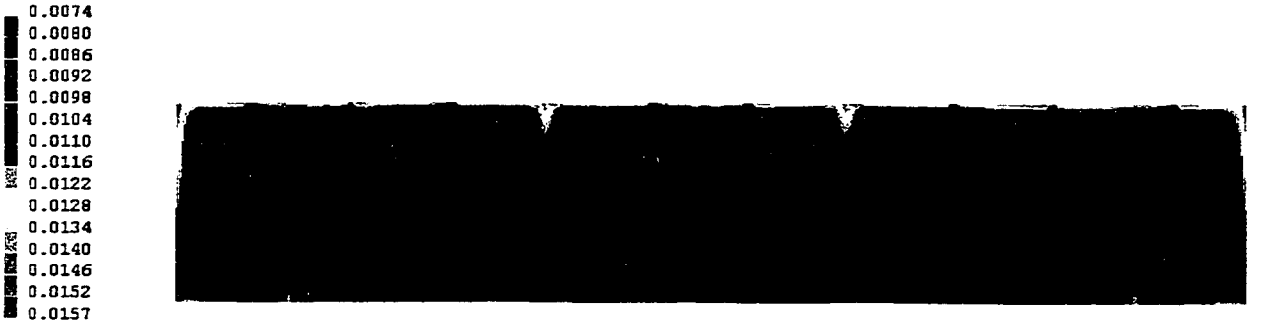

(c)

Figure 5.8. Contours of the liquid volume fraction (R2) at 57 m/s for (a) one outlet, (b) two-outlets, and (c) multiple outlets

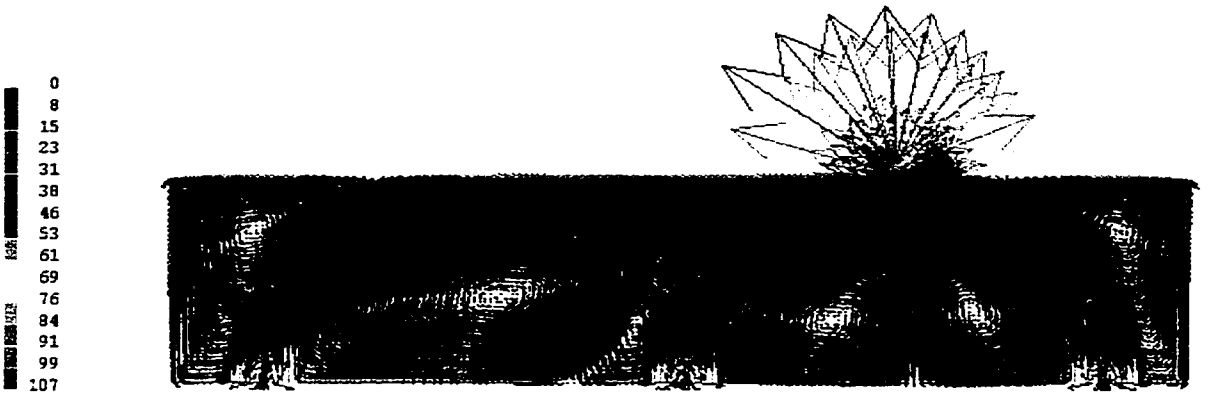

(a)

(b)

Figure 5.9 Six inlets (a) Velocity Field, and (b) Contour of R2

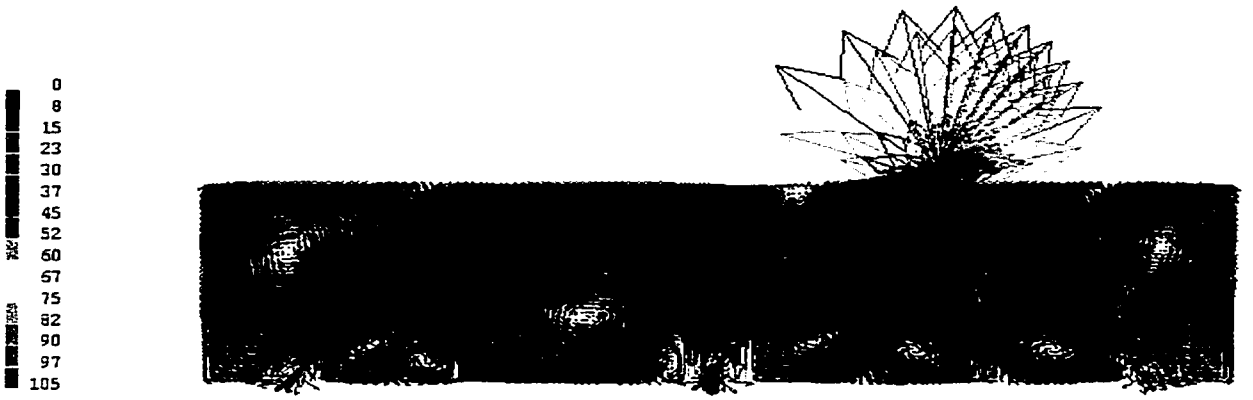

(a)

(b)

Figure 5.10. Eight inlets. (a) Velocity Field, and (b) Contour of the R2

(a)

(b)

Figure 5.11. Multiple Inlets and Multiple Outlets (a) Velocity field and (b) Liquid volume fraction (R2)

5.2.3 Effects of Internal Geometric Improvements

As with single-phase simulations, internal geometric changes like inserts or discs, have the potential of improving the flow distribution in the vessel, the same modifications have been applied to the two-phase situation. Figure 5.12 (a, b) illustrates the velocity flow fields and liquid volume fraction contours respectively with three discs inserted. Each disc has an inner (open) diameter of 0.4 m and an outer diameter of 1.6 m. These discs are placed 0.6 m above the incoming jets. Results (Figure 5.12 b) indicate that the situation becomes more complex now, with some liquid accumulating right on the disc itself and in its vicinity. From the velocity field it is clear that near the walls, there seems to be very high velocities.

As in the case of a single-phase flow, another improvement is applied on the disc, by lessening the open area available for flow. Figure 5.13 (a, b) show the velocity field and liquid volume fraction respectively for three discs again, but with an inner diameter of 0.2 m and outer diameter of 1.0 m. This arrangement leads to a more severe throttle of flow. The velocity field with this arrangement shows some improvement. The low velocity zones, which were visible in earlier cases, have been reduced in size. Also from the liquid volume fraction contour, it can be seen that the liquid accumulation at the vessel bottom as well as at the sides is reduced compared to earlier cases; however there seems to be high liquid concentration underneath the discs

Since the insert design heavily affects the flow distribution in the vessel, it would be worthwhile to investigate the effect of a conical insert in the vessel. The insert has 0.2 m diameter at the base which is gradually increased to 1.4 m at the top. Figure 5.14 shows the various plots for this configuration. From the velocity field plot, it can be seen that the

conical inserts act as a gradual flow distributor to each incoming jet. The size of the low velocity zones has been reduced in the middle of the vessel but increased elsewhere. The liquid volume fraction plots show that there is negligible liquid accumulation at the corners as well as at the tank bottom. Another positive aspect of this geometry of the insert is that the accumulation on the insert itself, which was a major drawback for other inserts seems to have been reduced. Thus it can be concluded that the conical inserts seem to be a promising geometry for improving the two-phase flow in the vessel.

5.2.4 Effects of physical properties of the fluid

All the cases considered so far were simulated for a 99:1 gas to liquid split by volume in the inlet mixture. Also the gas density was very low (1.36 kg/m^3). The possible effects of variations in the gas density on the flow profiles in the tank have been investigated. A total of four cases were simulated to gauge the effect of variation of the fluid property.

In case 1 the gas density was altered to 20 kg/m^3 (corresponds to high-pressure operation) keeping the gas to liquid split 99:1. Figure 5.15 (a) shows the gas volume fraction and liquid volume fraction respectively for this case. From the Figure it is clear that the liquid accumulation gets worse here when compared with that for the standard case (99:01) in Figure 5.15 (b).

In case 2 the gas to liquid split was changed to 95:05, i.e., the liquid fraction is increased with a subsequent decrease in the gas fraction. The gas velocity was 57 m/s and the gas density in this case was 20 kg/m^3. Figure 5.16 (a) depicts the liquid volume fraction for this case. It can be seen that the amount of liquid accumulation seems to have

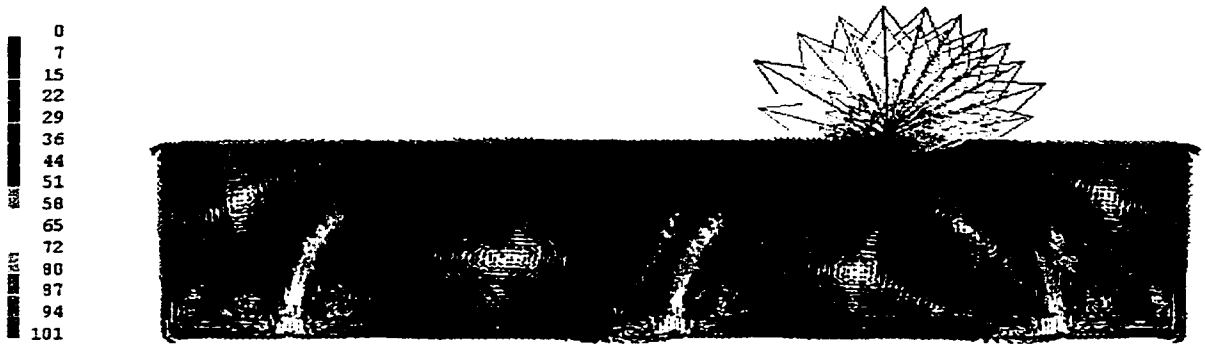

(a)

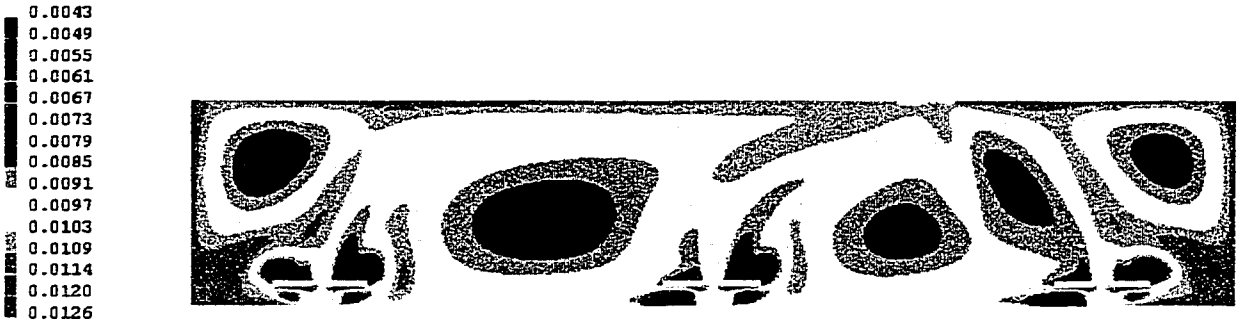

(b)

Figure 5.12. Annular disc 1.6 m OD and 0.4 m ID. (a) Velocity Field and (b) Contour of the Liquid volume fraction (R2)

(a)

(b)

Figure 5.13. Annular disc 1.0 m OD and 0.2 m ID. (a) Velocity Field and

(b) Contour of the Liquid volume fraction (R2)

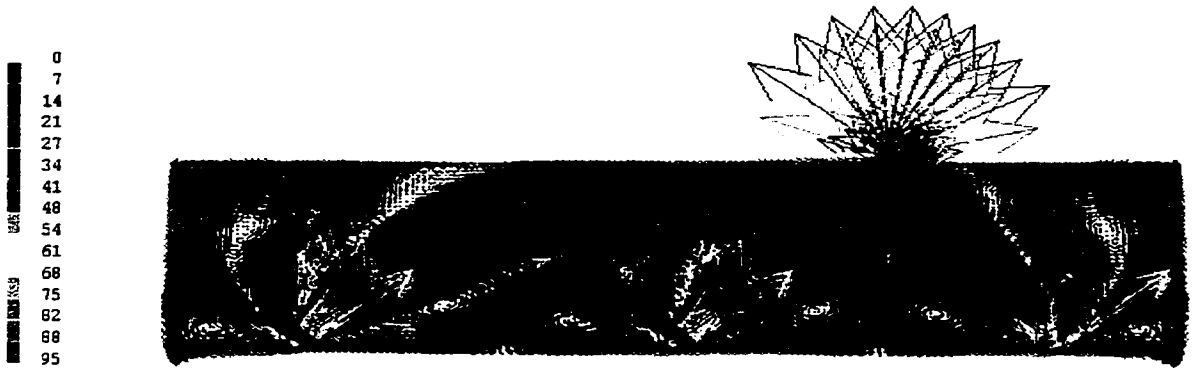

(a)

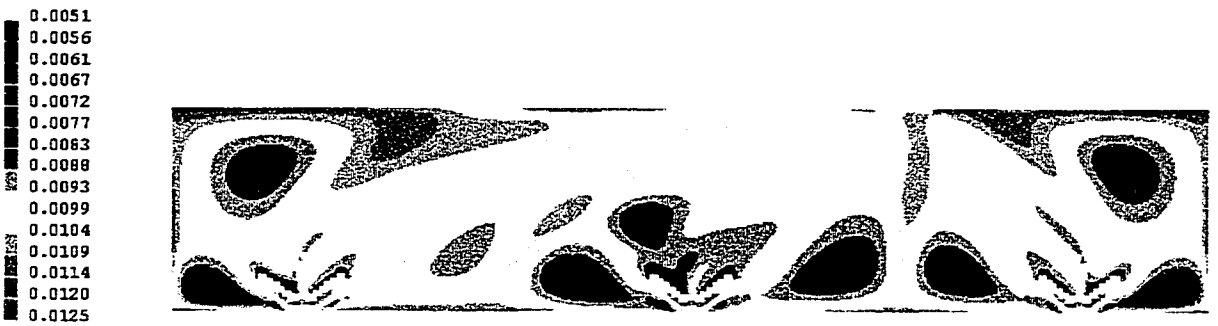

(b)

Figure 5.14. Conical Insert. (a) Velocity Field and (b) Liquid volume fraction (R2)

increased to about 50% (from 0.05 to 0.077) as compared to 30% when the split was 99:01. The results clearly underscore the importance of the effect of the split variation in a two-phase situation.

In case 3 the gas to liquid split was changed to 90:10 i.e. the liquid fraction is 10% of the mixture by volume. The gas velocity was 57 m/s and the gas density in this case was 20 kg/m^3. Figure 5.16 (b) depicts the gas volume fraction and liquid volume fraction for this case. It can be seen that the amount of liquid accumulation seems to have increased in comparison to case 2 to about 50% (from 0.1 to 0.149).

Figure 5.17 depicts the plot of the gas and liquid volume fractions at two locations in the vessel, at z = 25 and at z = 49, which corresponds to the topmost cell. It is clear from the plot that the liquid accumulation is higher (by almost 50%) at the top corners of the vessel compared to the center of the vessel. This shows that the liquid (heavy phase) tends to accumulate at the corners. This could lead to serious problems in case of polymeric flows or some complex two-phase situation.

In case 4 the gas to liquid split was kept at 90:10 but the gas velocity was increased to 70 m/s and the gas density in this case was 20 kg/m^3. Figure 5.18 depicts the liquid volume fractions for this case. It is clear from the figure that increasing the velocity from 57 m/s to 70 m/s (a 55.6% increase) does not yield any difference.

(a)

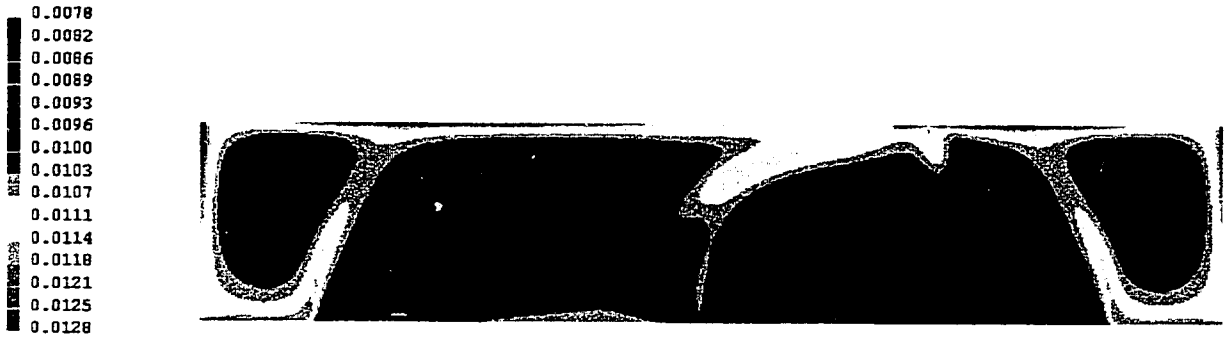

(b)

Figure 5.15. (a) Contour of R2 for gas density 20 kg/m^3. Gas to Liquid split (99:01) , and (b) Contour of R2 for the standard case

(a)

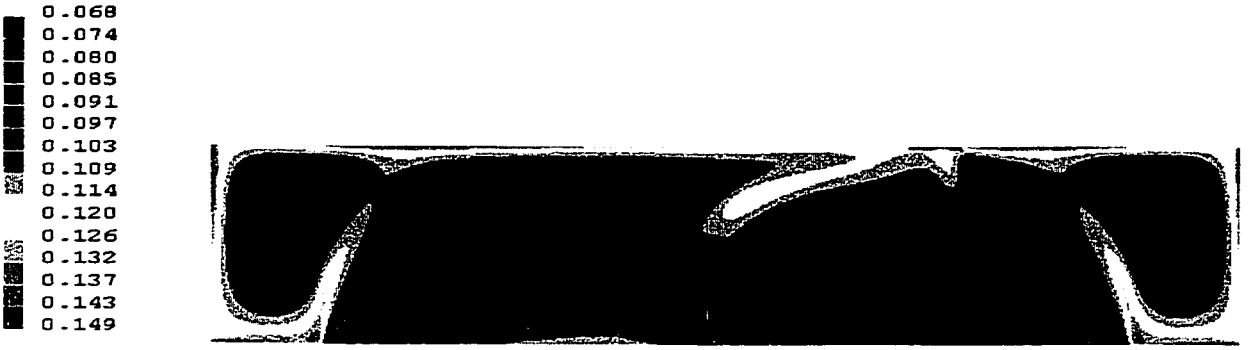

(b)

Figure 5.16. (a) Contour of R2 for gas density 20 kg/m^3. Gas to Liquid split (95:05) , and (b) Contour of R2 for gas density 20 kg/m^3. Gas to Liquid split (90:10) and velocity 57 m/s.

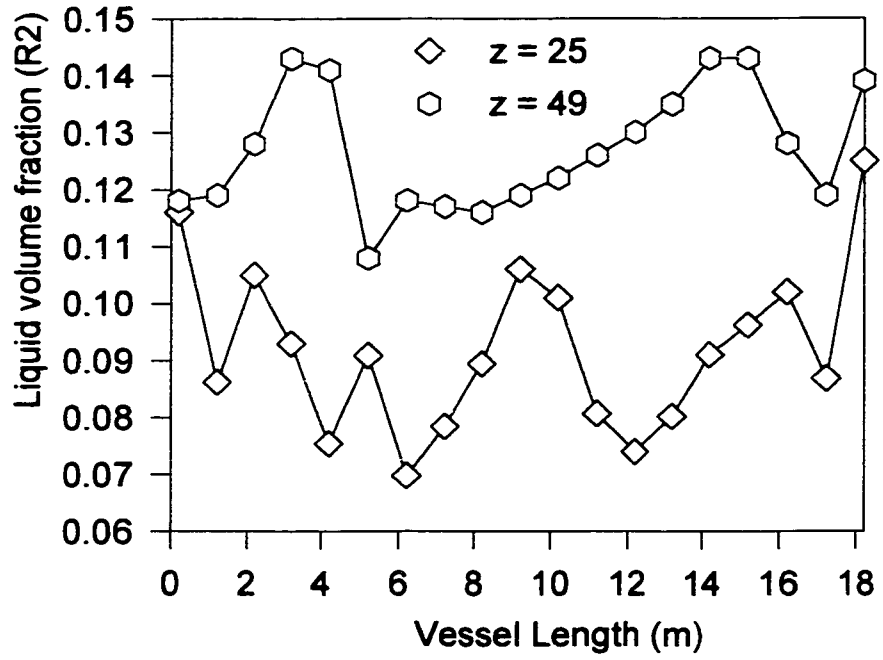

Figure 5.17. Comparison of R2 for the case with gas density = 20 kg/m^3 and liquid density = 600 kg/m^3, with Gas to Liquid split (99:01)

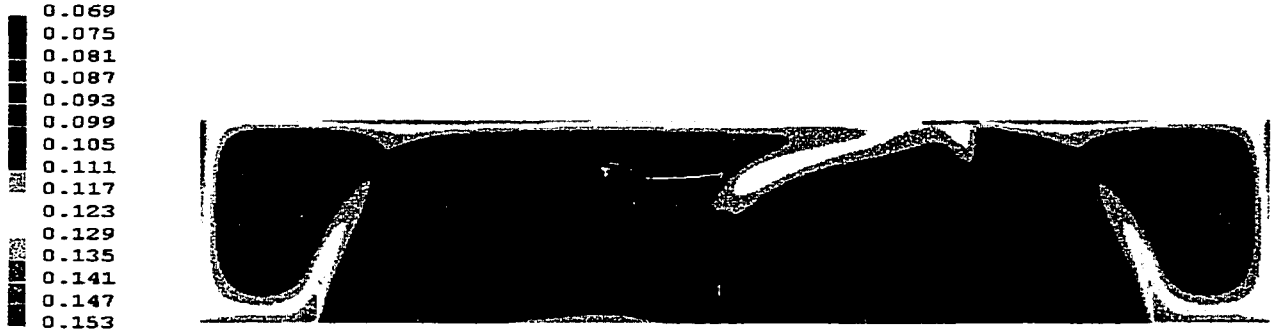

Figure 5.18. Contour of the liquid volume fraction (R2) for gas density 20 kg/ m^3,. Gas to Liquid split (90: 10) and velocity of 70 m/s.

Chapter 6

Results of Packed Bed Flow

6.1 Introduction

A detailed understanding of fluid movement within packed beds of catalyst particles is of fundamental importance in many industrial processes and especially in reaction engineering. Until now, most experimental and theoretical studies of fluid flow through packed beds has been restricted to descriptions of the bed in terms of macroscopic properties, averaged over the bed, such as pressure drop, permeability and dispersion. Nowadays a number of visualization techniques have been applied to study fluid transport through packed beds including conductance, capacitance, optical and X-ray tomography, and magnetic resonance imaging (MRI) techniques[51]. Mantle *et al.*[51] have reported their experimental results using MRI by taking in-situ measurements of flow velocity, diffusion and dispersion in packed beds.

As far as predicting flow distribution in packed beds using CFD is concerned, there are very few results available and those that are available are for lab-scale vessels[5].

In this investigation flow simulation was carried out in a partially packed vessel of industrial dimensions. The reactor dimensions remain the same as in the cases of single- and two-phase flow but there is a packed bed of 1.2 m height inserted 1.4 m above the vessel bottom (Figure 6.1). This means that out of the 49 cells in the z-direction, 12 cells located between 15-26 signify the packed bed. The analysis of flow through packed bed is

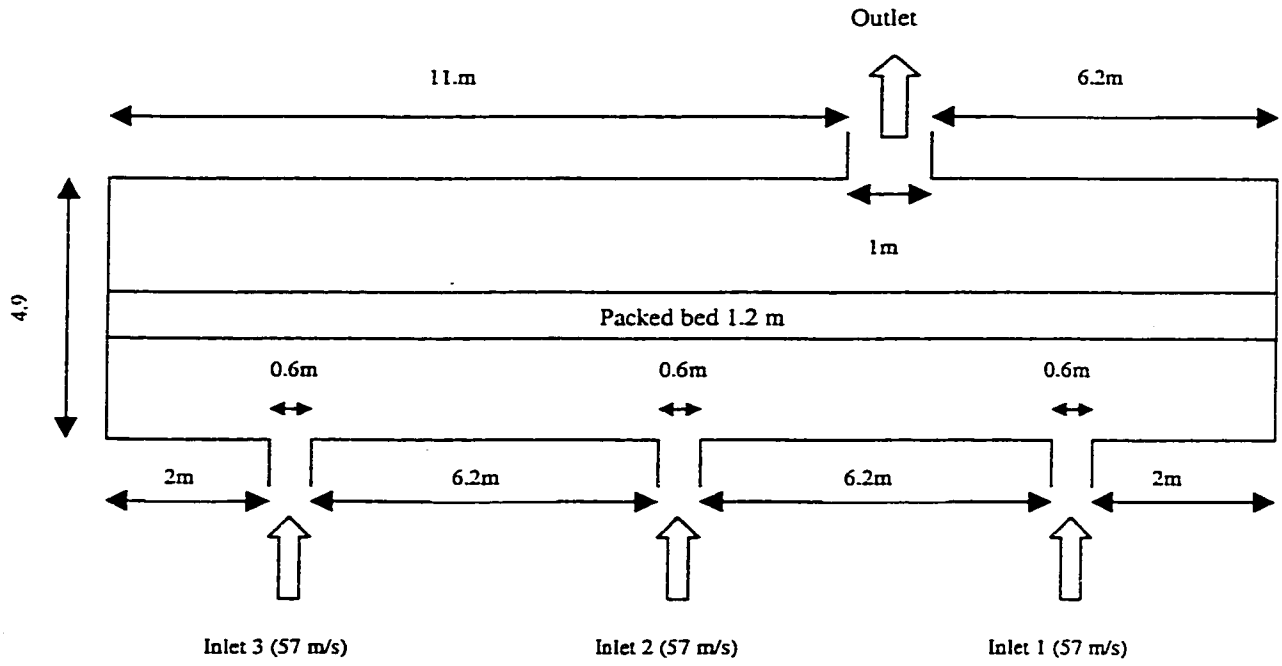

Figure 6.1. Schematic of the Packed Bed

done via two approaches. In the first approach the flow is resolved using the Darcy law model. In the second approach the flow through the packed bed is modeled using the modified Ergun equation.

Flow in porous media is modeled by addition of a momentum source term to the standard flow equations. The source term is composed of two parts, a viscous loss term and an inertial loss term.

Laminar flow in porous media can be successfully modeled by Darcy's law, which can be mathematically stated as

$$\Delta P = \frac{-\mu}{\alpha} v \qquad (6\text{-}1)$$

where α is the permeability and v is the superficial velocity. If the flow is such that the inertial loss term cannot be neglected, then the source terms must be calculated using the modified Ergun equations as explained in section 3.9.

The flow in the bed of the partially packed vessel considered in this study, may or not be in the laminar regime. The Reynolds number for a packed bed is defined as:

$$R_{ep} = \frac{d_p v \varrho}{(1-\theta)\mu} \qquad (6\text{-}2)$$

For a particle diameter of $1/8^{th}$ of an inch, and an injection velocity of 57 m/s (three inlets, each having a diameter of 0.6m), a fluid density of 1.36 kg/m^3, a viscosity of 2.96×10^{-5} Pa.s, a value of 157 is obtained for R_{ep}, where the superficial velocity is calculated based on the cross-sectional area of the converter.

The calculations for the three dimensional case differ from the two-dimensional case mainly due to the fact that the flow in the vessel is three-dimensional. For flow in porous media, it is generally accepted that the transition Reynolds number is about 10.

In summary, the flow regime in the packed bed of the partially packed converter is not clearly known, although it is likely to be closer, if not inside the laminar flow regime. To obtain the best results, simulation of flow in the partially packed vessel should be done using the source terms defined by the modified Ergun equation. However since the three-dimensional flow in the packed bed is likely to be significantly different from the two-dimensional in the present numerical model, the results are restricted to the following cases; (a) resolving the flow field with the assumption that the Darcy law is applicable and (b) resolving the flow filed using constant values of the source terms which are added to the momentum equations.

6.2 Simulation Results with the Darcy Law Model

Flow through porous media was resolved using the Darcy law. Such a type of flow may arise in catalytic beds and other highly resistive media. Numerically a patch is defined in the geometry where the Darcy's law is applicable and a coefficient is specified, which is the ratio of laminar viscosity/permeability. The permeability is calculated using the Darcy law, which can be mathematically stated as:

$$\alpha = -\frac{\mu v}{\Delta p / L} \tag{6-3}$$

where α is the permeability, μ is the fluid viscosity , v is the superficial fluid velocity based on the total bed area and $\Delta p / L$ is the pressure drop per unit length. The value of α

(a)

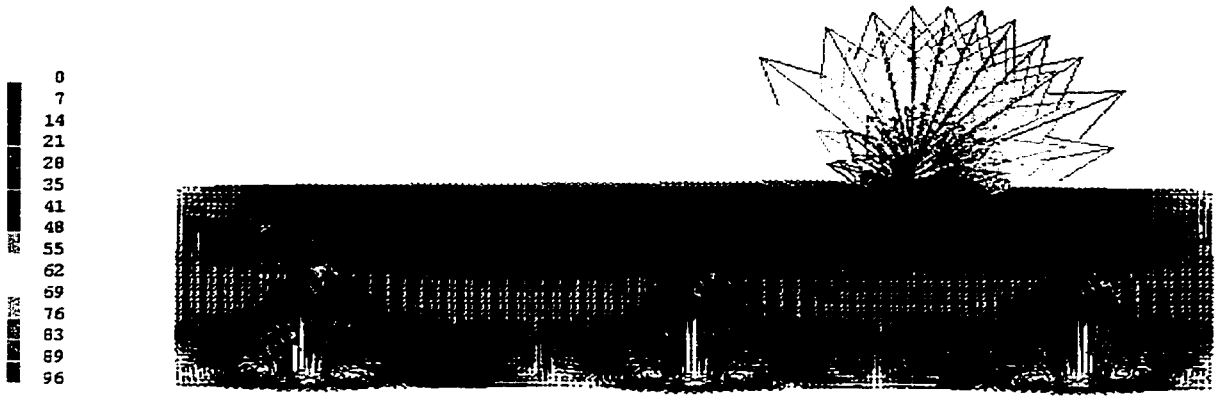

(b)

Figure 6.2. (a) Contours of the W1 velocity (z- direction) for the packed bed, and

(b) Velocity Field for the packed bed.

Permeability = $2.44e^{-8}$

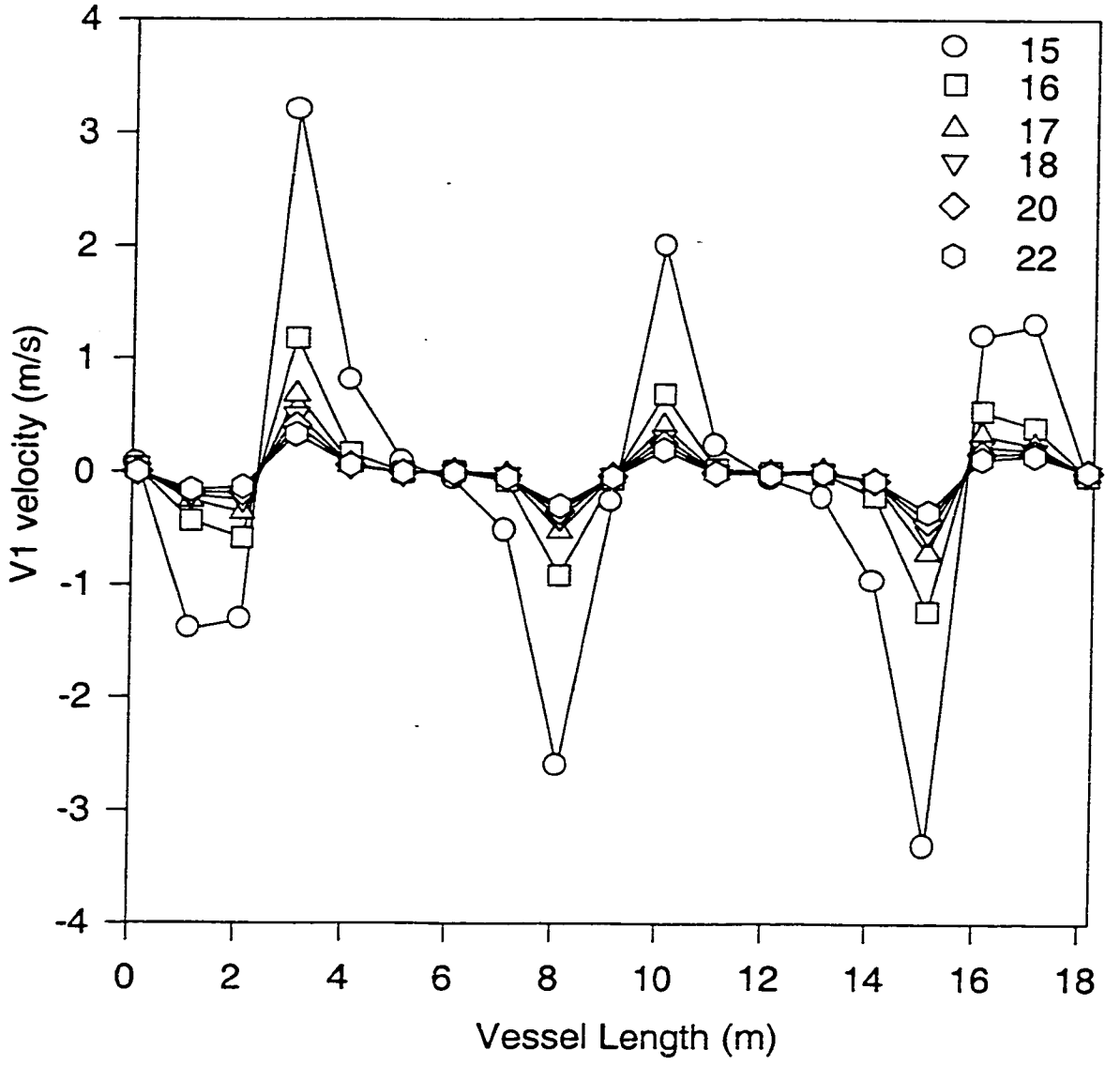

Figure 6.3 (a). A plot of V1 versus the vessel length at various positions in the packed bed

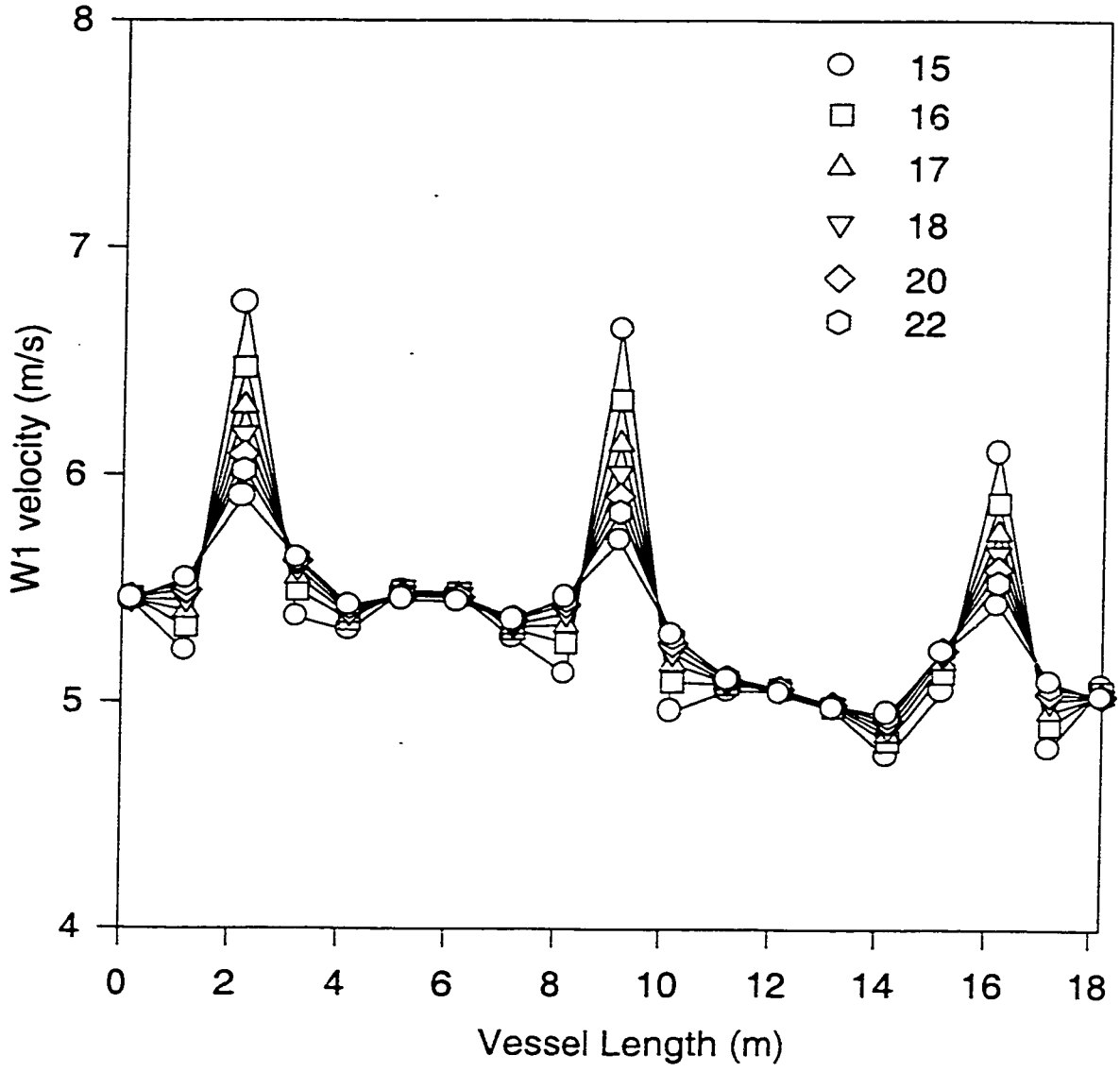

Figure 6.3 (b). A plot of W1 versus the vessel length at various positions in the packed bed

in this case is $2.44e^{-8}$ which yields the coefficient value (ratio of laminar viscosity to the permeability) to be 1213.14.

Figure 6.2 shows a plot of the contours of the velocity in the z- direction and the velocity field plots for this case. From the contour plot (Fig. 6.2 a) it can be seen that there is almost uniform flow in the packed bed, the bed acts as an even flow distributor in this case. Figure 6.3 (a, b) is a plot of the V1 and W1 velocities respectively for the vessel . Figure 6.3 (a, b) are reflections of the velocity field and contour plots, i.e., the first jet in the colored plots refers to the first jet from the right, whereas the same jet is depicted as the first from left in Figures 6.3 (a, b). These velocity values have been monitored at 15, 16, 17, 18, 20^{th}, and 22^{nd} cell in the packed bed. Figure 6.3 (a) shows clearly that in the lower part of the bed (slab 15) the velocity in the y-direction (V1) is significant i.e. of the order of $\pm$ 3 m/s. This V1 decreases to become of the order of $\pm$ 1 m/s in slab 16 and to less then $\pm$ 0.5 m/s in the remaining part of the bed.

Figure 6.3 (b) illustrates that the velocity in the z-direction (W1) is in the range of 5-7 m/s in the top part of the bed with the values in the first jet (nearest to the outlet) higher than the third jet by about 0.6-0.8 m/s. This means that most of the velocity is mainly in the z-direction. This is inline with theoretical predictions. The velocity varies in the bed from about 4 m/s to 7 m/s, which gives an indication of the highly resistive nature of the bed. From this it can be concluded that the near the first two inlets the catalytic bed sees more action and thus gets deactivated faster whereas near the third inlet which comprises about 50% of the bed, there is low activity and in practical situation the catalyst here sees very little action.It should be emphasized that these values of the velocities are applicable

for the 2-dimensional case. For the 3-dimensional case, these values are significantly different as the superficial velocity is

expected to be 0.54 m/s instead of 5.6 m/s. this means a change of Reynolds number for the packed bed will be reduced by a factor of 8.2 to about 19. This makes the packed bed Reynolds number much closer to the laminar regime whereas mentioned earlier Darcy's law is applicable.

6.2.1 Simulation results with modified Ergun equation

The modified Ergun equation was discussed in section 3.8. The friction factor terms for F_z and F_y for the packed bed are calculated from correlations (Equations 3.42 - 3.45). The bed is assumed to have a voidage of 0.5, which is typical for catalytic beds. The particle considered here are spheres of average diameter of $1/8^{th}$ of an inch. Figure 6.4 (a) show the result with $F_z = 10$ and $F_y = 10$ for the packed bed. There seems to be two zones, one in which the bed is underutilized and the other in which the bed is overutilized. The portion near the first two inlets has more activity as far as flow distribution is concerned as compared to that near the third inlet. This phenomena is also evident from Figure 6.4 (b) which is a reflection of the colored plot, wherein there seems to be a big low velocity zone between the second and third inlet and also between the third inlet and the wall.

Since the values of the friction factor have a pronounced effect on the flow distribution profiles, it was considered worthwhile to examine the effect of changes in the friction factor value. For the next case, the value of F_z is increased by 10 times the original value, i.e. $F_z = 100$, and $F_y = 10$. The results shown in Figure 6.5 depicts an almost similar trend to that with $F_z = 10$. Here the second jet has broken contact with the first one. Also evident from Figure 6.5 (b), is that there is lesser flow in the top half of the

vessel when compared with figure 6.4 (b), i.e. when the resistance in the z direction is higher the bed restricts the flow more than when the resistance is lower. In this case the areas of low velocity are more prominent.

In the last case, simulation has been carried out for a very high value of friction factors, viz. F_z = 5000, F_y = 5000. The results shown in Figure 6.6 show an almost uniform z velocity distribution in the vessel. This result is very much similar to that obtained with the Darcy law model with permeability of $2.44e^{-8}$. The plots show a uniform distribution in the packed bed inside the vessel. The results indicate that at this high value of friction factors, the bed acts as a uniform flow distributor. Figure 6.7 (reflection of the colored plot) are plots for z- directed velocity, which have been monitored from cells, 15-22. The results show higher velocities in the bed at the 15^{th} cell (bed entrance), but once the fluid enters the bed, the velocity starts to fall and eventually at the 22^{nd} cell, which is somewhere near the bed center, the velocity throughout the bed is almost constant at about 5.6 m/s.

(a)

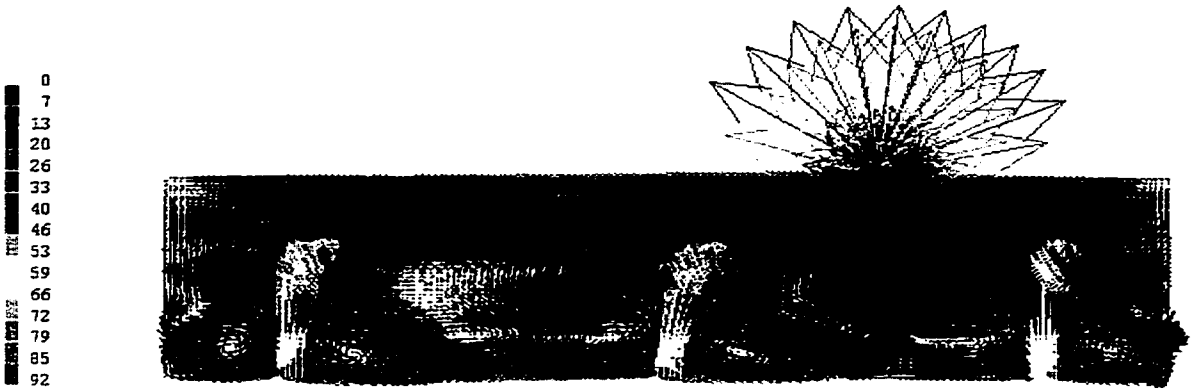

(b)

Figure 6.4. (a) Contour of W1 for the packed bed, and (b) Velocity Field for the packed bed.

($F_z = 10$ and $F_y = 10$)

(a)

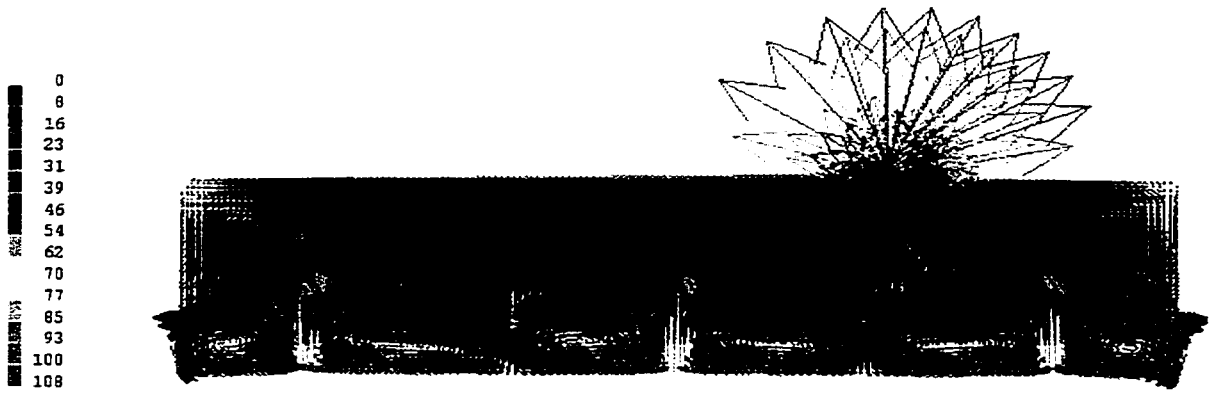

(b)

Figure 6.5. Contour of W1 for the packed bed, (b) Velocity Field for the packed bed.

(F_z=100, F_y=10)

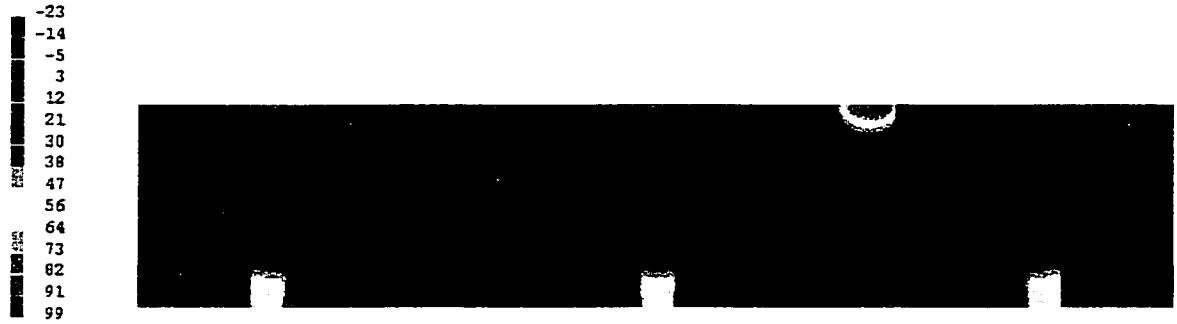

(a)

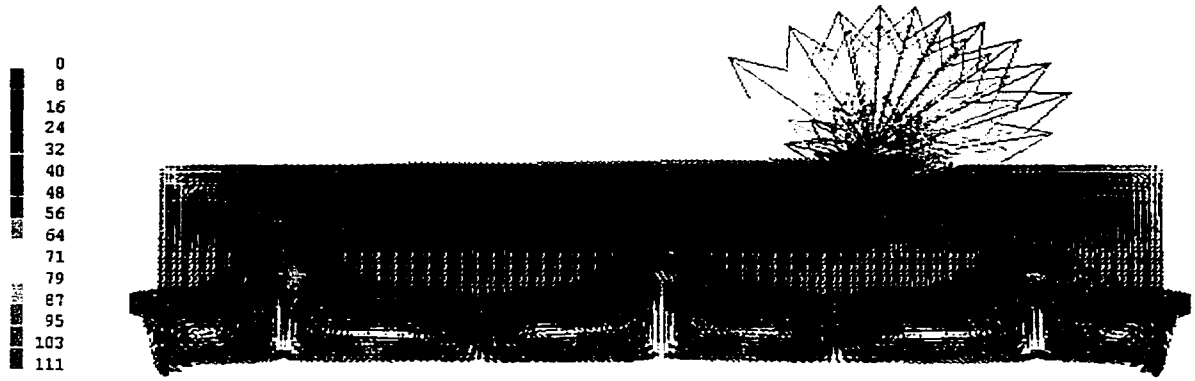

(b)

Figure 6.6. (a) Contours of W1 for the packed bed, and (b) Velocity Field for the packed bed.

(F_z =5000, F_y = 5000).

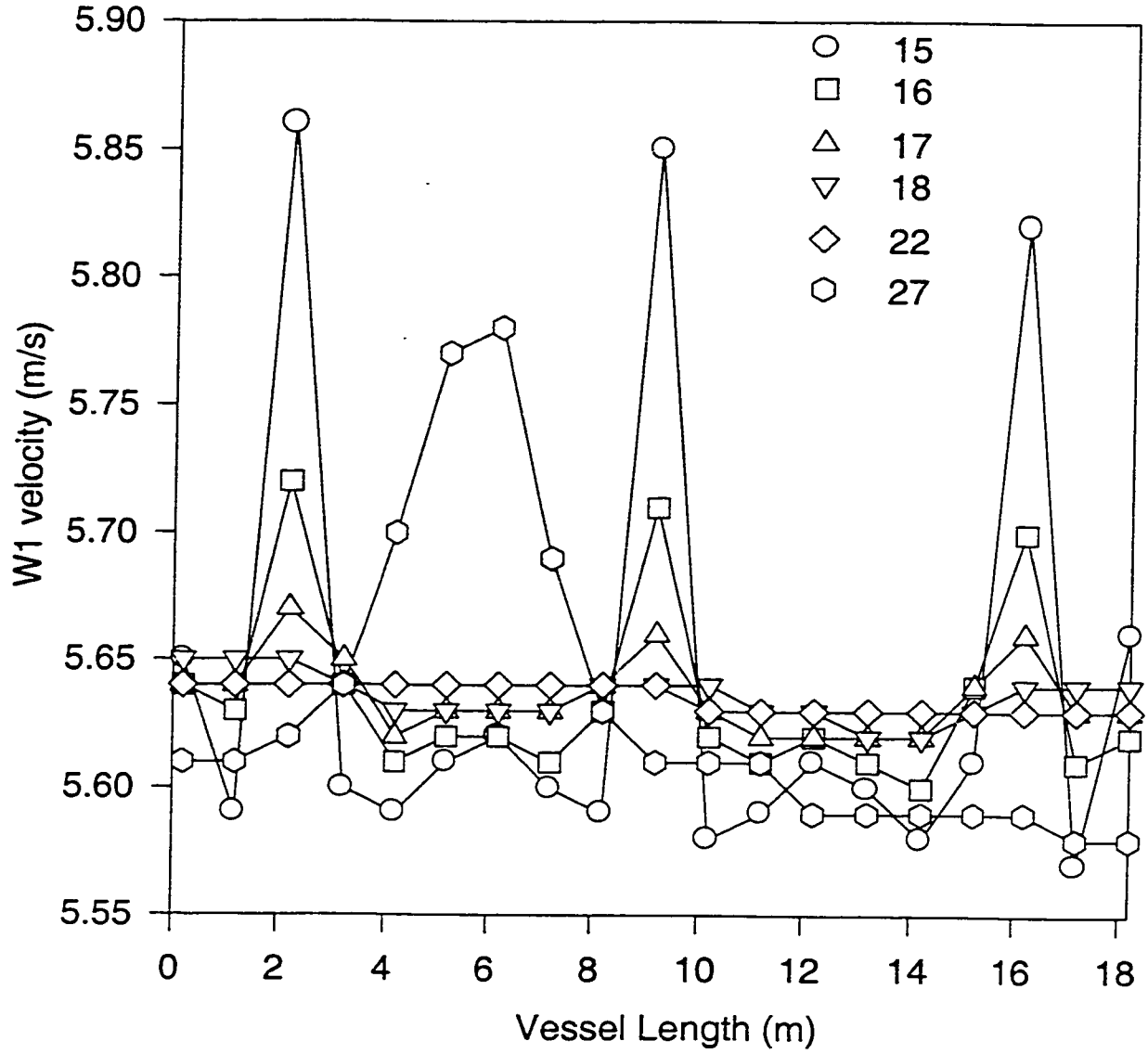

Figure 6.7. A plot of velocity in the z- direction for the packed bed with $F_z = 5000$ and $F_y = 5000$ at various positions in the bed

Chapter 7

Conclusions & Recommendations

The simulation studies carried out for the sulfur converter using CFD has underlined the importance of an intensive selection procedure for process industries. The model has been effective in emphasizing the importance of the vessel geometry as regards the flow distribution. The model also made clear the effects of variations of parameters like fluid flowrates, boundary conditions, split of phases in case of two-phase flow and the effect of the catalyst bed on the flow distribution in the vessel.

The results can be summarized for each type of flow condition as follows:

1. In the present geometry, there is a significant flow maldistribution in the vessel. In the region between the second and the third jet there is significant low velocity zoning. These low velocity zones are also larger near the walls.
2. The fluid flowrate has no pronounced effect on the flow situation in the vessel. The effects of increasing the velocity in the vessel from 45 m/s to 70 m/s did not produce any appreciable improvement.
3. The arrangements of inlets and outlets have a considerable impact on the flow situation in the vessel. The results clearly show that the present inlet / outlet design on the vessel is not a suitable one and some modifications on the outlet is desirable. The multiple outlet case also shows promising results.

4. The effects of having multiple inlets were not as promising as was expected. This may not be the optimal arrangement, but it highlights the importance of proper inlet selection in vessel design. The multiple inlets/multiple outlets case yields the best results as far as inlet/outlet modifications are concerned.

5. The flow situation can also be enhanced by inserting some form of disc or flow redistributors in the vessel. The results with a 0.2 m insert as well as that with a conical insert seems to be very encouraging. This alternative could be effective for the present vessel, if it is difficult to change the inlet/outlet arrangement as suggested above. The addition of insert can act as an economically favorable alternative. The results show that the conical insert can act as a good flow distributor in the vessel and if properly selected could lead to substantial improvements in the flow distribution. However, before recommending such inserts, careful consideration must be given to possible implications such as pressure drop and deposition of the dispersed phase on these inserts (two-phase flow).

6. With the two-phase situation, apart from flow maldistribution, another complexity arises which is the deposition or concentration of the liquid (heavy phase) at the corners of the vessel. This can lead to severe problems like precipitation or the formation of a pool of liquid, leading to surging of compressors in case of polymeric flows.

7. The effect of variation of fluid flowrate showed marginal improvement as far as minimizing the heavy phase (liquid) deposition at the corners.

8. The effect of different inlet / outlet arrangement for the two-phase case, gives the same results as that for a single-phase case. The multiple outlets in two-phase case

also was very promising. The use of 6 and 8-inlet cell shows that the 8-inlet cells gives slightly better results as far as liquid deposition (heavy phase) at the corners is concerned. The use of multiple inlets/outlet does not give encouraging results, as there seems to be more liquid accumulation at the corners.

9. The results with internal geometric improvements, i.e. addition of inserts in two-phase flow become more complex. Although the flow distribution shows improvement, there seems to be liquid deposition right in the vicinity of the insert. The results with a smaller insert (0.2 m ID) are encouraging. The conical insert gives the best result as far as addition of inserts is concerned. There is a good flow distribution in the vessel and the deposition or accumulation of the heavy phase (liquid) is almost zero.

10. The effects of physical properties were also investigated. The increase in gas density by about 20 times yields negative results. The flow situation gets worse in this case. The effect of increasing the liquid faction in the feed to about 10% from 1% deteriorates the situation further. When the velocity was increased with an increase in liquid fraction (10%), the results showed no appreciable change.

11. The packed bed analysis was done using two methods. The first method involved the Darcy law model. The model shows almost uniform flow in the packed bed. The packed bed acts as a huge resistance to the flow and acts as a distributor. The velocity in the bed is in the range of about 5.2 m/s. The bed seems to be underutilized in some areas (near the third inlet) and over-utilized near the first two inlets and the outlet. If this is the actual situation, this could lead to a faster deactivation of the catalyst in the zones near the outlet, which can consequently lead to operational problems in the vessel.

12. The results with the modified Ergun approach are also interesting. The friction factor values that have calculated form these equations were very high. The results with a high value of the friction factor shows an almost constant flow in the bed. This result is much similar to the Darcy model results for the higher permeability. When the friction factors were reduced to a much lower value, the results show the same short-circuiting of flow pattern as with the Darcy model with a lower permeability.

13. It can be concluded that the bed acts as huge resistance to flow and consequently can change the flow distribution pattern in the vessel.

14. The simulation results presented in this analysis have shown the importance of selecting a good design and operating conditions for industrial vessels. The current design of vessel investigated in this work is actually in use in industries. The analysis for different types of flows has shown that the present vessel design is very inefficient. The flow maldistribution resulting from such an inefficiency design will have a direct impact on the product quality and the economics of operation. The present investigation has been successful in analyzing this flow maldistribution and certain changes proposed could lead to a better flow distribution.

15. Since the flow in the vessel is in reality three-dimensional, a two-dimensional model used in this work, may not be a complete solution to the problem. A full three-dimensional model will be able to predict the flow distribution to a much better extent. The three-dimensional model is very important in case of the partially packed bed.

References

1. M. B. Abbott, and D. R. Basco, *Computational Fluid Dynamics*. Longman Scientific & Technical, Essex, England., 1989.
2. R. V. A. Oleimans, *Computational Fluid Dynamics for the Petrochemical Process Industry*, Kluwer Academic Press, Netherlands, 1991.
3. D. A. Coleman, *Computational Fluid Dynamics*: Understanding Unit Operations, BP Amoco Chemicals, PTQ, 1999.
4. R. Bird, W. E. Stewart, and E. N. Lightfoot, *Transport Phenomena*, John Wiley & Sons, New York, 1960.
5. P. Spicka, A. Martins, M. D. Dias, J. Lopez, and B. Carlos, Hydrodynamics of Gas-Liquid Flow in a 2D Packed/Unpacked Rectangular Reactor. *Chem. Eng. Sci.*, **54**(21), 5127-5137 (1999).
6. J. W. Wang and J. R. G. Andrews, Numerical Simulation of Flow in Helical Ducts, *AIChE J.*, **41**(5), 1071-1080 (1995).
7. H. F. Mier, J. J. N. Alves, and M. Mori, Comparison Between Staggered and Collocated Grids in the Finite-Volume Method Performance for Single and Multi-phase Flows, *Comp. and Chem. Eng.*, **23**, 247-262 (1999).
8. M. Abid, C. Xuereb, and J. Bertrand, Hydrodynamics in Vessels Stirred with Anchors and Gate Agitators, *Trans. I. Chem. Eng.*, **70**(Pt. A), 377-384 (1992).
9. D. Azbel, *Two Phase Flows in Chemical Engineering*, Cambridge University Press, Cambridge, England, 1981.
10. H. F. Rase, *Fixed Bed Reactor*, Butterworths Publishers, Ma, USA, 1990.

11. J. A. M. Kuipers, and W. P. M. Van Swaaij, Applications of Computational Fluid Dynamics to Chemical Reaction Engineering. *Reviews in Chemical Engineering*, **13**(3), 2-75 (1997).

12. C. K. Harris, D. Roekaerts, F. J. J. Rosendal, F. G. J. Buitendijk, Ph. Daskopoulous, A. J. N. Vreenegoor, and H. Wang, Computational Fluid Dynamics for Chemical Reactor Engineering, *Chem. Eng. Sci.*, **51**(10), 1569-1594 (1996).

13. M. Pipino, and R. O. Fox, Reactive Mixing in a Tubular Jet Reactor: A Comparison of PDF Simulation with Experimental Data, *Chem. Eng. Sci.*, **24B**, 5229-5241 (1994).

14. P. S. Harvey, and M. Greaves, Turbulent Flow in an Agitated Vessel, Parts I & II, *Trans. I. Chem. Eng.*, **60**, 195-210 (1982).

15. A. G. C. Lane, Ph.D. Thesis, Liquid Jet Mixing, Loughborough University of Technology, Loughborough, UK, 1981.

16. N. Zuber, and Z. Findlay, Average Volumetric Concentrations in Two-Phase Flow. *J. Heat Transfer*, **87**(3), 453-462 (1965).

17. G. B. Wallis, *One Dimensional Two-Phase Flows*, McGraw-Hill Book Company, New York, 1969.

18. L. S. Tong, and Y. S. Tang, *Boiling Heat Transfer and Two-Phase Flow*, Taylor & Francis, Washington, 1997.

19. E. Delnoij, J. A. M. Kuipers, and W. P. M. Van Swaaij, A Three-dimensional CFD Model for Gas-Liquid Bubble Columns, *Chem. Eng. Sci.*, **54**, 2217-2226 (1999).

20. Y. Jiang, M. R. Khadilkar, M. H. Al-Dahhan, and M. P. Dudukovic, Single Phase Flow Distribution in Packed Beds: Discrete Cell Approach Revisited, *Chem. Eng. Sci.*, **55**, 1829-1844 (2000).

21. V. V. Ranade, and Van den Akker, A Computational Snapshot Approach of Gas-Liquid Flow in Baffled Stirred Reactors, *Chem. Eng. Sci.*, **49**(24B), 5175-5192 (1994).

22. V. V. Ranade, Computational Fluid Dynamics for Reactor Engineering. *Reviews in Chemical Engineering*, **11**(3), 229-289 (1995).

23. M. H. Al-Dahhan, Y. Jiang, M. R. Khadilkar, and M. P. Dudukovic, Two-Phase Flow Distribution in 2D- Trickle Bed Reactors, *Chem. Eng. Sci.*, **54** (21) 5127-5137 (2000).

24. H. Delmas, and G. F. Froment, A Simulation Model Accounting for Structural Radial Nonuniformites in Fixed Bed Reactors, *Chem. Eng. Sci.*, **43**(5), 2281-2287 (Jun 1988).

25. T. Daszkowski and G. Eigenberger, A Revaluation of Fluid Flow, Heat Transfer and Chemical Reaction in Catalyst Filled Tubes, *Chem. Eng. Sci.*, **47**(9), 2245-2250 (1992).

26. J. J. Lerou, and G. F. Froment , Velocity, Temperature and Conversion Profiles in Fixed Bed Catalytic Reactors, *Chem. Eng. Sci.*, **32**, 853-861 (1977).

27. C. McGreavy, E. A. Foumeny, and K. H. Javed, Characterization of Transport Properties for Fixed Bed in terms of Local Bed Structure and Flow Distribution. *Chem. Eng. Sci.*, **41**, 787-797 (1986).

28. O. Bey, and G. Eigenberger, Fluid Flow Through Catalyst Filled Tubes, *Chem. Eng. Sci.*, **52**(8), 1365-1376 (1997).

29. I. Ziolkowska, and D. Ziolkowski, Modeling of Gas Interstitial Velocity Radial Distribution over a Cross-Section of a Tube Packed with a Granular Catalyst Bed, *Chem. Eng. Sci.*, **48**(18), 3283-3292 (1993).

30. G. W. Johnson, and R. S. Kapner , The Dependence of Axial Dispersion on Non-uniform Flows in Beds of Uniform Packing, *Chem. Eng. Sci.*, **45**, 3329-3341 (1990).

31. R. Berninger, and D. Vortemeyer, Die Umstromung von Hindernissen in Schuttungen. *Chem. Ing. Tech.*, **59**, 224 (1987a).

32. R. Berninger, and D. Vortemeyer, Der Einflub von Versperrung auf das reaktionstechnische Verhalten eines adiabaten Festbettreaktors, *Chem. Ing. Tech.*, **60**, 1052 (1987b).

33. J. Szekely, and J. J. Poveromo, Flow Maldistribution in Packed Beds, *AIChE J*, **21**, 769 (1975).

34. V. Stanek, *Fixed Bed Operations: Flow Distribution and Efficiency*, Ellis Horwood, Chichester, 1994.

35. V. Stanek, and J. Szekely, Three-dimensional Flow of Fluids through Nonuniform Packed Beds, *AIChE J*, **20**, 974-980 (1974).

36. D. D. Joseph, *AIChE Annual Meeting*, Flow Induced Microstructure and Direct Simulation of Liquid-Solid Flow, PTF Topical Conference, Miami Beach, FL, USA, 1998.

37. D. Vortemeyer and J. Schuster, Evaluation of Steady Flow Profiles in Rectangular and Circular Packed Beds by a Variational Method, *Chem. Eng. Sci.*, **38**(10), 1691-1699 (1983).

38. S. Ergun, Fluid Flow Through Packed Columns, *Chem. Eng. Prog.*, **48**(2), 89-94 (Feb 1952).

39. N. Dombrovski, E. A. Foumeny, and A. Riza, Know the CFD Codes, *Chem. Eng. Prog.*, **89**(9), 46-48 (1993).

40. H. D. Zughbi, and M. P. Schwarz, *CSIRO*, Simulation of Bath of Hismelt Research and Development, Rep 781, CSIRO, Australia, 1993.

41. H. D. Zughbi, *Final Report KFUPM*, Numerical Investigation of Two-Phase Flow at the Inlet of a SABIC Reactor, Dhahran, K.S.A, 2000.

42. D. B. Spalding, *A Guide To Phoenics Input Language*, CHAM, London, UK, 1992.

43. S. V. Patankar, *Numerical Heat Transfer and Fluid Flow*, Hemisphere Publishing Corporation, New York, 1980.

44. D. B. Spalding, Second International Conference on Physical Hydrodynamics, Washington D. C., 1978.

45. I. Kataoka, and M. Ishi, Mechanistic Modeling of Pool Entrainment Phenomenon, *Int. J. Heat & Mass Transfer*, **27**(11), (1984).

46. T. Miyahara, and T. Takahashi, Size of Droplets Produced in the Jetting Regime at Single Orifices, *J. Chem. Eng. Japan*, **17**(2), 218-220 (1984).

47. E. N. Ganic and W. M. Rohsenow, An Analysis of Dispersed Flow Heat Transfer using a Drop Deposition Model, Two-Phase Trans. & Reactor Safety, Oct. 18-20, Fort Lauderdale, Florida, USA. 1976.

48. H. C. Brinkman, Fluid Flow in a Porous Medium. *Appl. Sci. Res. Sect. A1*, **27**, (1947).

49. S. A. Orszag, V. Yakhot, W. S. Flannery, F. Boysan, D. Choudhry, J. Maruzewski, *Near Wall Turbulent Flows*, Elsevier Science Publishers, 1993.

50. POLIS Encyclopedia, Phoenics Online Information System, CHAM, London, UK. 2001.

51. M. D. Mantle, A. J. Sederman, and L. F. Gladden, Single-and Two-Phase Flow in Fixed Bed Reactors: MRI Flow Visualization and Lattice-Boltzman Simulations, *Chem. Eng. Sci.*, **56**, 523-529 (2001).

Vita

Name	Saifuddin Sheikh
D.O.B	09-10-75
Education	a) Diploma in Chemical Engineering from S.Polytechnic, Mumbai. 1994 b) Bachelors Degree in Petrochemical Engineering from University of Pune. 1997. c) PG. Diploma in Piping Design and Engineering from MIT, Pune. 1998 d) Masters in Chemical Engineering from KFUPM, Saudi Arabia. 2001
Experience	a) Site Engineer (September 1997 to March 1998) TATA-Honeywell (H.P.C.L refinery). Mumbai. b) Piping Design Engineer (April 1998 to January 1999) Dorr-Oliver India Ltd. Mumbai. c) Research Assistant (January 1999 to August 2001) Chemical Engineering Department. KFUPM. Saudi Arabia.
Publication	Saifuddin Sheikh, H. D. Zughbi, " Numerical Simulation of One- and Two- Phase Flows in a Tank" Annual AIChE Conference, Los Angeles, USA, November 2000.